Islamic University of Technology

Department of Mechanical and Production Engineering

MOLECULAR DYNAMICS SIMULATION OF TWO DIMENSIONAL MATERIALS

A Thesis by

Ahmad Fatehi Ali Mohammed Hezam

A.S.M Redwan Haider

Submitted in Partial Fulfillment
of the Requirements
for the Degree of

Bachelor of Science in Mechanical Engineering

May 2022

MOLECULAR DYNAMICS SIMULATION OF TWO DIMENSIONAL MATERIALS

AHMAD FATEHI ALI MOHAMMED HEZAM, 170011070

A.S.M REDWAN HAIDER, 170011061

Submitted in Partial Fulfillment
of the Requirements
for the Degree of

Bachelor of Science in Mechanical Engineering

DEPARTMENT OF MECHANICAL AND PRODUCTION ENGINEERING

May 2022

CERTIFICATE OF RESEARCH

This thesis titled "MOLECULAR DYNAMICS SIMULATION OF TWO DIMENSIONAL MATERIALS" submitted by AHMAD FATEHI ALI MOHAMMED HEZAM (170011070) and A.S.M Redwan Haider (170011061) has been accepted as satisfactory in partial fulfillment of the requirement for the Degree of Bachelor of Science in Mechanical Engineering.

Supervisors

_____

Mr.Sayedus Salehin

Assistant Professor

_____

Dr. Md. Rezwanul Karim

Associate Professor

Head of the Department

_____

Prof. Dr. Md. Anayet Ullah Patwari

Professor

Department of Mechanical and Production Engineering (MPE)
Islamic University of Technology (IUT)

DECLARATION

I hereby declare that this thesis entitled " MOLECULAR DYNAMICS SIMULATION OF TWO DIMENSIONAL MATERIALS." is an authentic report of our study carried out as requirement for the award of degree B.Sc. (Mechanical Engineering) at Islamic University of Technology, Gazipur, Dhaka, under the supervision of Dr.Md. Rezwanul Karim, Associate Professor, MPE, IUT in the year 2021

The matter embodied in this thesis has not been submitted in part or full to any other institute for award of any degree.

_____

Ahmad Fatehi Ali Mohammed Hezam
Student ID: 170011070

_____

A.S.M Redwan Haider
Student ID: 170011061

ACKNOWLEDGEMENTS

In the beginning we would love to praise Allah the Al-Mighty without whose guidance this work would have not been possible. Secondly, our parents who have relentelessly work hard for us to be in this position today. Our sincere gratitude towards our honourable supervisors Dr.Md.Rezwanul Karim and Mr. Sayedus Salehin for their guidance and encouragement throughout the project. We are glad to have Mohammed Raihan Uddin to guide us through the whole procedure with valuable directions.

We are greateful to our Co-superviors Dr.Yeasir Arafat and Mr.Md Akibul Islam for their relentless support and motivation. Their experstise of materials had given the thesis group an enormous advantage. Their construrctive ciristism and reviews had given the work a world class flavor.

We are thankful to Dr.Mohammad Tanvirul Ferdaous and Rafsan Subad for their logistical support. Their contribution made barriers easy to overcome.

Lastly, we also appreciate the prompt response of Dr. Nuwan Dewapriya and Dr. Jiang Xiujuan for their expert opinion during the progression of the work.

ABSTRACT

Ultra-thin materials like Graphene and Transition Metal dichalcogenides are a novel class of materials with robust applications in electronic devices. These 2D materials are one of the main driving forces behind the rise of nanotechnology. Therefore, researchers need to characterise such materials to find their suitable usage. These materials have multiple properties such as electronic, optical and mechanical. Mechanical properties such as elasticity, strength and plasticity define a material's usage. There are two common ways to investigate these materials. One such is Classical Mechanics, and the other is Density functional theory(DFT). This study focuses on the application of Molecular dynamics (MD) simulation to derive stress-strain relationships of such materials. LAMMPS is a tool that aids in performing the simulation. Interatomic potentials such as AIREBO and Stillinger-Weber potential are used to derive the required outcomes. The visual simulation results aid us in understanding and describing their fracture behaviour. In our work, we primarily focus on the temperature-dependent fracture to determine the ultimate tensile stress(UTS) of a material. Initially, we worked to examine the stress-strain relationship of armchair graphene monolayer due to varying temperatures from 300K to 2100K. Then, we thoroughly investigate molybdenum disulfide (MoS2) and molybdenum telluride (MoTe2) using the parameterised Stillinger-Weber potential. Finally, the fracture strength of MoTe2 is determined from 100K to 600K at an interval of 100K. The results for both armchair and zigzag are tabulated and plotted. We can observe that for each corresponding temperature, the armchair MoTe2 is stronger than zigzag MoTe2. Furthermore, we find that the young's modulus is unaffected due to the temperature change, which could help to determine the range and the application of the material in different field.

Keywords: 2D materials, molybdenum telluride, molecular dynamics, Stillinger weber potential, Fracture mechanics.

TABLE OF CONTENTS

LIST OF FIGURES

LIST OF TABLES

NOMENCLATURE

LAMMPS	Large scale atomic/molecular massively parallel simulator
TMDCs	Transition metal dichalcogenides
MD	Molecular Dynamics
CVD	Chemical vapor deposition
AR	Armchair
ZG	Zigzag
CPU	Central processing unit
GPU	Graphics processing unit
MoS_2	Molybdenum sulfide
$MoTe_2$	Molybdenum ditelluride
SEM	Scanning electron microscope
AFM	Atomic force microscopy
HEMTs	High-electron-mobility Transistor
NEMS	Nanoelectromechanical systems
TEM	Transmission Electron Microscopy
CWD	Charge Density Wave
MBE	Molecular Beam Epitaxy
LIB	Lithium ion batteries
NIB	Sodium ion batteries
MPI	Message-passing library
UTS	Ultimate tensile stress
Atomsk	Atom, Molecule, Material Software Kit
VESTA	Visualization for electronic and structural analysis

Chapter 1
INTRODUCTION

1.1. INTRODUCTION TO THE RESEARCH

The 2D materials are a novel class actively under research due to their extensive properties such as high conductance, tensile strength and mobility. Researchers are exploring more into these materials to find their potential usage in the industries such as electronics, composites, sensors and etc. The most eminent progress was the discovery of graphene, which has caused a revolutionary change. Graphene has attracted multiple researchers to investigate more about 2D Materials. The current technology also allows us to manipulate the properties as per requirement by adding new materials into such structures [1]. In addition, several other 2D materials are available in the literatures. These are silicene, Transition metal dichalcogenides (TMDs), Metal oxides, MXene and phosphorene [2]. Preparation of such materials can be as simple as using a scotch tape [3] to extract from bulk materials to complex processes like chemical vapor deposition (CVD) [4].

1.2. RESEARCH PROBLEM STATEMENT

The procurement process of such materials is costly since they are not found naturally in nature. Additionally, handling such materials requires advanced lab facilities with sophisticated logistics and equipment requirements. Therefore, very few researchers have access to such materials to explore more about their properties. Theoretically, there is a need for alternative ways to extract more information about such products via simulation. Thus, it reduces the possibility of any waste or misusage of materials. Researchers can use intuition for such data before directly using such materials for any experimental purpose. Classical and Quantum physics use fundamental laws to describe the atomic motion resulting from a change in different parameters [5]. Large-scale Atomic/Molecular Massively Parallel Simulator (LAMMPS) is software that simulates atomic motion in terms of classical physics [6]. Lammps uses classical molecular dynamics simulations (MD), that aids in modeling fluids and solids' chemical and mechanical behavior. The accuracy of the work depends on the potential interatomic file, which contains the function of atomic positions and other properties [7]. Atom.sk [8] using or Vesta [9] is open source software used to

create 2D atomic structures using the existing lattice parameters from the literature . LAMMPS simulation allows researchers to study the fracture mechanics of 2D materials qualitatively and quantitatively. The results help model fracture behavior for different materials and compare the data with other materials regarding strength, flexibility and rigidity. Ovito [10] visualizer is helps to observe the fracture mechanism.

1.3. OBJECTIVE OF THE STUDY

This research focuses on the mechanical behavior of the range of 2D materials available in the industry. The fundamentals of 2D materials, their categories, and classification were covered, along with the naming convention of different configurations. The prime ambition is to understand how the MD simulations work along with the supplements. The objective includes to learn how classical mechanics works and implements all three of newton's laws [11]. Once the structures are made using the respective software as mentioned earlier, the primary assignment is to run the LAMMPS code. We successfully learn to run uniaxial tensile loading on the material. 2D materials, in general, are exposed to static and dynamic loading, which causes mechanical deformations like wrinkle [12], buckle [13], tear [14] and fracture behavior [15]. The fracture mechanism of each material is crucial for research to understand the fracture pattern of different materials to prevet this unprecedented accidents by predicting the ultimate tensile stress and elastic modulus.we can identify the nature of the crack and the fracture strain at which the materials fail. Processing the quanitiative data produces stress-strain relationships we are invaluable information for designers. Researchers can use these reports to choose and compare between materials while designing a project or protoype.

1.4. SCOPES AND LIMITATIONS

MD simulation on materials allow characterizing the properties of materials in case of different conditions. The variation in conditions could be in temperature, defects, and doping. The material structure can be re-made into several options, and multiple simulations can be run upon it to understand how the materials behave in case of variations in parameters. The simulation results give results close to the accurate values. The results aid the researcher in understanding more about the materials and implementing them in different applications—the main drawback being the need for high computation power to run the simulations. The simulation uses Central

Processing Unit (CPU) cores to run the calculations. Additionally, the simulation can also be run in a Graphics processing unit (GPU), which requires extra configuration. The simulations can be run with parallel cores to speed up the process to get faster results. The initial investment of CPUs with such a configuration is quite expensive and consumes much electricity to give the output. Simulation time largely depends on the size of the sheet of material. A large sheet increases simulation time drastically; therefore, it takes several days to get a set of complete data sets. Furthermore, the CPU heats for continuous usage. Therefore, a code has to be prepared to stop the simulation when the ambient temperature surpasses the critical point of the material. Negligence in such a matter can end with a computer's motherboard melting, and fire can get ignited.

1.5. METHODOLOGY

The simulation process requires three files at once to initiate the process—the structural file, which contains the three coordinates for all the atoms in a sheet of material. Then the potential file contains the potential interatomic relationship. This file contains the function of relationships of how atoms behave when bought closer or taken away. Lastly, the instructions as a code written to command the LAMMPS simulator to carry out the task. The CPU process all the data using the governing equations to calculate stress-strain relationships.

1.6. CONTRIBUTION

This study concentrate on the temperature-dependent fracture of TMDs, with a particular emphasis on molybdenum ditelluride ($MoTe_2$). Each simulation was done with a varying temperature at 100K intervals from 100K to 600K. The simulation was conducted in both AR and ZG configurations for varying temperatures. The results were plotted together on a graph with the aid of Origin to compare the results. A general trend was discovered from the observation of quantitative data regarding the strength of the materials with varying temperatures and configurations. The code developed can be used for other thirty-four TMDCs available in the literature [16]. The Stress-Strain relationships can be calculated for this range of materials in a similar pattern in a similar pattern.

1.7. ORGANIZATION OF THE THESIS

The thesis has been divided into a number of chapters, Chapter 1 describe thesis layout and give the introduction of the thesis.

Chapter 2 represent the literature review and discuss the fundamentals and basic definitions in the 2D materials industry we will emphasize on graphene and TMDs such as molybdenum sulfide (MoS_2) and molybdenum ditelluride ($MoTe_2$).

Chapter 3 explain the methodology and will focus on how MD simulations work with the aid of LAMMPS and discuss in-depth the code and the supplement information required for the simulation to be complete. Where how to resolve different computational would be discussed and configuration-related issues to get more sensible data in line with the literature would be stated.

Chapter 4 would portray the results and discussion in a detailed manner where all the qualitative and quantitative results are compared.

Lastly Chapter 5, Summarize the findings and how the results could be close to more experimental data , the potential of this industry and the possibilities for future work would be conveyed.

Chapter 2

LITERATURE REVIEW

2.1.INTRODUCTION

In this chapter, different sub-sections will be discussed in the following section. In the sub-section, we introduce the rise of 2D materials. Materials have a fundamental parameter for all technological advancements through all ages. The sub-categories of 2D materials contain the key definitions of such materials and sample materials available in the literature. In the next section, we talk about graphene, which is made up of carbon atoms. The robustness of such materials and their dynamic capabilities is notable for their popularity. The contribution of these materials is widespread in industry for the decade. Besides graphene, the addition of Transition metal dichalcogenides (TMDCs) in the electronics industry due to their unique properties. Amongst the wide range of TMDCs, we focus solely on molybdenum disulfide (MoS_2) and molybdenum telluride $MoTe_2$. The objective of the section is to cover the state of the art of such materials to give an overview of all the possibilities. The current research also sheds light upon the progression in this field of science. The industry demands to learn more about the mechanical and electrical properties to find their best suitable application.

2.2. TWO-DIMENSIONAL MATERIALS.

Advancement of different civilizations depends on developing materials and some metals in particular are so influential that naming of several centuries begin with them. The discovery of copper, bronze and iron is revolutionary in history. We are undergoing another revolution of technology known as the age of nanotechnology. The potential of such materials is much beyond their visual capabilities. Researchers are continuously working on novel materials by playing with different chemical compositions and processes. The advent of potential technologies to visualize these materials on a nano-scale have broadened the possibility for more research. The dimensionality is a key parameter that defines its properties [17].

In nanotechnology, carbon nanostructures pioneering since the beginning of the invention of graphene by Nobel Laureates Geim and Novoselov [18]. Theoretical investigation into graphene shows its robust characteristic from mechanical and electronic perspectives [19]. The discovery of graphene leads to the exploration of other 2D materials, which also have many possibilities. Apart from graphene, there are other 2D materials such as metal oxides and transition metal dichalcogenides. The unique properties adds more varieties to the comprehensive list of superconductors, semi-conductors, semi-metals and insulators for the electronics industry [20]. Table.1 lists all the possible 2D materials enlisted in the literature.

Table 1. Family of 2D materials.

<table>
<tr><td>Graphene Family</td><td>Graphene</td><td>h-BN</td><td>BCN</td><td>Fluoro-graphene</td><td>Graphene Oxide</td></tr>
<tr><td rowspan="2">2D chalcogenides</td><td rowspan="2">MoS_2 , WSe_2</td><td colspan="2" rowspan="2">Semi-conducting dichalogenides: $MoTe_2$, $ZrSe_2$</td><td colspan="2">Metallic dichalogenides : $NbSe_2$, NbS_2</td></tr>
<tr><td colspan="2">Layered Semiconductors: GaSe, GaTe</td></tr>
<tr><td rowspan="2">2D oxides</td><td>Micas, BSCCO</td><td>MoO_2, WO_3</td><td rowspan="2">Perovskite: $LaNb_2O_2$</td><td colspan="2">Hydroxides: $Ni(OH)_2$</td></tr>
<tr><td>Layered Cu-oxides</td><td>TiO_2, MnO_2</td><td colspan="2">Others.</td></tr>
</table>

2D materials characterization is 1-atom thick sheets that detaches from the bulk mass as layers stand without substrate. Layers up to 10 atoms thick are often kept under consideration as 2D materials [17]. 2D materials have somewhat large lateral dimensions in contrast to their thickness [21]. The lateral to transverse ratio is quite large. In 2D material, adjacent atoms in the same plane connects via covalent bonding, while layers of 2D materials holds together by comparatively weak interlayer Van Der Waals coupling [22].

2D materials have recently drawn much attention in the science community because of their promising electrical, mechanical, physical, substance, and optical properties [23]. The 2D materials have high Young's modulus, ultra-low weight, high strength, high anisotropy, and outstanding carrier mobility between the in-plane and out-of-plane mechanical properties. Furthermore, a Weak Van Der Waals connection between layers permits them to slide effectively with the application of shear stress, resulting in a change of lubrication properties. In order to

ensure the best use of the novel mechanical and mechanoelectrical transduction properties. 2D materials utilization is a wide-going application, including adaptable hardware, strain sensors, nanogenerators, and imaginative nanoelectromechanical frameworks (NEMS) [22].

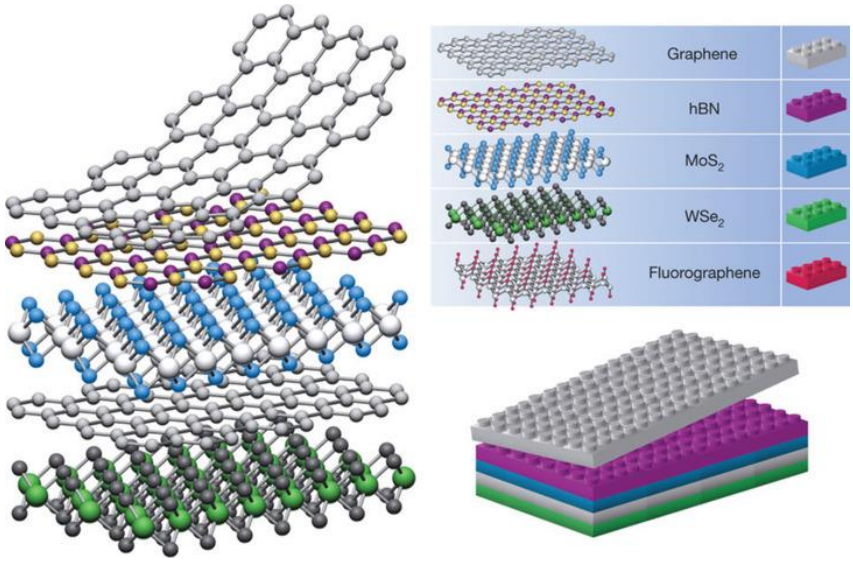

Figure 1 : Schematic diagram of a hetero-structured 2D material. Reproduced from Geim, A.K., et al., 2013. Van der Waals heterostructures. Nature 499, 419–425.[24].

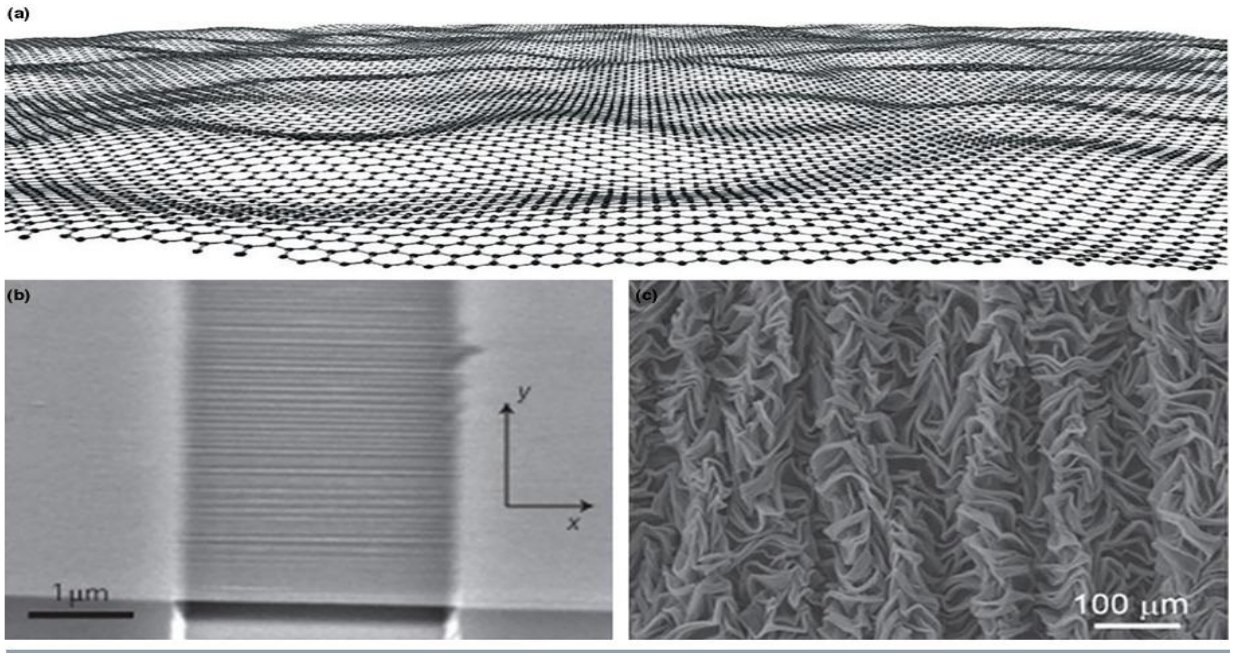

Figure 2: (a) Schematic of Rippled graphene (b) SEM images of wrinkled graphene and (c) SEM images of crumpled graphene. Nature 446 (2007) 60–63, Nat. Nano 4(2009).[25].

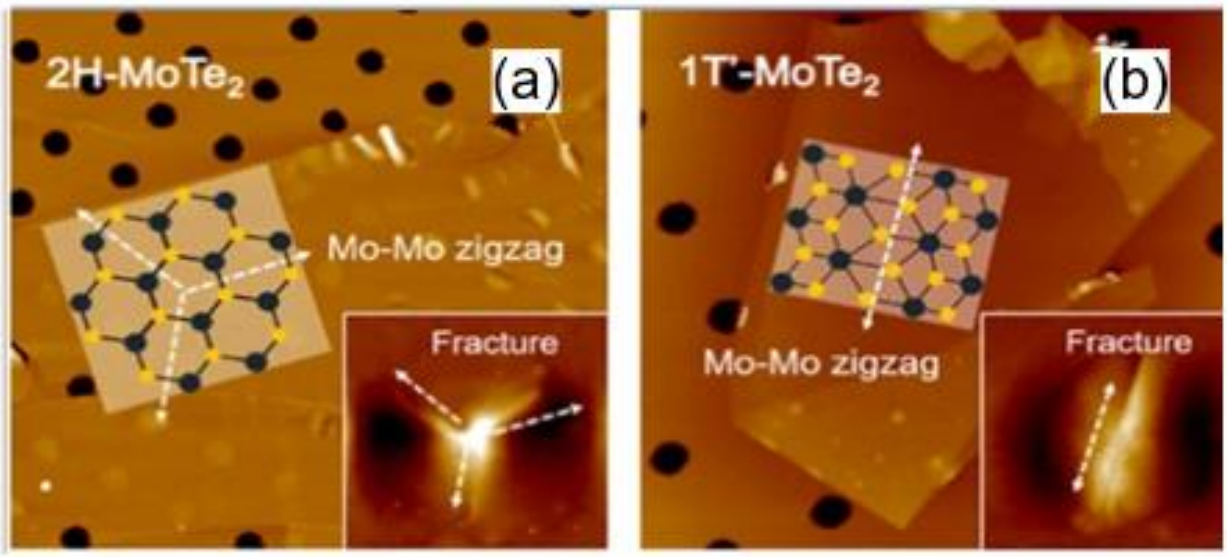

Figure 3: AFM images of the (a) 2H-$MoTe_2$ flake that covers tens of holes. Inset shows its crystal structure defined by the SHG experiment (b) 1T'-$MoTe_2$ flake that covers tens of holes. Inset shows its crystal structure defined by the SHG experiment. Nano Lett. 2019, 19, 2.[25].

2.3. GRAPHENE

Research in 2D material is ramping ever since the identification of graphene in 2004. A simple adhesive tape peels off layer after layer of graphene from graphite [26]. *Graphene* is a carbon allotrope of a single layer of sp^2 hybridized carbon in a 2D honeycomb lattice structure. In simpler terms, a single layer of isolated graphite is graphene. Every atom in graphene is bonds with the three nearest atoms by σ-bond and contributes one atom to the conduction band. The same type of bond is also available in carbon nanotubes and polycyclic aromatic hydrocarbon, partially in fullerenes and glassy carbons [27][28]. Conduction bands leads to graphene's one of the most valuable properties making it a zero-overlap semimetal [26]. Graphene conducts both electricity and heat along its plane very efficiently.

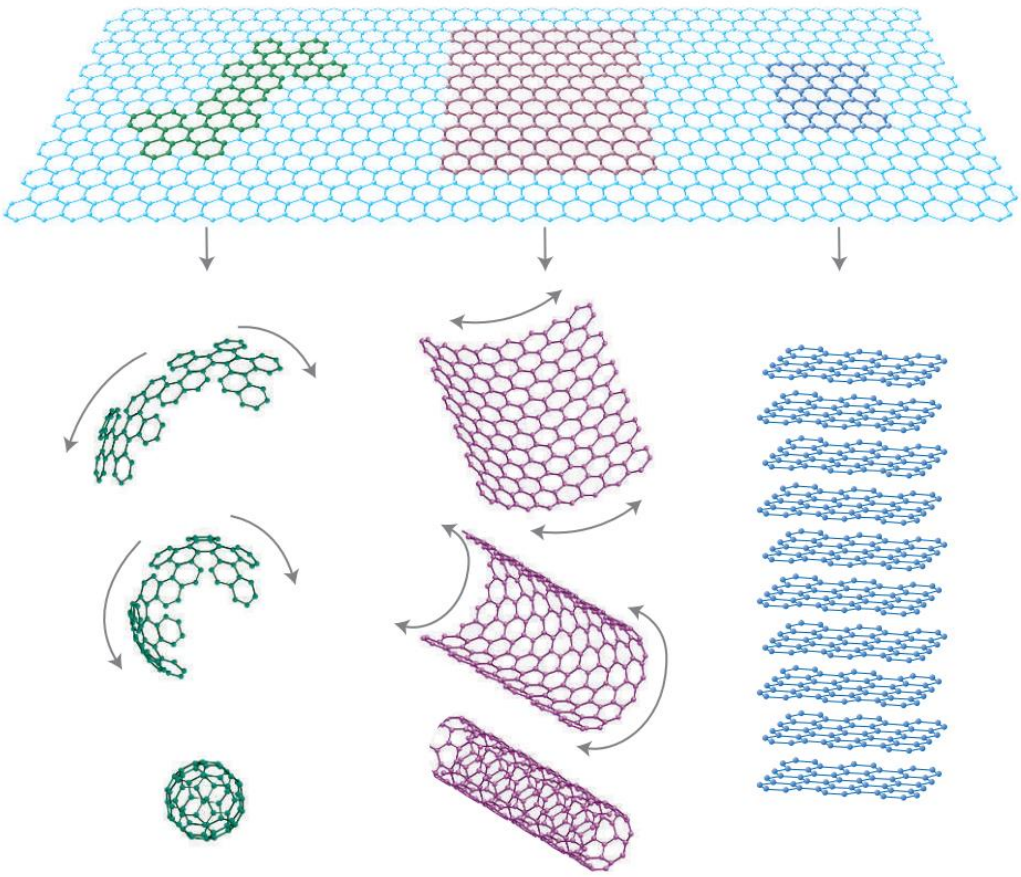

Figure 4: Mother of all graphitic forms. Graphene is a 2D building material for carbon materials of all other dimensionalities. It can be wrapped up into 0D buckyballs, rolled into 1D nanotubes or stacked into 3D graphite [26]. Nat. Mater.

Graphene is an essential and valuable nanomaterial because of its outstandingly high rigidity, electrical conductivity, straightforwardness, and being the slenderest two-layered material [29]. Interest in innovative work of graphene encompasses from semiconductors, gadgets and electric batteries to composites.

In theoretical prediction, the 2D material family expands out to more than 1,000 individuals [30]. Many of these materials undergo synthesis experimentally [31]. 2D materials are sorted into four types –

(i) Graphene family
(ii) Chalcogenides
(iii) 2D oxides
(iv) Xenes

as displayed by their nuclear designs, shown in Fig.5 .

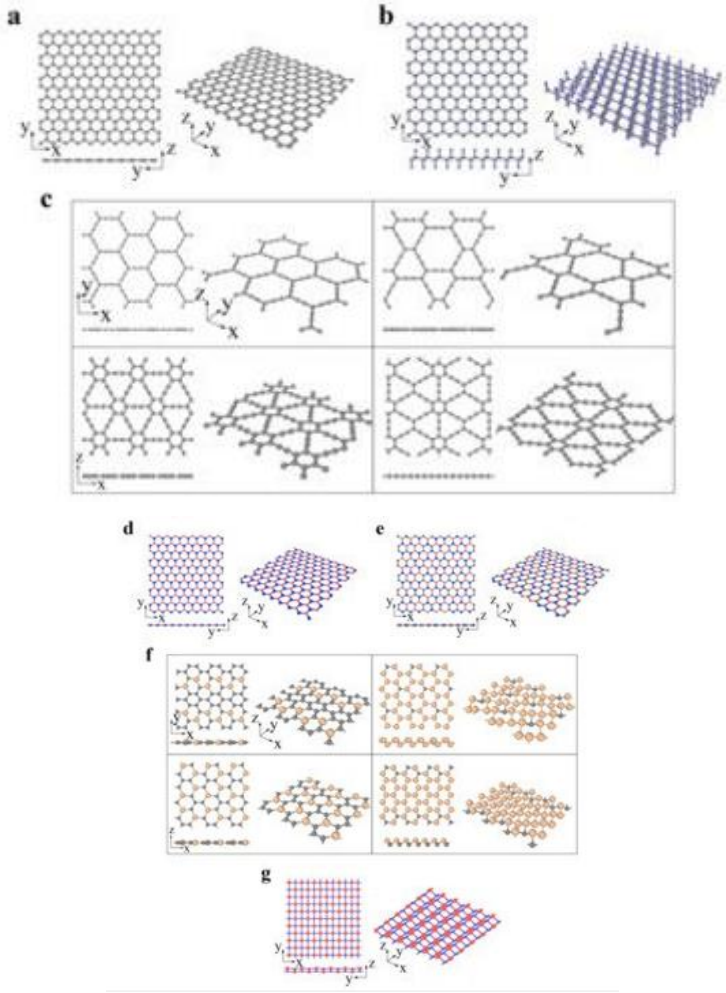

Figure 5: The graphene family: (a) graphene (gray atom represents C), (b) CX (X = H, F, Cl; gray and blue atoms represent C and X, respectively), (c) graphene (α-graphene, β-graphene, γ-graphene and 6,6,12-graphyne from left to right, top to bottom; gray atom represents C), (d) h-BN (red and blue atoms represent B and N, respectively), (e) BCN (reproduced from Ref. [32]; red, gray and blue atoms represent B, C and N, respectively), (f) SixC1−x(x = 2/10, 5/6, 2/6, 14/18 from left to right, top to bottom; gray and yellow atoms represent C and Si, respectively) (reproduced from Ref. [33]), (g) TiC (reproduced from Ref. [34]; red and blue atoms represent C and Ti, respectively) [35].

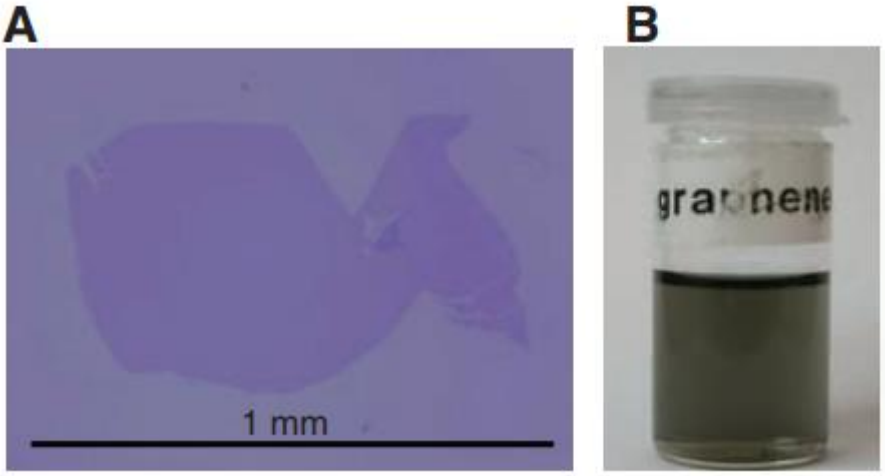

Figure 6: (a) Large graphene crystal prepared on an oxidized Si wafer by the scotch tape technique. [Courtesy of Graphene Industries Ltd.] (b) Left panel: Suspension of microcrystals obtained by ultrasound cleavage of graphite in chloroform. Right panel: Such suspensions can be printed on various substrates. The resulting films are robust and remain highly conductive even if folded. [Courtesy of R. Nair, University of Manchester] Nat. Mater. 8, 203 (2009).[36].

Fig.5(a–g), the family of graphene includes its variants made up of various hybridized carbon atoms or heterogeneous components. The saturated carbon atoms (sp^3 hybridization) bind with non-carbon elements in fluoro-graphene, chloro-graphene, and graphene oxide, generating an alternating pattern. The network of sp- and sp^2-hybridized carbon atoms that make up carbon allotropes (such as graphene) is made up of sp- and sp^2-hybridized carbon atoms. The graphene structure can be thought of as acetylene chains replacing incomplete aromatic C–C connections in graphene. α-, β-, γ- and 6,6,12-graphyne are produced by complete, 2/3, 1/3, and 5/12 substitutions, respectively (Fig.5c)[37][38]. Graphene structures have fascinating semiconducting properties that make them feasible for electronic devices. Their inherent nanopores and structures make them potential candidates for gas separation, filtration, and water desalination [39][40].

Two or more elements can replace the initial carbon atoms to generate more complex layered structures, such as h-BN (Fig.5d), boron–carbon–nitrogen (BCN) (Fig.5e) [32], and SixC1x (Fig.5f) [33], in a similar way to graphene. A 2D material having a tetragonal configuration, like the similar hexagonal structure above, is found to be extremely stable. In the side view, TiC with p(pi)–d(pi) bound (Fig.3g) is buckled into a zigzag configuration. It has anisotropic features because of its unique structure.

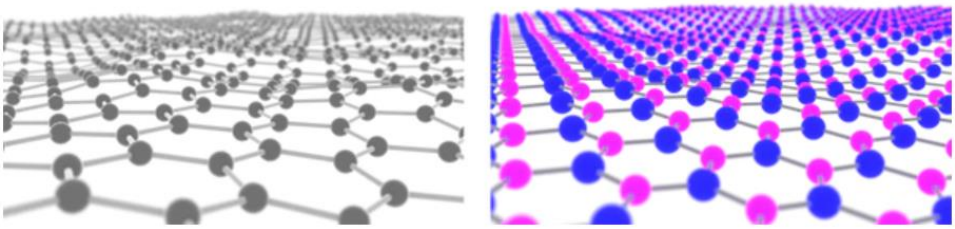

Figure 7:Hexagonal Graphene (left) and Hexagonal Boron Nitride (right)[41].

In Fig.7 Although Graphene (left) and Hexagonal Boron Nitride (right) both are 2D and both have hexagonal lattice structure, they possess very different physical properties. Hexagonal boron nitride is a wide-bandgap insulator while graphene is an excellent electrical conductor.

Graphene is optically transparent, absorbing just 2% of transmitted light and has the greatest tensile strength. Even the weight of a football might be supported by a single monolayer of graphene that is only 0.3 nm thick [42]. Hexagonal boron nitride (h-BN) is an isomorph (similar crystallographic appearance), but instead of carbon, it comprises boron and nitrogen atoms. It is a wide-bandgap insulator, unlike graphene, which is an excellent conductor [43].

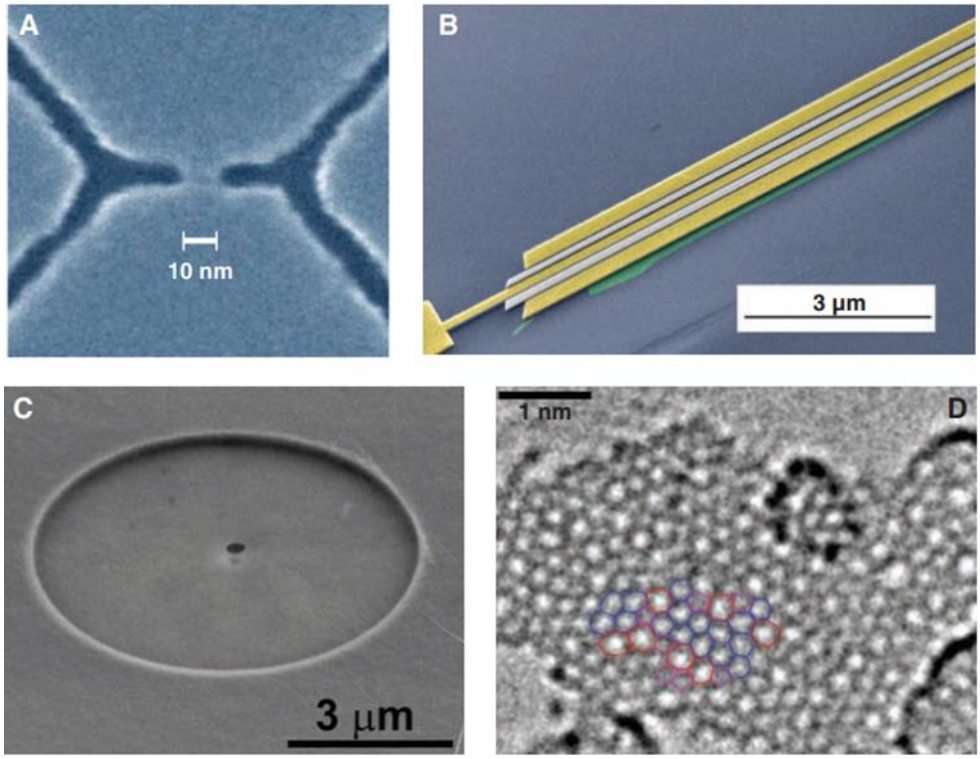

Figure 8: (a) Graphene nanoribbons of sub-10-nm scale exhibit the transistors action with large on-off ratios. (b) graphene-based HEMTs. (c) Graphene-based NEMS. (d) Ready to use: Graphene membranes provide an ideal support for TEM. Science 324, 1530 (2009).[44].

The application of graphene in different markets is depended on the production rate of such materials. Previously, the conventional techniques were used to extract small amount of graphene at time. Currently, more advanced techniques are in practice to prepare graphene in multiple shapes and sizes. There is a big challenge in the optimization of the quality of graphene and the method of production. Such processes are as follows:

(i) Liquid phase and thermal exfoliation
(ii) Chemical vapour deposition
(iii) Synthesis on SiC

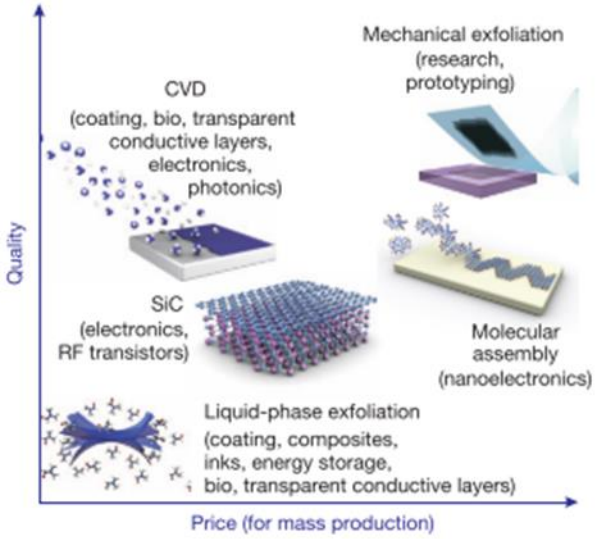

Figure 9: Several methods of mass-production of graphene. Nature 490, 7419 (2012).[45].

In Fig.9 represent a several methods of mass-production of graphene depicted, which allow a wide choice in terms of size, quality and price for any particular application[45].

2.4. TRANSITION METAL DICHALCOGENIDE

The transitional metal dichalcogenide (TMDC) MX_2 represents a class of developing 2D material known as chalcogenides. MX_2 has two layers of chalcogen atoms X sandwiched between two layers of transitional metal atoms M (Mo, W, Nb, Ta) and chalcogen atoms X (S, Se, Te). Fig.15 shows the all the elements that can react together to form a TMCS compound.

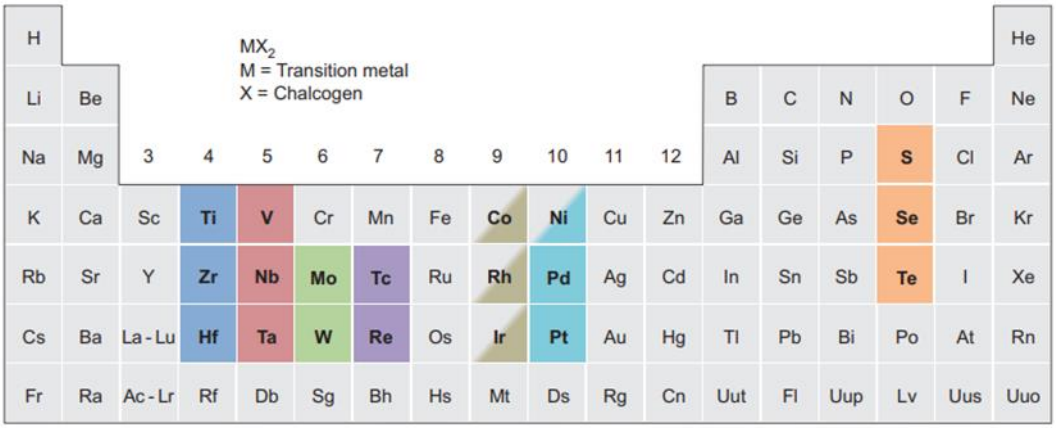

Figure 10: There are around 40 distinct stacked TMD compounds. In the periodic chart, the transition metals and three chalcogen elements that primarily crystallize in such layered structures are indicated. Nature Chemistry 5, (2013).[46].

MX_2 is commonly divided into two phases: 2H and 1T [47][48][49]. Till now, there is much research into the 2H phases. In Fig.10 the MX_2 (M = Mo, Nb, W, Ta; X = S, Se, Te) tends to be in the 2H phase in equilibrium, whereas MX_2 (M = Zr, Hf; X = S, Se) tends to be in the 1T phase [78][79]. Under certain conditions, the transition from 2H to 1T phases can occur [47][48][49].

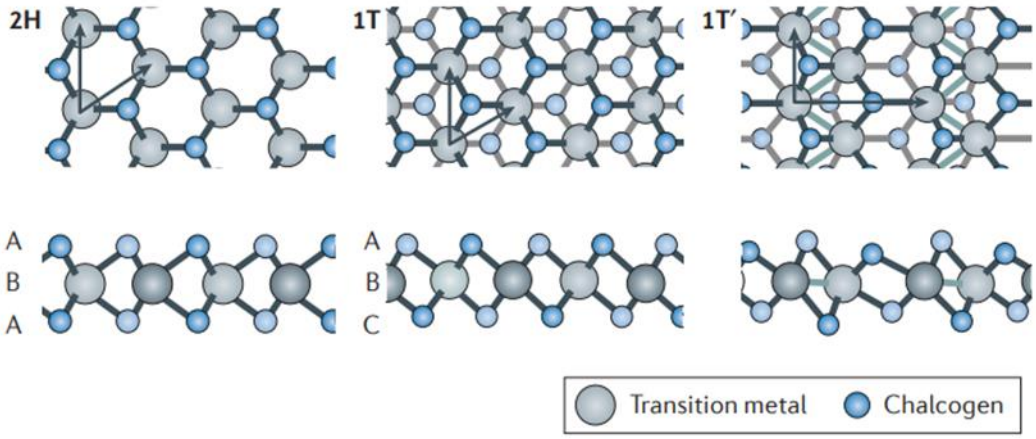

Figure 11: Structure of TMDs. Atomic structure of single layers of transition metal dichalcogenides (TMDCs) in their trigonal prismatic (2H), distorted octahedral (1T) and dimerized (1T′) phases. Lattice vectors and the stacking of atomic planes are indicated.[50]

TMDCs are two-dimensional semiconductor materials with distinct mechanical, electrical and optical characteristics. For the applications of advanced semiconductor devices, the materials can substitute for graphene (metallic substance) and hexagonal boron nitride (hBN, insulator). TMDC growth techniques is a focus in this section. TMDCs require a different approach because of the various chemicals and growth processes. TMDCs have a unique property of charge density wave phases supported by the fermi momentum theory [51]. A slight distortion causes the modulation of the electronic charge density. The phenomena of CWD depend on the crystalline phase and the chemical composition of the material. A functional relationship is derived between the temperature and pressure, which is shown in the Fig.12.

In addition, TMDC doping for customizing characteristics by adding alien materials into the structure. This affects the mobility, bandgap and contact resistance of the impure material. Furthermore, doping can alter the magnetic characteristics too [52]. Fig.13 shows how doping affects the conductivity of TMDCs.

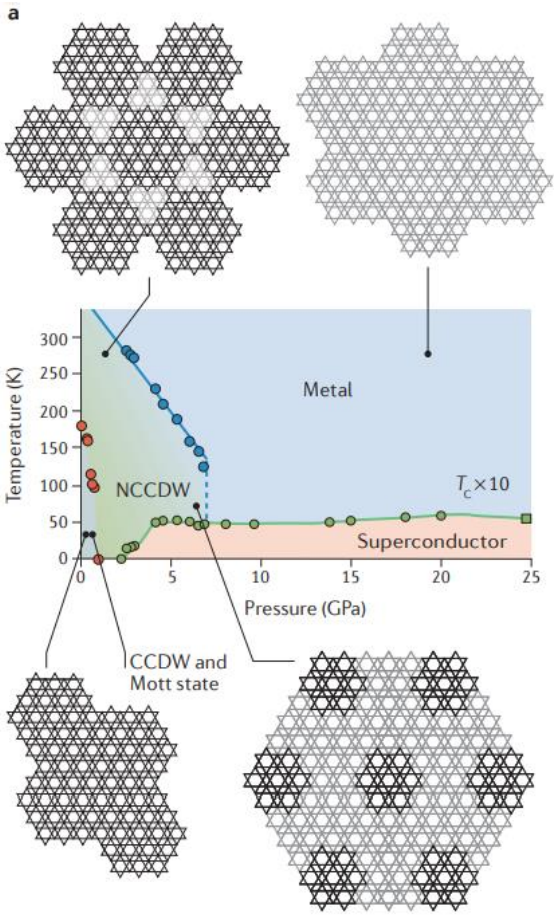

Figure 12: Temperature–pressure phase diagram of 1T TaS_2 showing various charge density wave (CDW) phases. The deformation patterns corresponding to the different phases are shown[53].

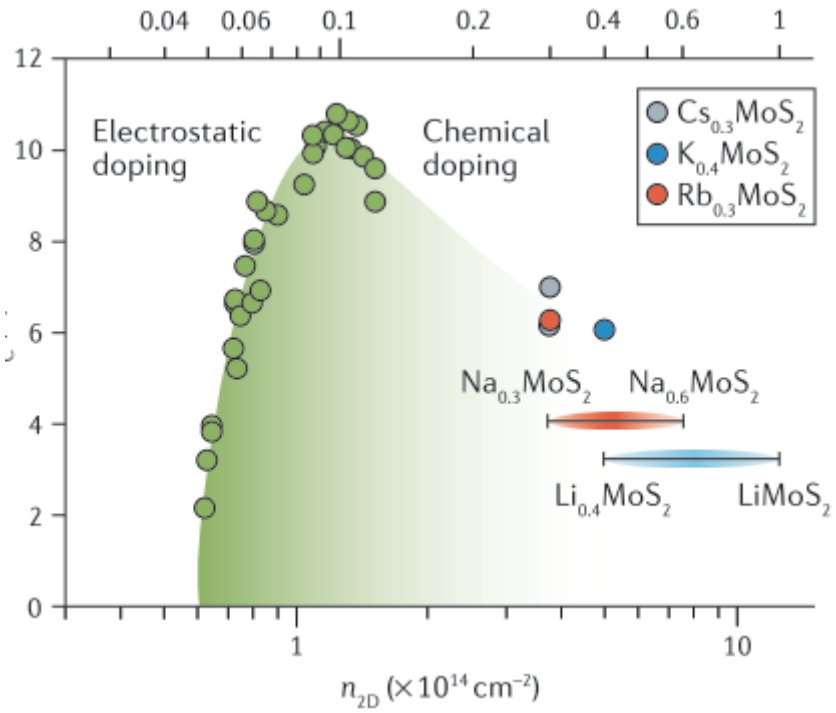

Figure 13: Phase diagram of superconductivity in electrostatically and chemically doped 2H MoS_2[53].

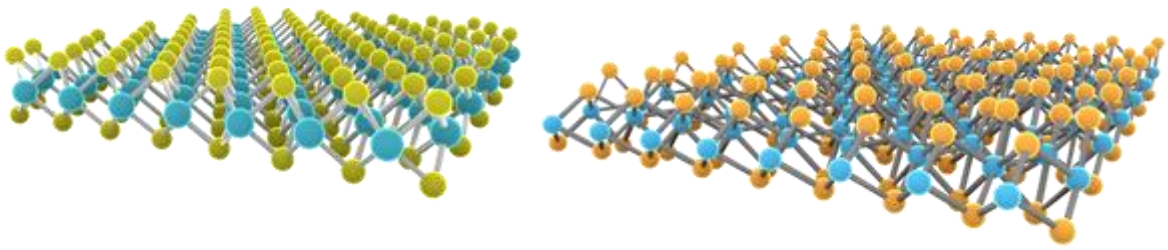

Figure 14: Molybdenum disulphide (MoS_2) in the left. Tungsten ditelluride (WTe_2) in the right. Both are transition metal dichalcogenides with a two-dimensional structure. WTe_2 tends to adopt the metallic 1T phase , whereas MoS_2 favours the semiconducting 2H[54].

The best thing about these materials is that they are not just remarkable for LIBs; they are in usage as an electrode for Na-ion batteries (NIBs), an excellent cost-effective alternative to LIBs [55]. TMDCs based on metal sulfides, such as MoS_2, react with Li atoms to create lithium sulfide, which causes phase changes in electrode systems [56]. Yang et al. [55] used first-principle simulations to study the potential of different TMDCs when used as NIB electrode material. The findings indicate low energy barriers for Na surface diffusion in TMDCs and notable phase transitions in several transition metal sulfides. MoS_2 and WSe_2 are the most commonly investigated

TMDCs for LIB electrodes. Su et al. [57] were among the first to reveal MoS_2's excellent performance capabilities as a NIB anode with ultrathin designs. Similar to graphene, utilization of defective MoS_2 form with antisites, vacancies and grain boundaries increases its specific capacity [58].

The Li adsorption increase is principally responsible for the performance enhancement of defective MoS_2. Chen et al. [59] created a tubular MoS_2 structure that connects with carbon nanotubes in 2016(CNTs). CNT is used extensively in this structure to address the issue of structural deterioration in MoS_2 as a result of conversion processes, resulting in an anode with long cycle life. TMDCs have a fundamental structural and chemical stability limitation, making them rely on other composite materials to use their electrode capabilities entirely [60].

Table 2: Summary of TMDC materials and properties.

	-S_2	-Se_2	-Te_2
	Electronic Properties		
Nb	Metal; superconducting; CDW	Metal; superconducting; CDW	Metal
Ta	Metal; superconducting; CD	Metal; superconducting; CDW	Metal
Mo	Semiconducting 1L: 1.8 eV Bulk: 1.2 eV	Semiconducting 1L: 1.5 eV Bulk: 1.1 eV	Semiconducting 1L: 1.1 eV Bulk: 1.0 eV
W	Semiconducting 1L: 2.1 eV 1L: 1.9 eV Bulk: 1.4 eV	Semiconducting 1L: 1.7 eV Bulk: 1.2 eV	Semiconducting 1L: 1.1 eV

TMDCs crystals are generally from the extraction and filtration of natural minerals. These minerals contain bulk amounts of TMDCs as large crystal structures. These natural crystals or synthetic crystals are source of thin flakes of TMDCs. Sheets of TMDCs is a output of mechanical peel-off using sticky tapes [61]. This process help researchers to understand more about the materials; however, this method is not scalable for mass production. Alternatively, liquid-phase exfoliation using an organic solvent is a well-known technique that makes the thickness of the flakes controlable [62]. These are conventional method in usage for early-stage investigation. Fig.16

portrays scalable methods to produce adequate amounts for mass usage. Fig.16 (a) shows molecular beam epitaxy (MBE) which uses ultra-thin vacuum chambers to collect the deposition on a hot substrate [63]. The highest quality TMDCs are is due to chemical vapor deposition (CVD), illustrated in 16 (b). The set-up is much simpler than MBE and the overall cost is much less in this process. The final method is similar to CVD but uses MOCVD's metal-organic gas phases [64]. Fig.16 (c) shows how this method works.

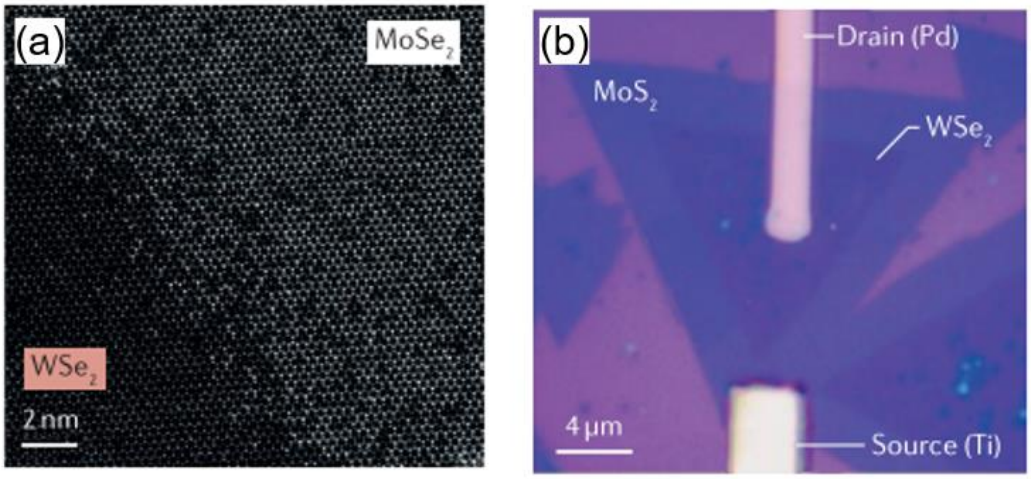

Figure 15: Examples of synthesis of 2D TMDC lateral hetero-structures. (a) High-angle annular dark-field scanning transmission electron microscopy image of the lateral hetero-structure formed between $MoSe_2$ and WSe_2. (b) Optical image of a p–n junction based on a MoS_2 /WSe_2.[65].

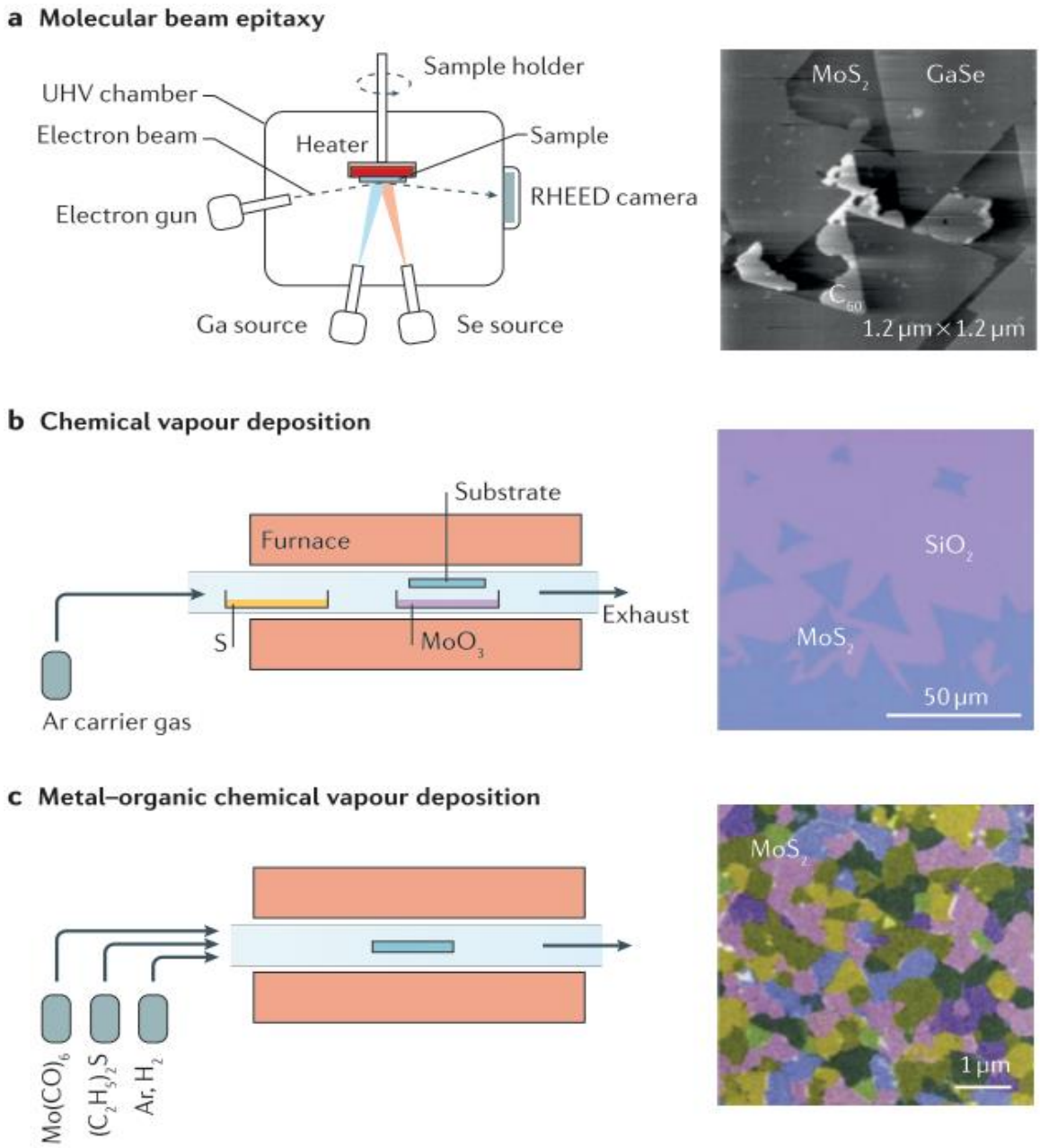

Figure 16: Growth methods for the synthesis of ultrathin TMDCs. (a) In molecular beam epitaxy. (b) Chemical vapor deposition (c) Metal–organic chemical vapour deposition. Nature Reviews Materials 2, 8 (2017).[53].

The electronic properties of these materials are essential for applications. In general, the dissimilarity of the electronic properties of TMDCs is result of variation in band structure with bulk to monolayer transitions [66]. DFT [67] calculations can be applicable to calculate the energy gap of TMDCs on the basis of well-known Hohenberg and Kohn theorems. DFT [67] furnished a legitimate foundation for the improvement of computational techniques for obtaining records approximately the energetics and structure properties of (atoms and) molecules at a much lower

cost than traditional wave function techniques[67]. It is a method of theoretical investigation of solids [68]. Using ab initio DFT simulations, this bandgap alteration is possible just by applying mechanical stresses [69]. While the electronic properties of graphene is unchanagble due to tensile stress, TMDCs are sensitive to both tensile and shear stress. In addition, much less strain is essential to vary the bandgap of TMDCs compared to graphene. Mechanical stress decreases the bandgap of semiconductor TMDCs, leading to a direct to the indirect bandgap thus causing a semiconductor to metal transition.

Table 3: Electronic character of different layered TMDCs

Group	M	X	Properties
4	Ti, Hf, Zr	S, Se, Te	Diamagnetic. Semiconducting (Eg = 0.2~2 eV).
5	V, Nb, Ta	S, Se, Te	Superconducting. Narrow band metals (ρ ~10–4 Ω.cm) or semimetals. Charge density wave (CDW). Paramagnetic, antiferromagnetic, or diamagnetic
6	Mo, W	S, Se, Te	Sulfides and selenides are semiconducting (Eg ~1 eV). Tellurides are semimetallic (ρ ~10–3Ω cm). Diamagnetic.
7	Tc, Re	S, Se, Te	Diamagnetic. Small-gap semiconductors..
10	Pd, Pt	S, Se, Te	Sulfides and selenides are semiconducting (Eg = 0.4eV) and diamagnetic. Tellurides are metallic and paramagnetic. $PdTe_2$ is superconducting.

TMDCs monolayer can absorb rays in the near-infrared and visible spectra region. Its primary determination by a direct transition between the valance and the conduction band that states around k and k' points[70]–[73]. When there is no excitonic effect in the case of 2D, it is often indicates a step function. A spectrum originating from the energy-independent joint density of states and transition matrix elements near parabolic band edges. Prediction of very large exciton binding energies is common by theoretical studies [38][42], and recent observations verify them based on optical spectroscopy [79]–[82] and scanning tunneling spectroscopy[54][55].

Apart from these, 2D TMDCs also possess higher-order excitonic quasiparticles. In the case of doping monolayer of TMDCs trions (bound state of two electrons and one hole or two holes and one electron) is possible [80], [84]. Thus promising possibilities of trions application for room-temperature electrical transport of absorbed light energy [85] and creating high-temperature and high-density quantum coherent states of excitons [86]. TMDC monolayers exhibit electronic characteristics ranging between superconducting and semiconducting depending on their chemical composition. A direct bandgap in the 1–2 eV region, group-4 TMDC monolayers (e.g., WS_2, MoS_2, $MoSe_2$, and WSe_2) display semiconductor behavior. An indirect bandgap exists in TMDC bilayers and multilayers.

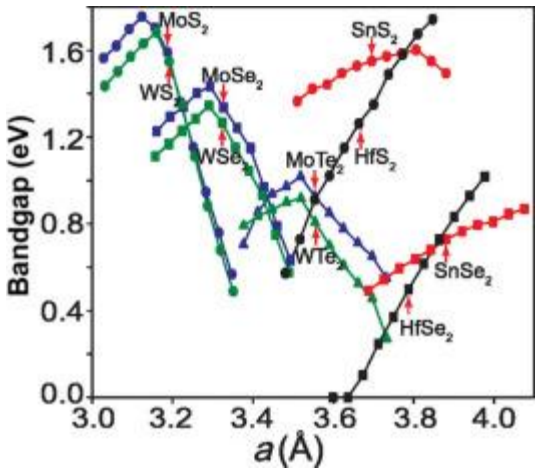

Figure 17: Theoretical bandgap for various MX_2 monolayers as a function of lattice constant changed by uniform isotropic strain ranging from 5% to 5%. Each monolayer's equilibrium lattice constant is indicated by a red arrow.

TMDC monolayers are presently being studied in photonics, spintronics and valleytronics [87][88][71]. In addition, circularly polarized light with orthogonal polarizations can treat different valleys individually [87][89]. Furthermore, because TMDC monolayers lack surface dangling bonds, they make vertical heterostructures without lattice matching. The edges of TMDC nanoribbons can have intriguing qualities like increased catalytic activity [90]. Therefore, various applications like dye-sensitized solar cells [91] or robust electrocatalysis, which might be helpful for hydrogen production[92]. Edgy topology, Quantum confinement and electrical interaction between edges for very narrow nanoribbons [40] are three main principles that explain the dynamic behaviors owing to edges.

Photonics applications: The observations of the Purcell effect, coupled exciton–polaritons, lasing in 2D TMDC optical cavities, and single-photon emitters have opened new opportunities for their photonic applications and development. Characteristics like tough light-matter interactions that initiate from the strong excitonic effects in 2D TMDCs are a crucial feature of these exciting phenomena [93].

Superconductivity: In their phase diagram, all bulk TMDCs with a charge density wave (CDW) [94] also display superconductivity. There are indeed two phenomena. Two-phase can either coexist or compete. In TMDCs, the superconducting phase can be either inherent or prompt by chemical doping, electrostatic doping or applied pressure[95].

Mobility engineering: The mean free path of charge carriers, spin or valley determines the applicability of 2D materials for applications established on quantum transport. In this the charge carrier mobility determines the suitability of application of the charge carriers as they are directly related to the mobility of the carriers. Although theoretically predicted principles for the charge-carrier mobility for 2D TMDCs [96]–[98] are very promising, in practice, the mobility is hindered by disorder and scattering sources.

2.5. MOLYBDENUM SULFIDE

Molybdenum disulfide (MoS_2) is a TMDC with honeycomb-shaped lattice[73]. Molybdenum disulfide (MoS_2) has a layered hexagonal arrangement composed of covalently bonded S and Mo atoms. A plane of Mo atoms is covalently inserted between two planes of S atoms in an intercalating trigonal-prismatic pattern. In Bulk MoS_2, S-Mo-S layers attach through Van der Waals forces resulting in a bandgap of 1.8eV [99].

Comparing with graphene, MoS_2 is more resilient to buckling due to a greater bending modulus by a factor of seven [100]. Mechanical property verification of MoS_2 via investgation using density functional theory (DFT) [101], experiments [102] and reactive potentials such as reactive empirical bond-order (REBO) [101], [103], [104] and ReaxFF [105], [106]. Literature shows that it a has high Young's modulus of about 0.2 TPa and the fracture stress beyond 10 GPa.

Molecular dynamic (Lammps) simulation reported that for a single layer MoS_2 the young's modulus equals 152.8 GPa in the armchair directions. In addition, the fracture strain and fractures tress are observed to be 0.131 and 13.89 GPa, respectively [107].

Temperature, layer number and stacking order of multiple layers have effect on the stress-strain curve and elastic properties. For example, it has been observed that Elastic constants, fracture strain and fracture stress of single layer structures decrease with the temperature rise. However, the increased layer number has minimal effect on the stiffness of the multilayer[107].

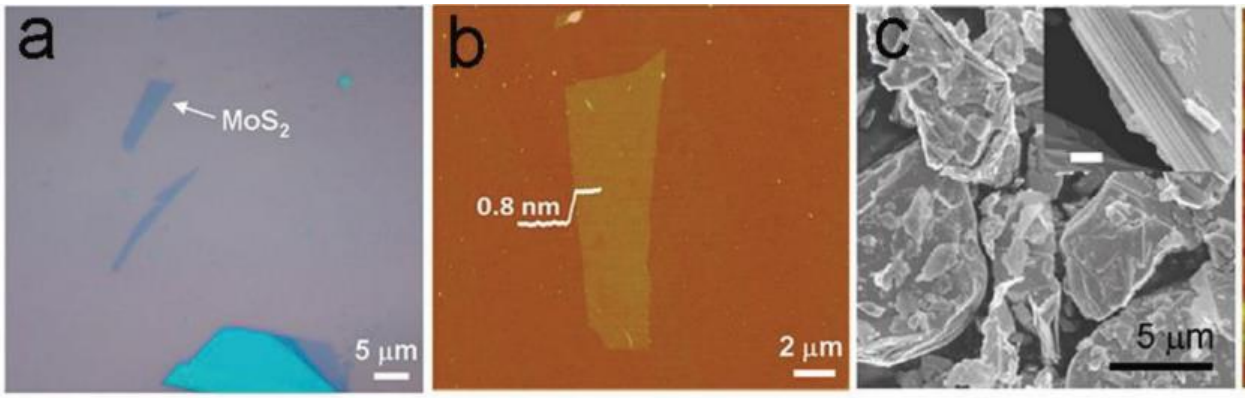

Figure 18: (a) Optical microscopy image of monolayer MoS_2. (b) AFM image of monolayer MoS_2(c) SEM image of MoS_2 powder. Small Methods 11, 2 (2018).[108].

From classical molecular dynamics simulations (Lammps) on the tensile response of the 2H- MoS_2 monolayer in an armchair (X-direction) and zigzag (Y-direction) directions. At a temperature of 300 K using the ReaxFF force field. In case of the armchair configuration, the fracture starts at a tensile stress of 25.5% and the specimens fail at 27%. For a zigzag configuration, the corresponding values are 24.6% and 28.9%, respectively [129].

Classical molecular dynamics simulations (Lammps) were used to observe the single-layer fracture mechanics of MoS_2. It turns out that for a flawless single-layer MoS_2 (crack-free and non-porous), the fracture classification is a brittle fracture[109]. Bonds in the armchair direction have greater resistance to crack transmission than in the zigzag direction.[109].

Temperature affects the mechanical properties of samples with cracks and pores. As an effect of increasing temperature, both failure stress and strain are weakened.

MD (Lammps) simulations of the failure mechanism of armchair and zigzag cracks in MoS_2 monolayer sheets under mixed fracture modes. Modes I and II anticipate that both chair and zigzag cracks preferentially and disseminate along a zigzag surface, similar to graphene [15].

Strain rate, size, and chirality also affect the young's modulus and thermal conductivity of a single layer of MoS_2. From classical molecular dynamics simulations (Lammps), the elastic modulus is affected by both the chirality and the width of a single MoS_2 layer [110].

The modulus of elasticity decrease with decreasing width for both the zigzag and armchair single layer MoS_2. Although this differs from the size-dependent trend observation[111], it is similar to the results found in graphene nanoribbons[112]. In addition, the relative thermal conductivity of the single-layer armchair MoS_2 at 300K decreases with increasing strain rate[110].

The defect and grain boundary influence the mechanical properties of mono- or polycrystalline MoS_2. Classical molecular dynamics (MD) simulation (LAMMPS) shows a lower tensile strength of polycrystalline MoS_2, suggesting that GBs, vacancy as well as oxygen doping significantly degrade the mechanical properties of MoS_2 [113].

2.6. MOLYBDENUM DITELLURIDE

Molybdenum (IV) telluride, also known as molybdenum ditelluride or simply molybdenum telluride. Molybdenum and tellurium compound with the formula $MoTe_2$, equals 27.32 percent molybdenum and 72.68 percent tellurium by mass. It can form two-dimensional sheets that can be broken down into transparent and flexible monolayers. It is a semiconductor with the ability to glow. It belongs to the transition metal dichalcogenides family of materials [114].

$MoTe_2$ is black when in its powdered form [115]. Sticky tape peels off very thin $MoTe_2$ crystals. Red light may pass through them when they are thin, roughly 500 nm thick. Even the thinnest layers have the potential to be orange or translucent. Wavelengths longer than 6720 transmits and shorter wavelengths severely experience resistance. An absorption edge appears in the spectrum. At 77 K, this edge becomes 6465. This is a deep red color [116].

$MoTe_2$ is found in three crystalline forms with layered structures that are quite similar: hexagonal (2H-$MoTe_2$), monoclinic (1T-$MoTe_2$), and orthorhombic' (1T'-$MoTe_2$). It crystallizes in the hexagonal system at ambient temperature, analogous to molybdenum disulfide [117]. Flat crystals are platy crystals [118]. $MoTe_2$ has a specific gravity of 7.78 gcm^3 with unit cell sizes of a=3.519 c=13.964 [117]. In a trigonal prism, each molybdenum atom is surrounded by six tellurium atoms, with a spacing of 2.73 between the Mo and Te atoms. [117] Molybdenum sublayers are sandwiched between two sublayers of tellurium atoms, and the three-layer structure is then stacked [119]. Each layer has a thickness of 6.97 mm [116]. Two tellurium atoms in the same sublayer subtend an angle of 80.7° within this layer. At the molybdenum atom, the tellurium atoms on one sublayer lie exactly

above those on the lower sublayer, forming an angle of 83.1°. 136.0° is the other Te-Mo-Te angle across sublayers. Within a sublayer, the spacing between molybdenum atoms is 3.518. The spacing between tellurium atoms in a sublayer is the same as this. 3.60 is the distance between a tellurium atom in one sublayer and the atom in the other [120]. Only the van der Waals force holds the layers together [121]. The tellurium atoms are 3.95 atoms apart throughout the strata [120]. The centre of a triangle of tellurium atoms on the top of the layer below is align with the tellurium atom at the bottom of one layer. As a result, the layers are in two distinct places [120]. The crystal is readily split on the plane between the three-layer sheets [119].The sizes alter with temperature, with a=3.492 at 100 K and 3.53 at 400 K. Thermal expansion causes “c” to vary from 13.67 to 14.32 in the same range [119]. 2H-$MoTe_2$ is another name for the hexagonal form, where "H" refers to hexagonal and "2" indicates that the layers are in two separate places. $MoTe_2$ crystallizes in the monoclinic 1T form (β–$MoTe_2$) at temperatures over 900 °C, with space group P21/m and unit cell sizes of “a=6.33”, “b=3.469”, and “c=13.86:”, with an angle of 93°55′. Rod-shaped crystals are in the high-temperature form. This polymorph's density is 7.5 gcm^3, whereas it normally 7.67 gcm^3. Around the molybdenum atoms, tellurium atoms create a distorted octahedron [118]. Rapid cooling can bring this high-temperature form, known as β–$MoTe_2$, down to room temperature [122]. $MoTe_2$ may live below 500 °C in this metastable form [123]. The crystal shape of metastable β–$MoTe_2$ transforms to orthorhombic when it is cooled below 20 °C. The monoclinic angle c moves to 90°. This shape is known β' or, more misleadingly, T_d [124].

The temperature necessary to transition from α- to β-$MoTe_2$ is 820 °C, however, if Te is lowered by 5%, the required transition temperature rises to 880 °C [123]. According to K. Ueno and K. Fukushima, when the form heats in a low or high vacuum, it oxidizes to create MoO_2 and no reversible phase changes occur [125].

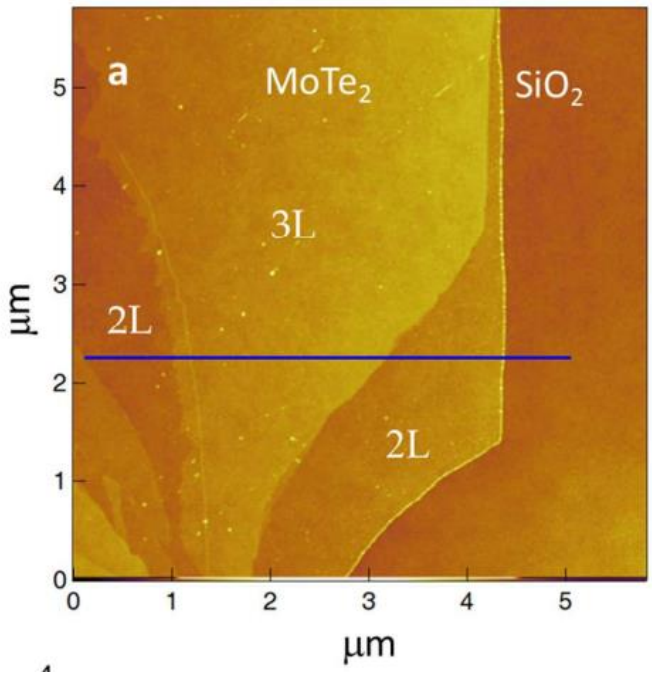

Figure 19: Optical image of a $MoTe_2$ single crystalline flake, after mechanical exfoliation, used for Raman spectroscopy in conjunction with atomic force microscopy. ACS Nano 40 (2020).[126]

In nanoindentation, biaxial deformation of suspended membranes is commonly utilize to study the elastic characteristics of structurally isotropic two-dimensional (2D) materials. However, in the case of biaxial deformation, the elastic characteristics and the fracture mechanics of anisotropic 2D materials remain entirely unknown. $MoTe_2$ exhibits polymorphic behavior having isotropic (2H) and anisotropic (1T′ and Td) phases, making it an ideal single-stoichiometric material system for studying these essential concerns. Using a combination of temperature-variant nanoindentation and first-principles computations, we present the elastic properties and fracture behaviors of biaxially deformed, polymorphic $MoTe_2$ [127].

A tensile strain of 0.2 percent brings the 2H-1T′ phase transition temperature of $MoTe_2$ down to ambient temperature. A substantial temperature-stress coefficient, which derives from a huge volume change and negligible latent heat, enables first-order SM transition, enhancing conductance by 10,000 times [128].

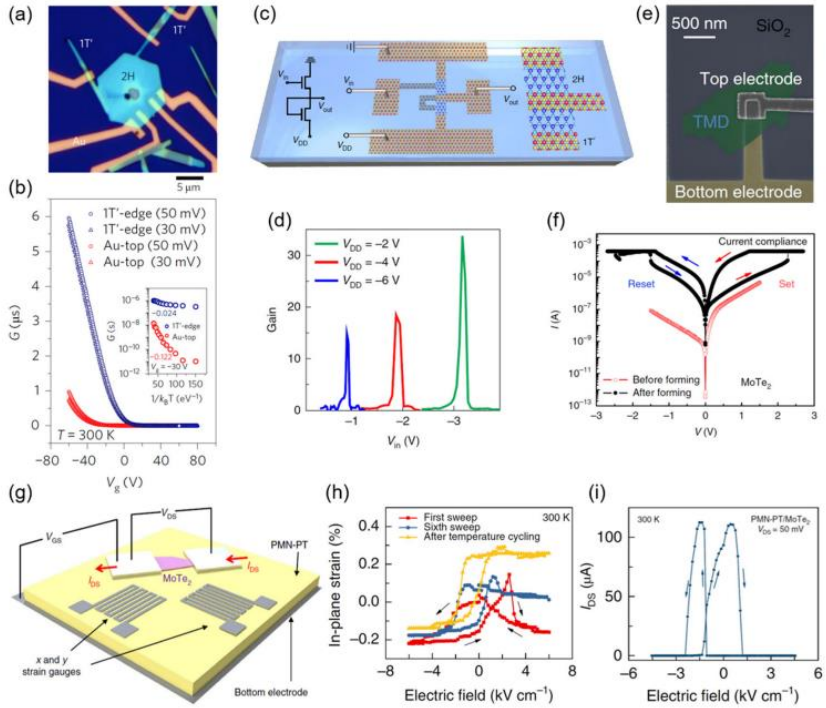

Figure 20: Applications of $MoTe_2$ hetero-phase homojunctions in electronic devices. (a) Optical microscope image and (b) transfer characteristics of a coplanar contacted 1T0–2H-$MoTe_2$ transistor (c) schematic diagram and (d) signal gains of a hetero-phase $MoTe_2$ inverter, Reprinted with permission from 2019 Springer Nature; (e) SEM images and (f) I–V characteristics of a vertical $MoTe_2$ RRAM device, Reprinted with permission from 2018 Springer Nature; (g) schematic diagram, (h) measured strain curves, and (i) strain-induced operation of a ferroelectric strain $MoTe_2$ FET, Reprinted with permission from 2019 Springer[4].

The effective moduli of the three phases differ by less than 15% due to comparable atomic bonding. As a result of their unequal distribution of bonding strengths, the breaking strengths of distorted 1T′ and T_d phases are only half that of the 2H phase. Both isotropic 2H and anisotropic 1T′ phase fractures satisfy the theorem of minimum energy, creating triangular and linear fracture patterns along the orientations parallel to Mo–Mo zigzag chains, respectively. Our findings give a reference database for the elastic behaviors of many $MoTe_2$ phases, but they also provide a universal technique for mechanical exploration of any isotropic and anisotropic 2D material [128].

Various applications based on polymorphic $MoTe_2$ transistors are almost reaching exhaustion, such as $MoTe_2$ radiofrequency (RF) transistors with excellent air stability and a remarkable cutoff frequency (320 MHz with a 5 m gate length), an ultrashort-gate-length 1T0–2H-$MoTe_2$ FET based

on a CNT gate with a trivial subthreshold swing (73 mV dec1) and a high on/off current ratio (~10^5) [129].

Arrays of hetero-phase $MoTe_2$ logic inverter creation by tellurizing patterned distinct precursors, which displays outstanding logic-level conservation, good air stability, and eligibility for IC consisting of numerous cascaded inverters (Fig.20c,d) [129]. Hou et al. found a reversible phase transition between few-layer 1T0 and 2H-$MoTe_2$ in a FET configuration under the electric-field-induced strain created by a ferroelectric substrate [130]. This innovative transistor switching approach avoid the concerns of static and dynamic power intake in conventional FETs. Moreover, they obtain substantial nonvolatile alterations in channel conductivity between two states at ambient temperature. (Fig.20 g–i) showing that the sub-nanosecond low-power nonvolatile strain switching technique has a lot of promise in applications like logic and memory

In this chapter, the literature background has been explored and the overview of the 2D represented thoroughly with concentration on graphene, molybdenum sulfide (MoS_2) and molybdenum ditelluride ($MoTe_2$).

Chapter 3
MOLECULAR DYNAMICS SIMULATION

3.1. INTRODUCTION

Previously, all types of research using theoretical or experimental framework to perform investigation upon different materials. Theoretical solutions involve multiple mathematical equations that leads to solutions. These results help to justify and understand their behavior. Alternatively, experimental research extract results from a system using the measurement of specific parameters by varying independent parameters.

The results produce a functional relationship. However, it is very laborious to solve problems using the following methods. In some cases, the experimentation is highly costly and nearly impossible due to the lack of adequate resources. In order to come up with faster results, the introduction of high-speed computers enable researchers to mimic different systems. Simulation systems are models in a computer using theoretical and experimental knowledge to perform computer simulations. The results from the computer may have a lower accuracy but give an idea of the pattern of data or results.

At the nano-scale, molecular dynamics simulations are applicable [131] —this is a computer simulation tool that can investigate atomic movements and physical properties. The calculation is done using classical mechanics. Therefore, takes into consideration newton's laws of motion.

The three basic requirement for the simulation to run [131]:

i) Interatomic Potential: information on atomic interaction .
ii) Integration of equations of motion.
iii) Initial Conditions: velocities and positions.

The accuracy of results depends on the potential file. This file contains the potential energy as a function of the position of the atoms away from other atoms. Concept development from experimentation updates the relationship curves for more accurate simulation results.

LAMMPS (Large-scale Atomic/Molecular Massively Parallel Simulator) is a simulator that runs using Molecular dynamics simulation code. It can model nano-scale to macroscopic systems as the MD simulation position to the other tools dipicted in Fig.21 using various atomic potentials and

boundary conditions. Recently, a considerable amount of research is under pogress on the field of 2D materials. In collaboration with Lawrence Livermore National Laborator and three other companies, Sadia National laboratories develop the LAMMPS open-source[132]. The first version development started using Fortran and later shifted C++. LAMMPS can be built on a CPU or Desktop and run on parallel computing facilities. In addition, it is applicable to run LAMMPS on facilities with a message-passing library (MPI) feature. In LAMMPS, parallelism is applicable to scale up computing capabilities using parallelism. Therefore, along with appointing CPUs, Graphical processing units (GPUs) can be coupled to speed up the simulation. Furthermore, the open-source feature allows further modification and extension of capabilities as per the user's requirement[6], [11], [133].

This chapter will further discuss about different simulations on 2D materials using LAMMPS. Initially, different mechanical deformation due to loading. Then, the research objectives of using LAMMPS to investigate the fracture mechanics of materials. An overview of the current status quo of nanotechnology's experimental and computational progress. Then, a brief description of the methodology of how the LAMMPS simulation works. Lastly, a summary of the application of the developer package.

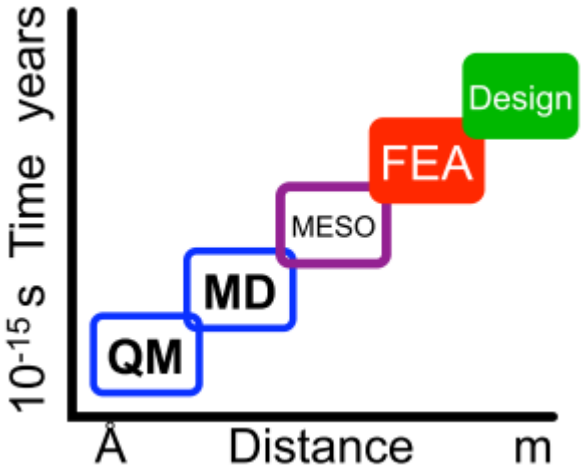

Figure 21: Time vs size relationship for simulation model[134].

3.2. MECHANICAL DEFORMATIONS

Materials inside any electronic device are always undergoing adverse conditions. Certain parameters affect the extrinsic properties of the materials. Therefore, engineers need to understand their behavior when such material interact with different environments. The behavior helps optimize the usage by developing functional relationships that govern their properties. Development of predictive models can identify materials' yield points or failure criteria. Generally, 2D materials are exposed to two different types of loading conditions that are as follows:

i) Static Loading [135] : Load on the material is fixed or stationary.

ii) Dynamic loading [136] : Load on the material varies with time.

The main difference between them is the time of application of the load. Faster loading is considered dynamic and vice-versa; slow loading is known as static loading. In the first case, the loading remains constant and is applied in a specific orientation without any movement. In the case of dynamic loading, there are further sub-categories such as harmonic, periodic, and non-periodic. The behavior of mater varies also varies depending on conditions. Researchers observe different phenomena to characterize them using phenomena to explain them better.

The deformation which are notable in literature are wrinkle/crumple [12], buckle [13], tear [14] and fracture [137]. Fig.3.2 shows samples of deformations.

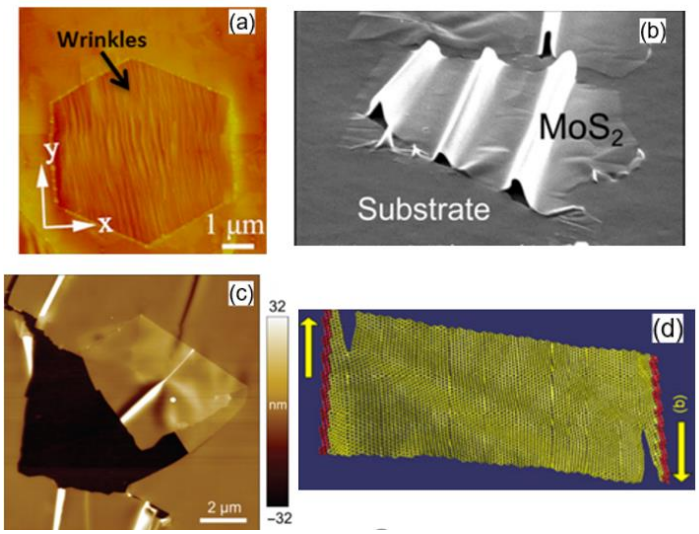

Figure 22: (a) An AFM image of a hexagonal graphene flake with wrinkle formation.(b) Buckling formation on MoS2 (c) AFM topographic image of an internal tear in graphene (d) Failure modes observed in molecular dynamics simulations.

3.3. RESEARCH OBJECTIVES

Literature talks about the intense investigation done on how such loading conditions affect the structure of 2D materials. Graphene, along with other two-dimensional materials, has a variety of applications in micro-electromechanical systems (MEMS) and nanoelectromechanical systems [73][72]. Investigation of mechanical and fracture properties of 2D materials is essential to predict their behavior when incorporated into nano-scale devices. Superlatively, it is a recommendation to characterize the material properties via uniaxial tensile stress. However, on a nano-scale, such experiments are pretty complex. Alternatively, the most widely common process for 2D materials is atomic force microscopy [138] and nano-indentation [139].

The research objective is to learn the usage of MD simulation on different 2D materials. Learning how to gain an in-depth understanding of the simulator works and its functionality. Understanding the fundamental knowledge in deriving a stress-strain relationship of materials. Our work also covers the different parameters that affect the fracture mechanics of the material—finally, the application of LAMMPS in 2D materials to observe the fracture behavior in uniaxial stress. Visual results can also explain the mechanics of fracture due to tensile stress. Alteration of several parameters like temperature and strain rate produces a behavior change [140] Similarly, the material alters by applying vacancy [141] or doping the materials with foreign atoms [142].

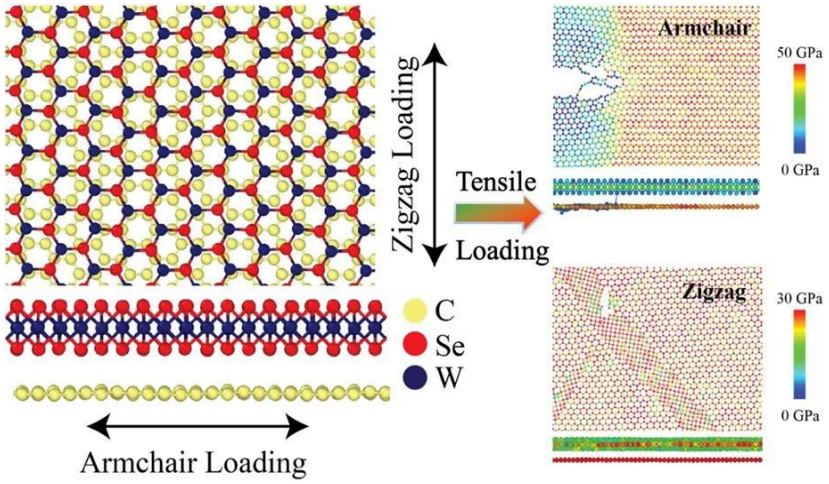

Figure 23: The fracture of graphene under tensile load. a) armchair b) zigzag Computational Materials Science 188 (2021)[143].

3.4. STATE-OF-THE-ART

The current simulation research focus on the stress-strain analysis of materials using MD and DFT simulations. The objective is to predict fracture mechanics of graphene and other novel 2D materials. Fig.24 shows snapshots of the fracture pattern of materials in both armchair and zigzag configurations. The images provides insight on mechaics of fracture within the material. There are relatively similar works less to this. For example, M. A. N. Dewapriya et al. [144] investigate the effect of temperature on the fracture of graphene. M.C. Wang et al. [145] shows the effect of defects on graphene's fracture mechanics. X Wang et al. [15] use MD simulation to fracture and crack propagation in a single monolayer of MoS_2.

Similarly, M.S.R. Elapolu et al. [146] perform a similar investigation on multi-layers of MoS_2. Furthermore, Luiz et al. [147] investigate the fracture pattern and elastic properties for TMDC with MoX_2 (X = S, Se, Te) configuration. Finally, Shoaib et al. [148] simulate the results for the mechanical properties of $MoTe_2$ films.

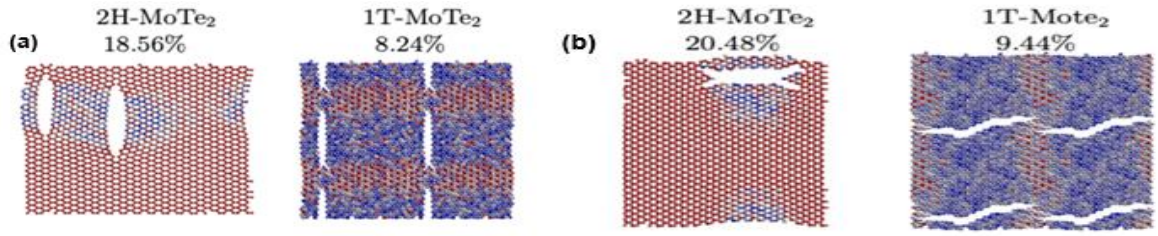

Figure 24: Representative MD snapshots of the fracture dynamics for the (a) 2H-$MoTe_2$ & 1T-$MoTe_2$ armchair (b) 2H-$MoTe_2$ & 1T-$MoTe_2$ zigzag monolayers at 300K. Condens. Matter 2020, 5, 73.[149].

3.5. METHODOLOGY

The simulator requires three different elements to initiate the simulation process which are as follows:

i) *Atomic structure file:* File that contains the all the information regarding the material. These includes atom type, coordinates, shape and size.

ii) *Interatomic potential:* Describes the interaction between the pairs of atoms or groups of atoms.

iii) *Input Script:* File that contains the input script that contains all the constraints, ensembles and boundary conditions for the simulation to run.

Atomic structure file: There are three ways to produce the atomic structure file. Create this file directly by adding an extra line in the instructions. This process requires the size and mass of the material as the input. Create using an atom.sk [8]. Atom.sk is an open-source tool that generates the data file for materials *ab into* calculations. A simple command line, e.g., shown in Fig 25 , generates the material. The third method of producing volumetric data files uses VESTA [9]. VESTA is unique compared to the other two methods since it aids in visualizing and creating the structure simultaneously. VESTA uses ball-stick, wireframe, space-filling, and dot surfaces to represent the material model. Additionally, it uses different color codes to distinguish the different types of atoms. Fig 27 shows some examples of a lattice made using VESTA.

```
atomsk unitcell.xsf -duplicate 2 2 6 \
  final_cell.cfg
```

Figure 25: Example Command line for atom.sk

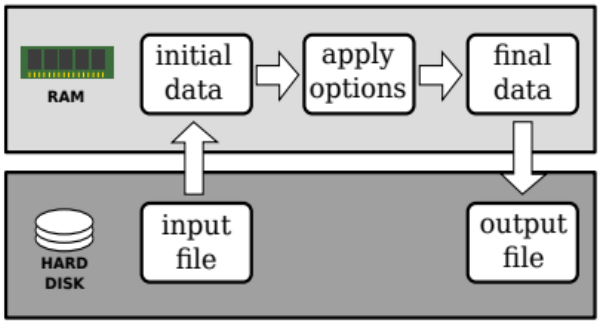

Figure 26: Workflow of the default operating mode of atoms.

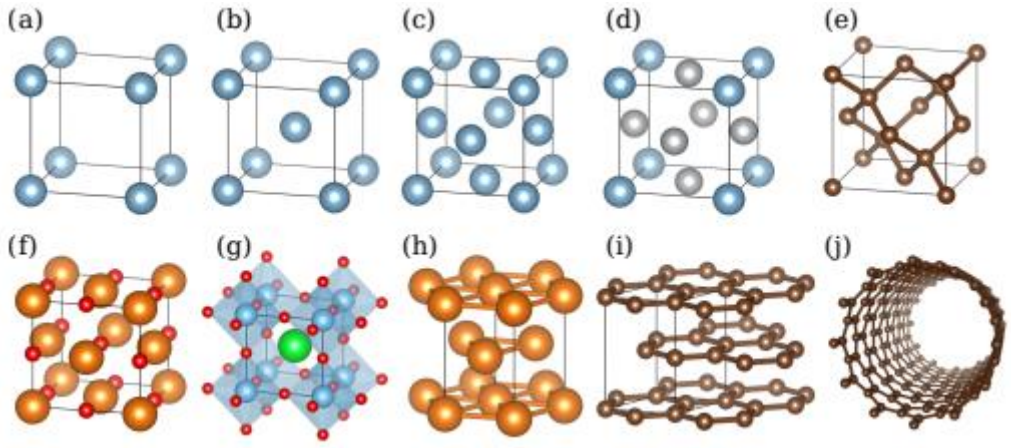

Figure 27:Some examples of lattices that can be generated with Atomsk, as visualized with VESTA. . The unit cells appear as thick black lines. (a) Simple cubic. (b) Body-centered cubic. (c) Face-centered cubic lattice. (d) The $L1_2$ structure of Ni_3Al. (e) The carbon diamond lattice. (f) The rocksalt lattice of NaCl, MgO, or LiF. (g) The cubic perovskite lattice of $SrTiO_3$. TiO_6 octahedra are shown in transparent blue. (h) The hexagonal close-packed lattice. (i) The carbon graphite lattice. (j) A (10,0) carbon nanotube.

Interatomic Potential: The potential file contains the force field that contains the potential energy as function positions or distances. Fig.28 shows an example of the relationship between interatomic energy and distance. These potential files are obtained using phenomenological methods to select parameterized mathematical formulas. The outcome depends on the interaction of neighboring atoms. A simulation may use a combination of two or more interatomic potentials in the case of simulation for TMDC (MX_2) simulation. For example, one potential models the covalent bonds of X-M-X, and the other potential model is for the van der Waals bond between X-M-X layers. In our work, we use Stillinger–Weber (SW) potential, which describes the interaction of atoms inside a TMDC and the coupling between them. The computationally intensive and complex development of potential files enables the simulator to give more accurate results.

Moreover, generic physics equations are undergone modification using experimental data. Notable potential files which are currently in usage are AIREBO[150], REBO [151] and Tersoff , which include bond orders. These are known as pairwise potentials. The potential files applicable in the case of charge variables are ReaxFF [152] and COMB [153]. Fig.29 illustrates the computational cost of developing potential files over time. The upward trend depicts that researchers have opted for faster computing instead of older, cheaper models.

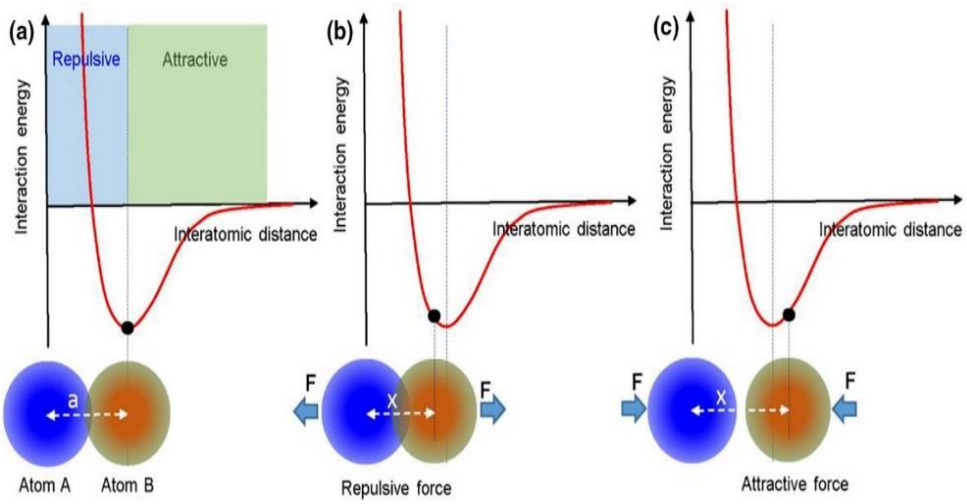

Figure 28: Example of interatomic potential curve.

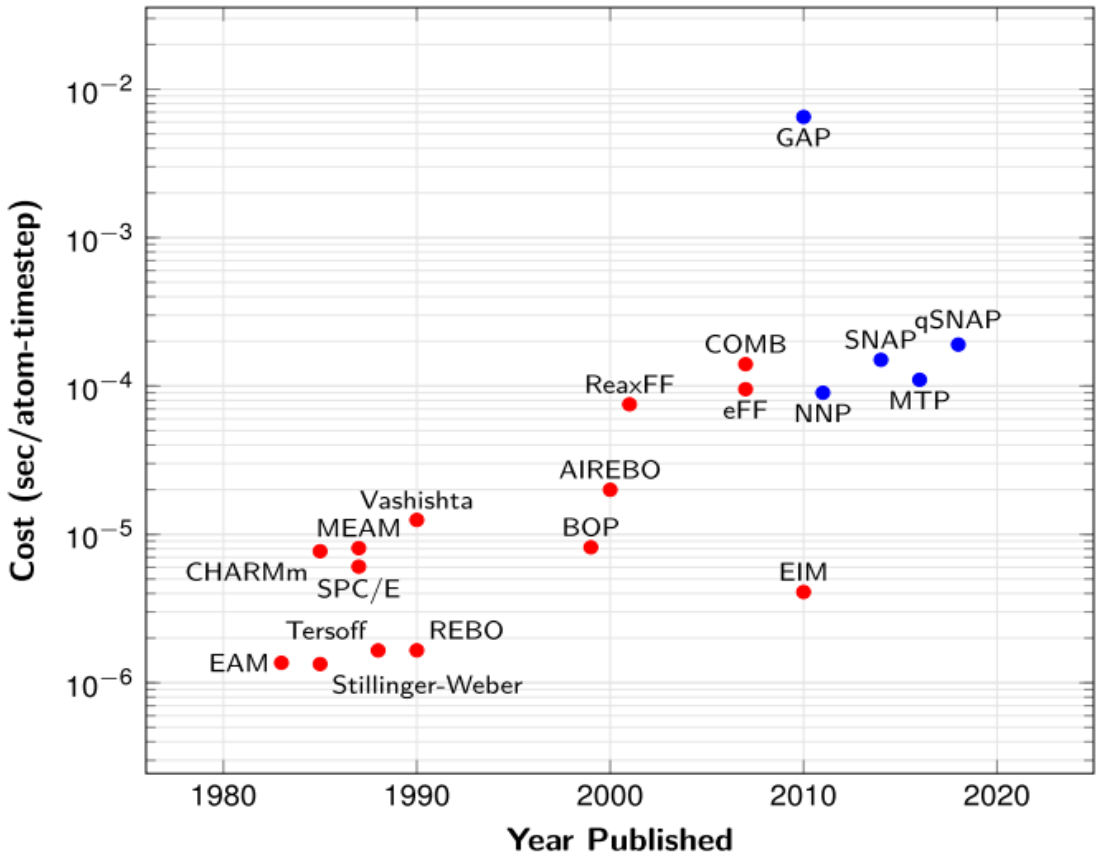

Figure 29: Comparison of the computational cost on a per-atom, per-timestep basis of various manybody potentials (red) and several machine learning interatomic potentials (blue), as implemented in LAMMPS. Computer Physics Communications 271 (2022)[154].

Input Script: The LAMMPS input scripts are designed to provide a dynamic amount of flexibility to users to implement different forms of material modeling. The feature allows a user to customize a model by changing a few lines in the input script or adding novel interatomic potential files, diagnostics, and constraints. The three key features of flexibility:

i) Flexibility via input script options: Customization without programming
ii) Flexibility via source-code styles: Writing codes to extend capabilities.
iii) Flexibility via use of LAMMPS as a library

The performance accelerates using advanced hardware such as multi-thread CPUs and GPUs. Application of Algorithms such as the rendezvous algorithm [155] to create an intermediate decomposition of data, allowing entry and exit processors to identify all the intermediate data. This aid in distributing the workload in an extensive computing system. LAMMPS enables the MPI parallelism protocol. Therefore, the simulation can run across parallel CPUs connected by a network.

In molecular dynamics (MD) simulations, different conditions can be under itertative simulation process. First, a different set of governing equations is put into use by choosing the right ensemble format. These parameters are the number of atoms, volume, temperature, and enthalpy/energy. For instance, in the case of the NPT ensemble, all the other parameters remain constant except for volume. Other ensembles are NVE, NVT, and NPH. Then comes the boundary conditions, which are typically periodic and non-periodic. The periodic boundary condition, for instance, encloses the material in a single box that can replicate to an infinite number of translations in all directions. Additional information includes thermosetting settings, pressure control, harmonic constraints, bond angle constraints, etc.

MD program runs using time integration algorithms; this integrates the equations related to the motion of intermingling atoms and produces their trajectory. Some familiar integrators available are a velocity-verlet integrator, rigid body integration, etc.

The simulation starts after introducing randomization to distort the symmetry in the material. Since atoms are symmetrically equivalent the equations cannot perform any calculation. There is no net force on the atom until they are in asymmetric condition. Thus, atoms shall remain idle. Fig.30 shows the flowchart of the MD simulation.

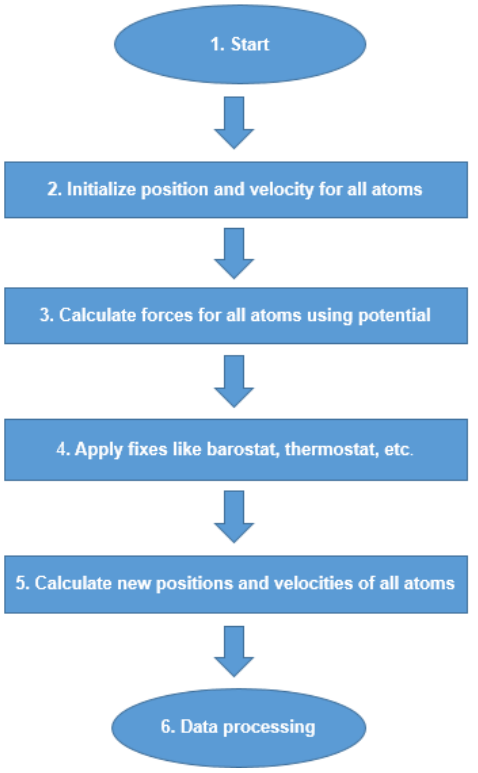

Figure 30: Flowchart of MD Simulation.

Once the simulation is over, the simulator provides two different output files. It is first the user-defined system (log file) that contains the per atom calculations. This data file needs processing to plot graphs and other empirical relationships. Another file contains the simulation video of the whole process. The video segments depend on the time step chosen for the simulation. The video is played using OVITO [10], a 3D visualization software that post-process the atomistic data. Fig.31 shows the interface of the OVITO software. The whole simulation can be played back and forth to understand the material's behavior as the code runs. In Fig.32 , a graph was plotted using the data files extracted after the simulation was complete. Finally, Fig.33 summarizes the whole LAMMPS simulation and gives a clear fundamental understanding of the steps in the process.

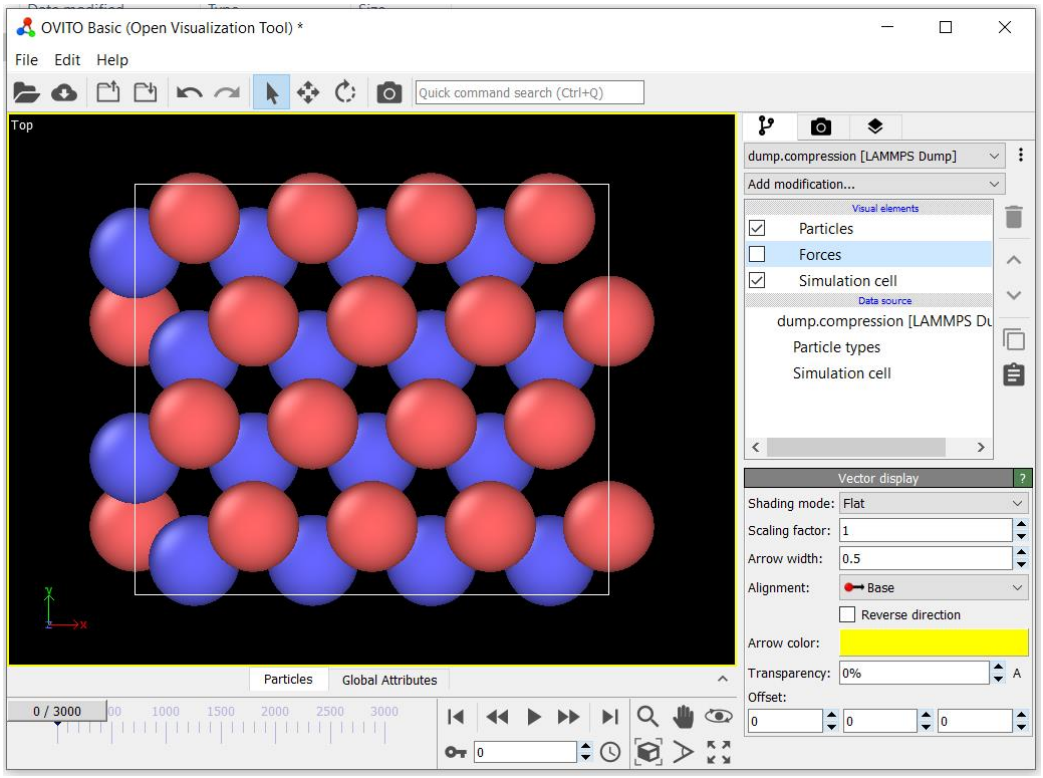

Figure 31: Screenshot of the main window of OVITO.

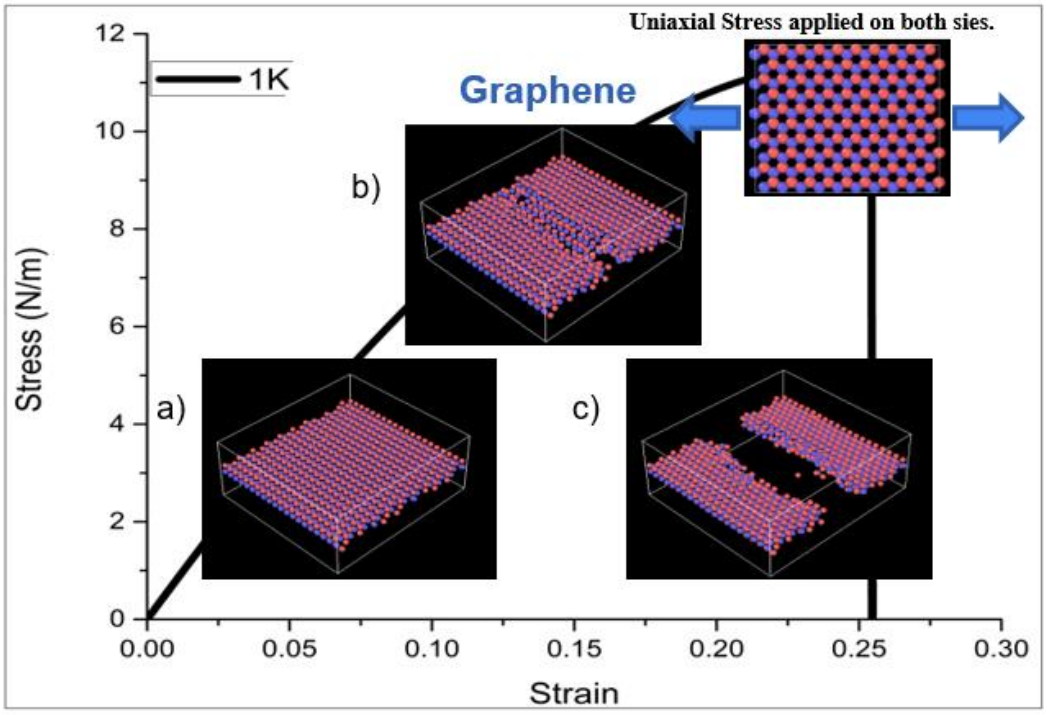

Figure 32: (a) Monolayer Graphene sheet representing a 2D material before and during initial uniaxial tension applying (b) Initialization of fracture in the sheet (c) The 2D sheet after complete fracture.

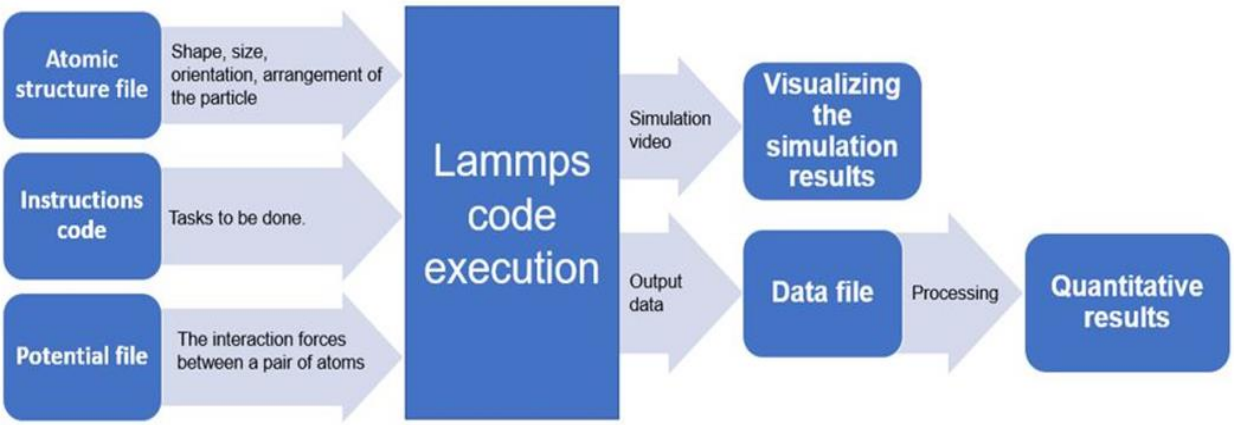

Figure 33 : Step by step procedure of LAMMPS simulation.

3.6. BUILDING LAMMPS USING CMAKE

CMake allows users to compile LAMMPS alternative to the traditional manual customization of files.

This allows beginners to easily compile software if they want to modify or extend the capabilities of LAMMPS. CMake uses a twostep process to produce a functional simulator with new capabilities. Initially, generate a new building environment inside a new directory. Then the compilation of all the executables and libraries.

The parametrized SW potential [156] for TMDCs is the most common interatomic potential file for conducting simulations on two-dimensional materials. Figure 37 shows that bond angles are not considered in the general SW potential; therefore, there is a need for modification for LAMMPS. Incorporating two inequivalent angels into the code increases the accuracy of the result. After the modification, Jiang et al [157] testes the strain-induced buckling on a composite TMDC heterostructure. The modified code uses a bending angle of θ=80.581 for all TMDCs.

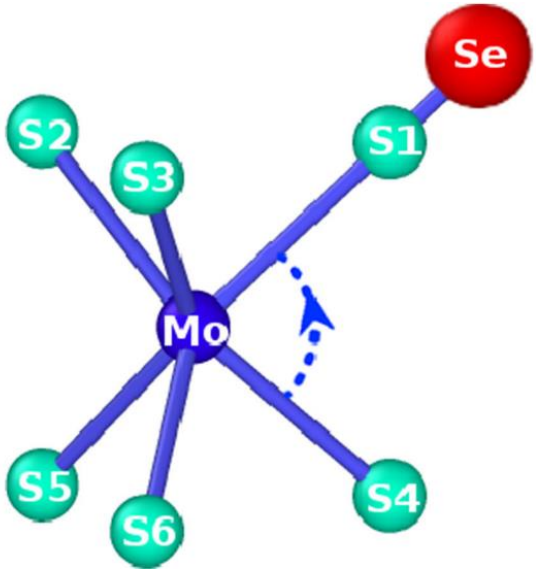

Figure 34: Local environment around atom Mo in the MoS_2 hexagonal lattice with the Mo layer sandwiched by two S layers. Atoms S1, S2,and S3 are in the top group of the MoS_2 layer. Atoms S4, S5,and S6 are in the bottom group of the MoS_2 layer. Atom S1 is substituted by atom Se. Note that the bending of angles like θ_{MoS1S6} is not considered in the SW potential, and a modification is necessary for LAMMPS to exclude this term in the three-body SW potential. Acta Mechanica Solida Sinica 32, 1 (2019).[158].

The following five steps modifies the LAMMPS using CMAKE [133].

i) Downloading the CMake Developer Packages for Lammps.

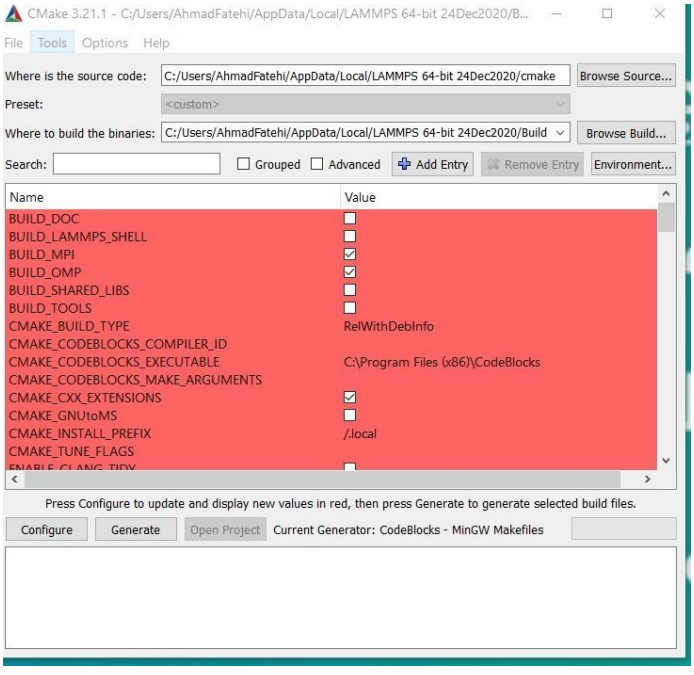

ii) Editing the SW file using CodeBlocks.

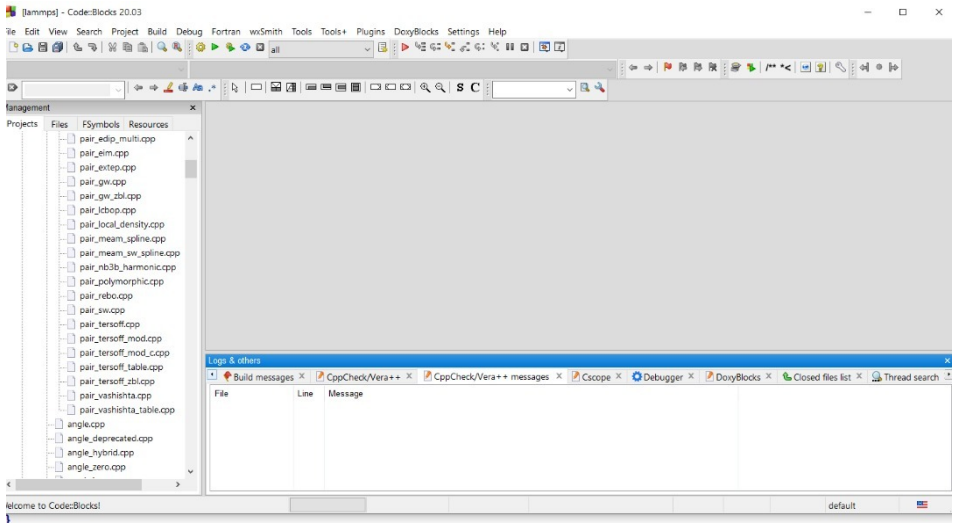

iii) Adding the additional code into SW file

```
  expgsrainv2 = exp(gsrainv2);

  rinv12 = 1.0/(r1*r2);
  cs = (delr1[0]*delr2[0] + delr1[1]*delr2[1] + delr1[2]*delr2[2]) * rinv12;
  delcs = cs - paramijk->costheta;
  if(fabs(delcs) <= 0.25)
{
delcs = delcs; }
else if(fabs(delcs) < 0.35)
{
delcs = delcs * (0.5+0.5*sin(3.142*(delcs-0.25)/(0.35-0.25)+0.5*3.142));
}
else
{
delcs = 0.0;
}
  delcssq = delcs*delcs;

  facexp = expgsrainv1*expgsrainv2;

  // facrad = sqrt(paramij->lambda_epsilon*paramik->lambda_epsilon) *
  //          facexp*delcssq;

  facrad = paramijk->lambda_epsilon * facexp*delcssq;
  fradl = facrad*gsrainvsq1;
  frad2 = facrad*gsrainvsq2;
  facang = paramijk->lambda_epsilon2 * facexp*delcs;
  facang12 = rinv12*facang;
  csfacang = cs*facang;
  csfac1 = rinvsq1*csfacang;

  fj[0] = delr1[0]*(fradl+csfac1)-delr2[0]*facang12;
  fj[1] = delr1[1]*(fradl+csfac1)-delr2[1]*facang12;
  fj[2] = delr1[2]*(fradl+csfac1)-delr2[2]*facang12;
```

iv) Generating modified SW file using compiler.

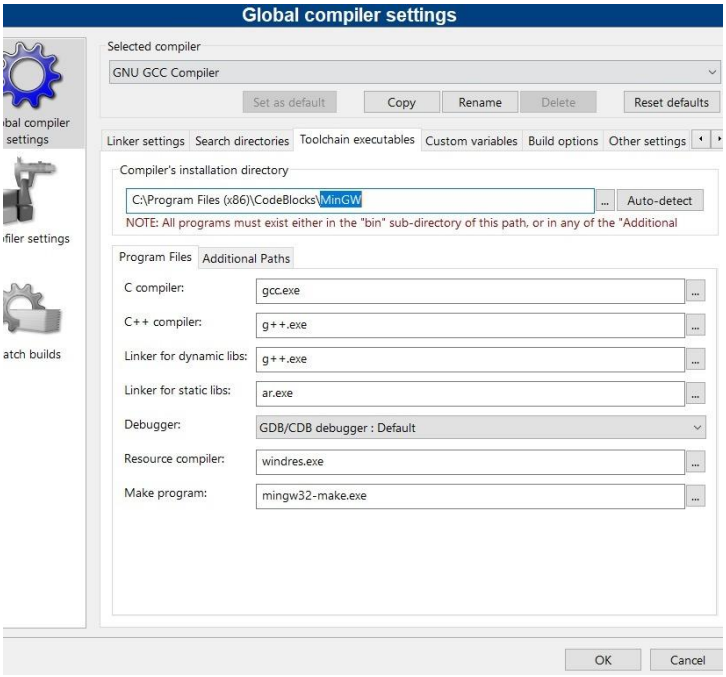

v) Running sample Simulation using modified SW potential to test for results

3.7. SOFTWARE & APPLICATIONS

Structure Makings

Simulation Visualizer

Data Processing

MD Simulator

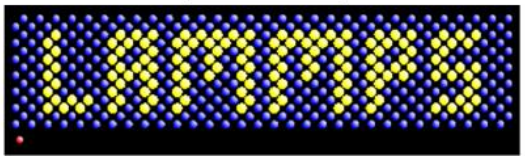

Download links:

1. https://atomsk.univ-lille.fr/dl.php
2. https://jp-minerals.org/vesta/en/download.html
3. https://lammps.sandia.gov/download.html
4. https://www.ovito.org/windows-downloads/
5. https://www.python.org/downloads/
6. https://www.mathworks.com/downloads/
7. https://www.python.org/downloads/

In this chapter, MD simulations has been clarified and the of LAMMPS software as tool for MD simulation used to discuss in-depth the code and the supplement information required for the simulation to be complete. different computational configuration-related and issues were solved.

Chapter 4

DATA GENERATION OF UNIAXIAL STRESS ON 2D MATERIAL , RESULT & DISCUSSION

4.1. INTRODUCTION

In this chapter, the structure of different 2D materials, Graphene, MoS2 and MoTe2, is investigated along with their fracture stress under different Temperature. First validation of the stracture is showm. Second the validation of the three material computational experiment result to the literature. Third Sample of the fracture behavior in both directions Zigzag and armchair is presented.Finally the result of MoTe2 computational experiments finging the fracture stress and Young's modulus under different temperatures of range 100K to 600K under 100K interval are discussed .

4.2. STRUCTURE OF 2D MATERIALS

The 2D materials are anisotropic in general and have two configurations based on the two directions x and y axes in Nano level, as shown in the two pictures of MoTe2 Fig. 35-36 are depicting the two configurations. As the strain is applied uniaxially to different sheet sizes and different materials, the configuration of sheet being a Zigzag or an Armchair would play a significant role to the Fracture stress and Fracture behavior. Therefore, All the simulations for different Temperatures have been run in both directions(configurations). following Fig. 35-45 are presenting some key results related to 2D materials structures.

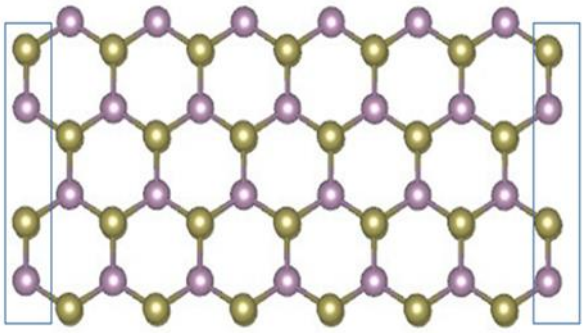

Figure 35: Zigzag direction of 2D material.

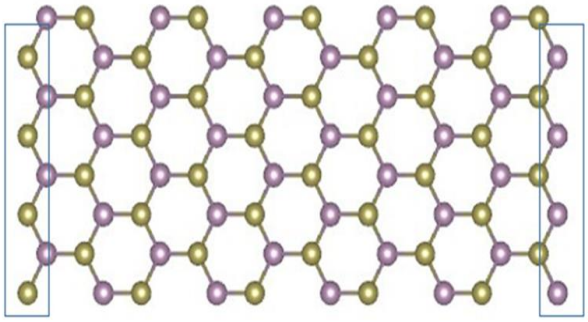

Figure 36: Armchair Direction of 2D material.

4.2.1. Graphene

The Graphene sheet was made in two different ways using MATLAB code and VESTA Atomic Database.

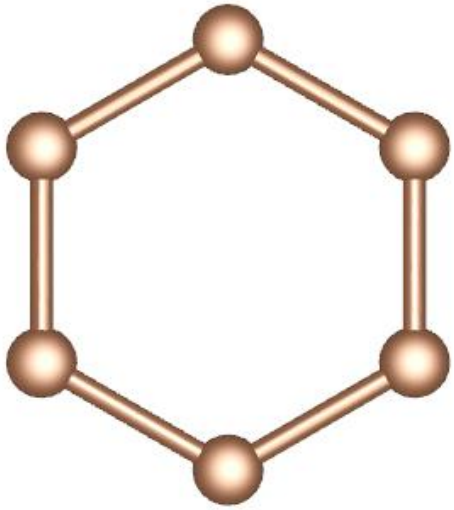

Figure 37: Graphene unit cell[159].

Fig.37 shows the VESTA snapshots of the unit cell of graphene and with the parameters where a, b and,c are the length in Armastrong of the unit cell in three dimensions and α, β, γ, are the mutual angles of the lattice unit cell shown in the Table.4.

Table 4 : Graphene 2D Sheet lattice parameters [160]

Lattice Parameters	a(Å)	b(Å)	c(Å)	α(°)	β(°)	y˙(°)
	2.465	2.465	1.423	90	90	120

The Parameters are given in the Table.4 have been cross checked with literature for the latest accurate values as VESTA provides such modification accessibility.

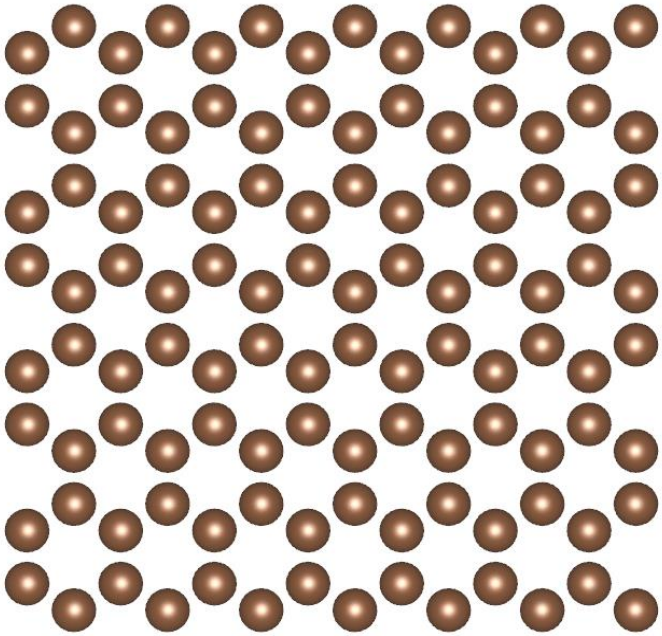

Figure 38: Graphene Sheet[161].

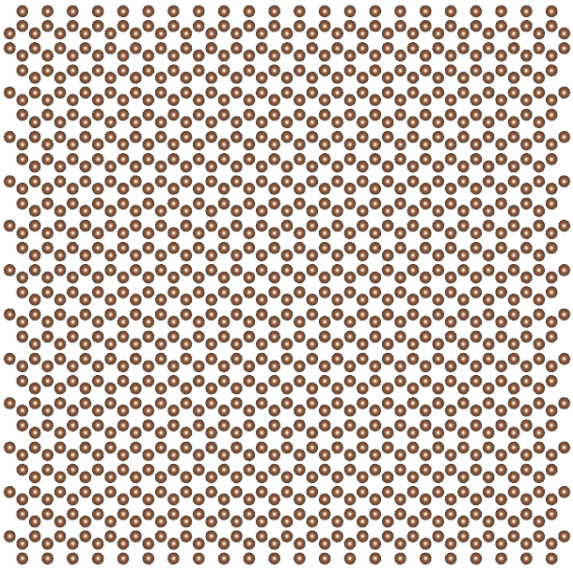

*Figure 39: Graphene 5*5 nm Sheet made in VESTA*

Fig.38 shows a magnified graphene sheet, according to the literature, regenerated using MATLAB code with 1008 atoms. The second Fig.39 is made in VESTA with 1008 atoms. Both of the snapshots are taken from the VESTA visualization environment.

4.2.2. MoS_2

The MoS_2 Material components exist in the Database of VESTA to construct the unit cell compound. However, for the validity of the parameters unit cell of MoS_2 was downloaded from an open-source Database called Crystallography with the proper referencing of the parameters to published Journals. following Fig.40-42 are presenting some key results related to MoS_2 Structure.

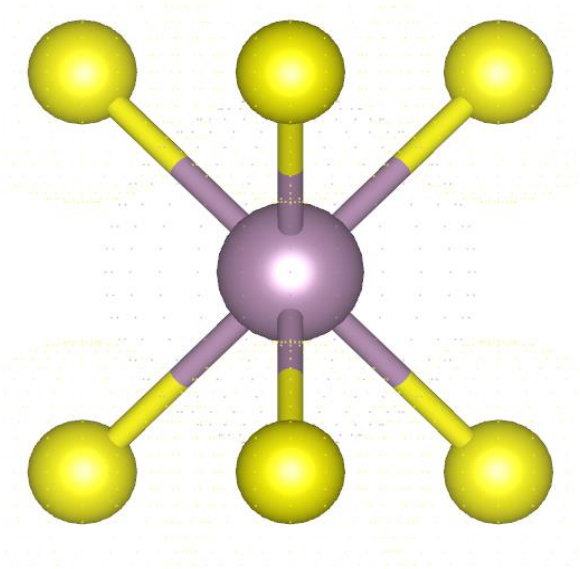

Figure 40: MoS_2 unit Cell [162].

Fig.40 is a snapshot taken from VESTA shows the MoS_2 unit cell after processing, and the Table.5 below shows the lattice parameters.

Table 5: MoS_2 2D sheet parameters [163].

Lattice Parameters	a(Å)	b(Å)	c(Å)	α(º)	β(º)	y˙(º)
	3.15	3.15	12.3	90	90	120

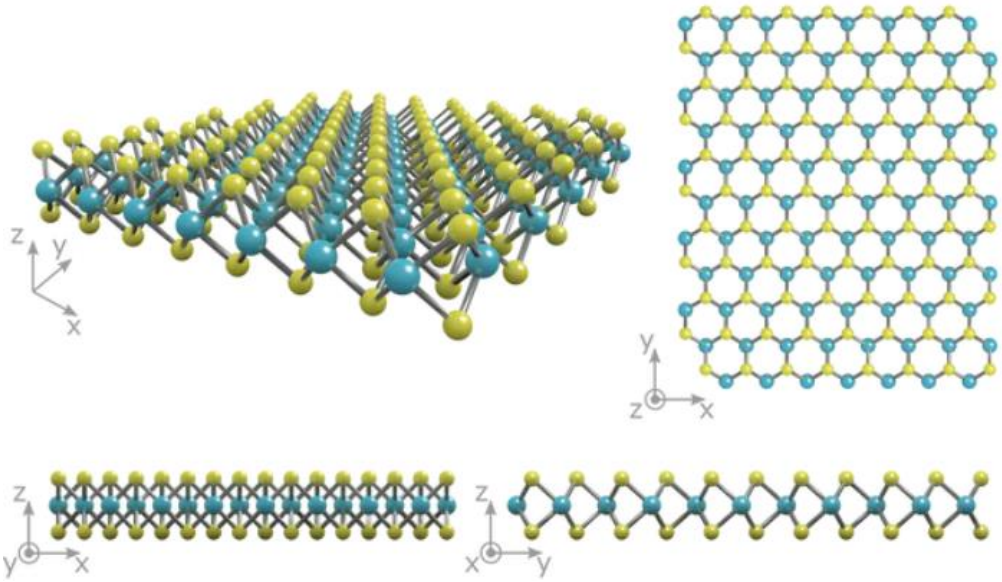

Figure 41 : The crystal structure of monolayer MoS_2 showing a layer of molybdenum atoms (blue) sandwiched between two layers of sulfur atoms (yellow)[164].

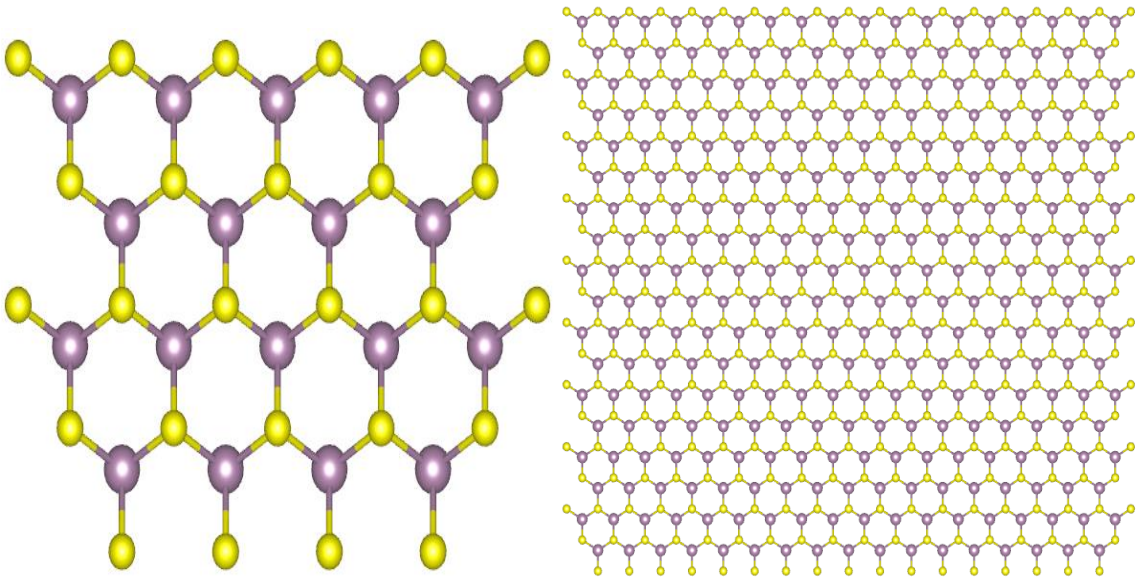

*Figure 42 : 1.2*1.1nm, and 5.4*5 nm MoS_2 sheets made in VESTA.*

Fig.41 The VESTA snapshots show the sheet after the duplication and proper aligning of the material to work in LAMMPS, which was done in ATOMSK; there are two sheets size made one of the 48 atoms and another 918 atoms; the small size helped for reducing the time of the simulation in the initial trial and error configuration of some coding parameters, then with more parameters are stable the larger sheet is introduced.

4.2.3. $MoTe_2$

It is prime material and is worked with after the confident has been built replicating the result of the general and easier to simulate (Graphene) then replicating the values for similar material (MoS_2) which belong to same Family of TMDs. Wherease the code and extra resources are available in internet for MoS_2 while there is not much rescource available for $MoTe_2$. The following Fig. 46-48 are presenting some key results related to $MoTe_2$ Structure.

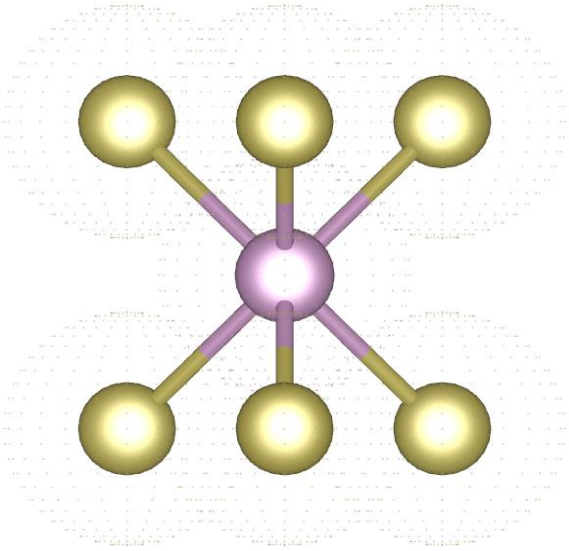

Figure 43: $MoTe_2$ Unit cell [162].

The $MoTe_2$ Material components exist in the Database of VESTA to construct the unit cell compound. However, for the validity of the parameters unit cell of $MoTe_2$ is downloaded from an open-source Database called Crystallography with the proper referencing of the parameters to published Journals.

Fig.43 is a snapshot taken from VESTA shows the $MoTe_2$ unit cell after processing, and the Table.6 below shows the lattice parameters.

Table 6: $MoTe_2$ 2D Sheet lattice parameters[165].

Lattice Parameters	a(Å)	b(Å)	c(Å)	α(°)	β(°)	y˙(°)
	3.519	3.519	13.964	90	90	120

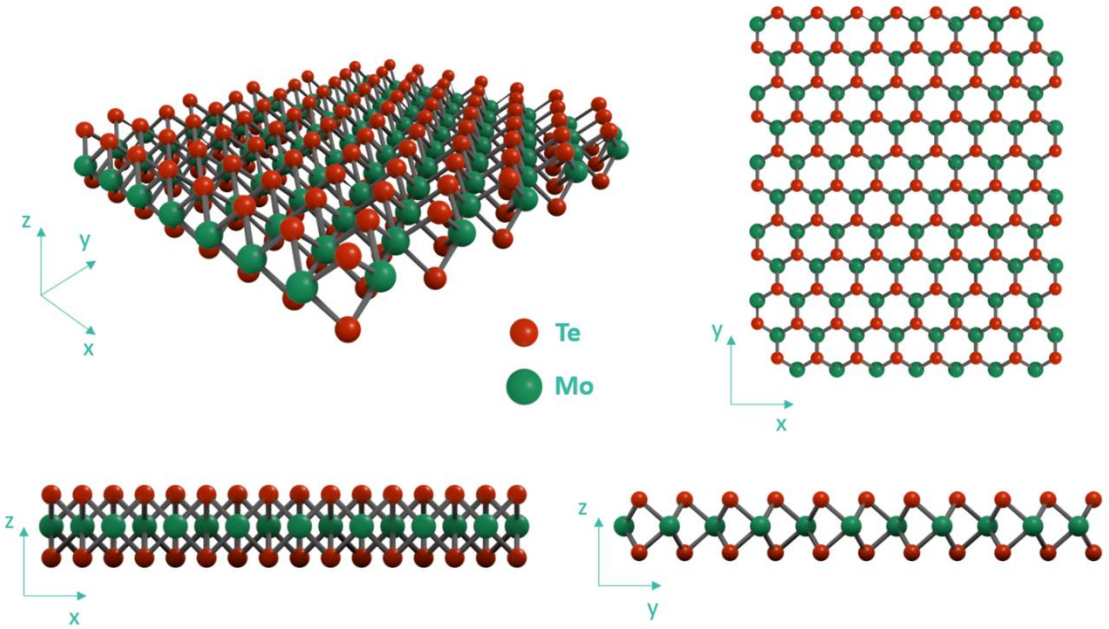

Figure 44 : The crystal structure of monolayer $MoTe_2$ showing a layer of molybdenum atoms (black) sandwiched between two layers of sulfur atoms (red)[166].

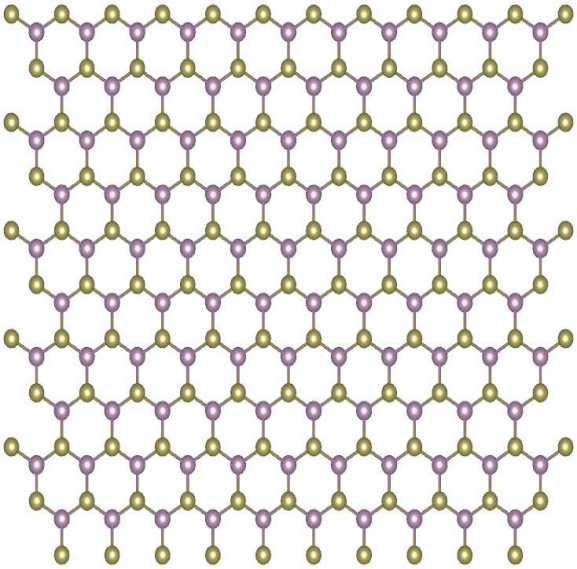

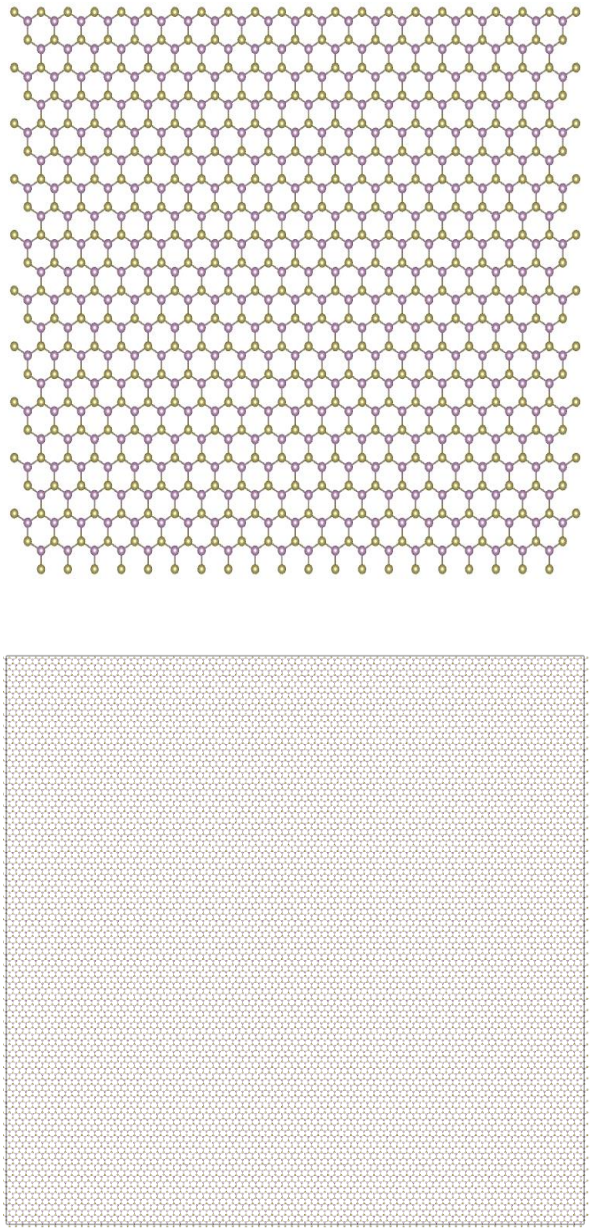

*Figure 45 : Shows sheets of different sizes in follow order up to down , small to big and more significant 3.5*3.0 nm,7*6 nm and 30*30nm Sheets, respectively, the snapshot taken from VESTA.*

Fig.45 VESTA snapshots show the sheet after the duplication and proper aligning of the material to work in LAMMPS, which is done in ATOMSK, there were many sheets with different sizes made, but only three are used frequently; the Smallest of 300 atoms, one of 1200 atoms, and the primary size where the result is drawn from was 25800 atoms. the small size helped reduce the simulation time in the initial trial and error configuration of some coding parameters. Then sheet of 30*30nm is used in the computation workstation to obtain the final result.

4.3. VALIDATION OF 2D MATERIALS AGAINST LITERATURE

The structure of the material was prepared as decriped in perivous section, then the intended simulation experiment code, and the potential file were finalized. The result obtained was validated against similer work. the validity of the codes and potential files is checked; therefore, any further usage of the simulation setup would be reasonably accepted.

4.3.1. Validation of Graphene.

Graphene with initial coding experience in LAMMPS using AIREBO potential run to investigate the capability of reproducing the data for a wide range of temperatures from 300K to 2100K as the final target is to investigate the fracture strain of $MoTe_2$ under a broader range of Temperatures then what already explored. following Fig. 46-54 are presenting some key results related to Graphene Validation.

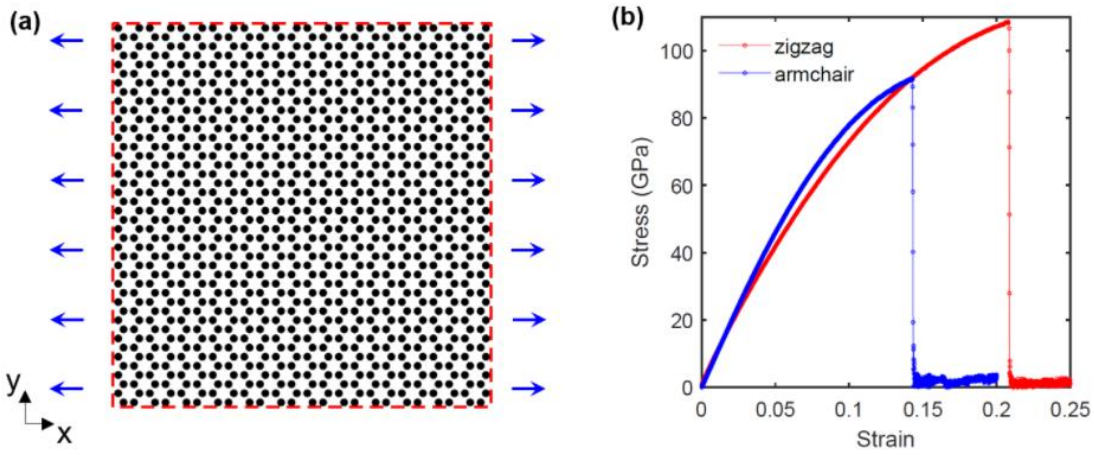

Figure 46 : (a)Uniaxial Stress on Graphene (b) Stress-strain curve for armchair and zigzag [161].

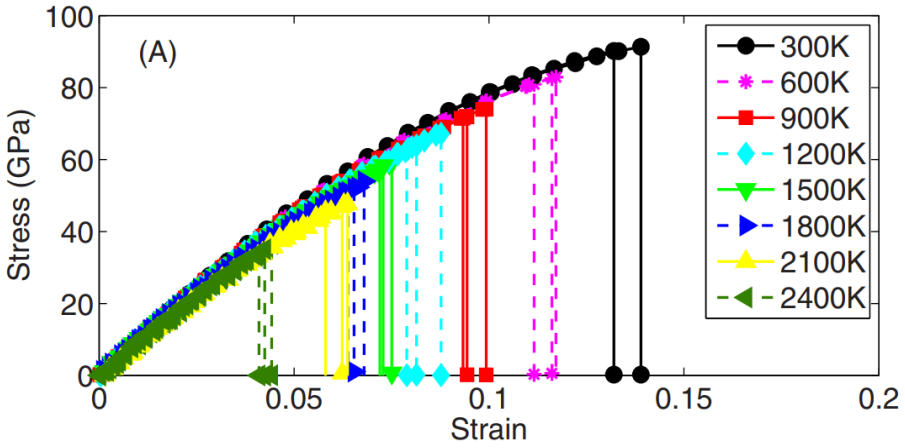

Figure 47 : Nominal strain vs stress of graphene under uniaxial tensile test along the armchair direction at various temperatures[167].

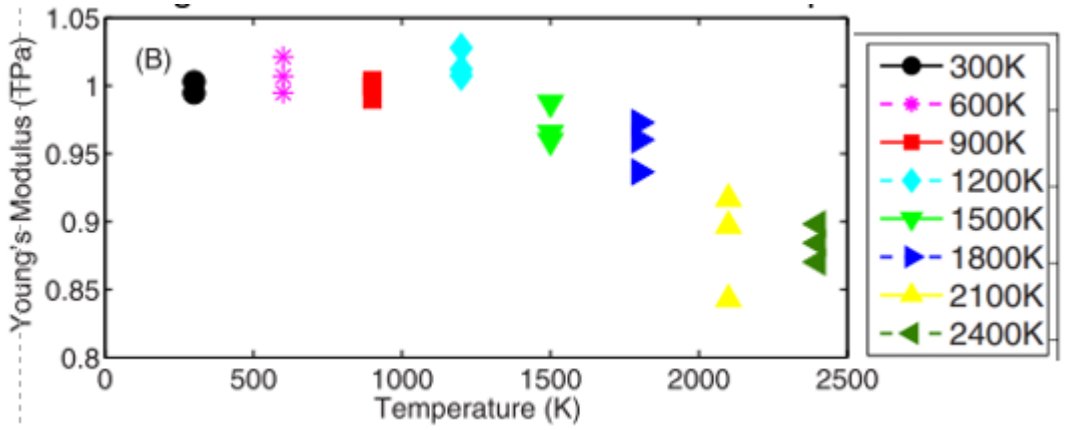

Figure 48: Variation in Young's modulus of graphene with temperature under uniaxial tensile test along the armchair direction[167].

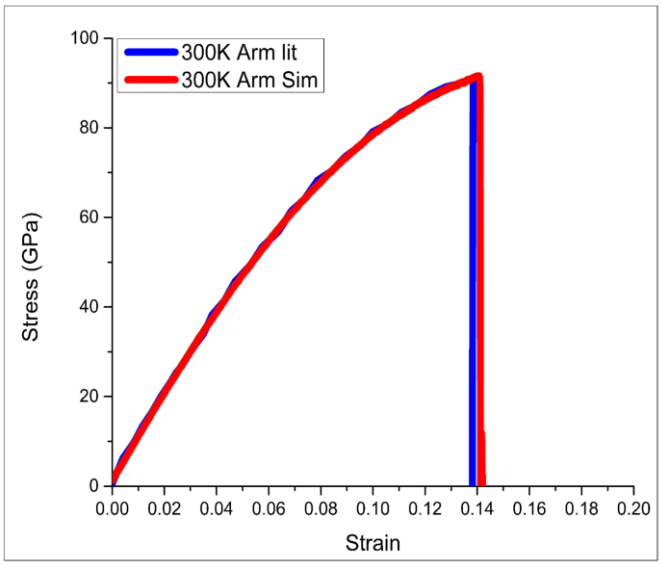

Figure 49 : Graphene comparison of Stress-Strain curve at 300K for armchair simulation. (lit- Literature & Sim- Present study)

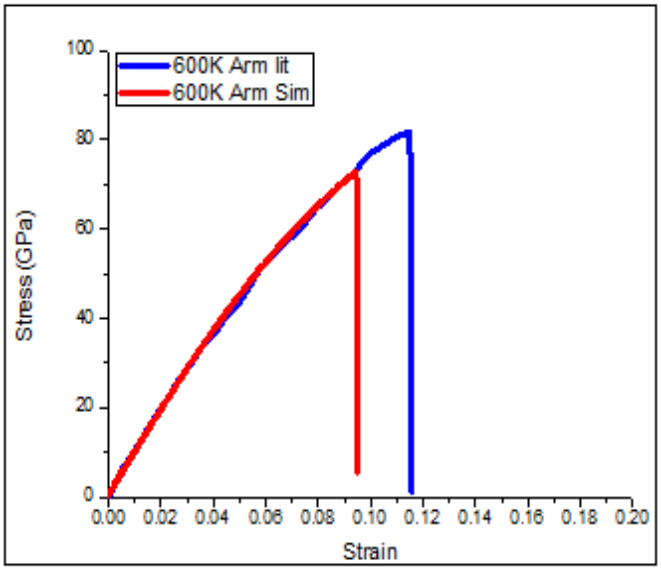

Figure 50: Graphene comparison of Stress-Strain curve at 600K for armchair simulation.(lit- Literature & Sim- Present study)

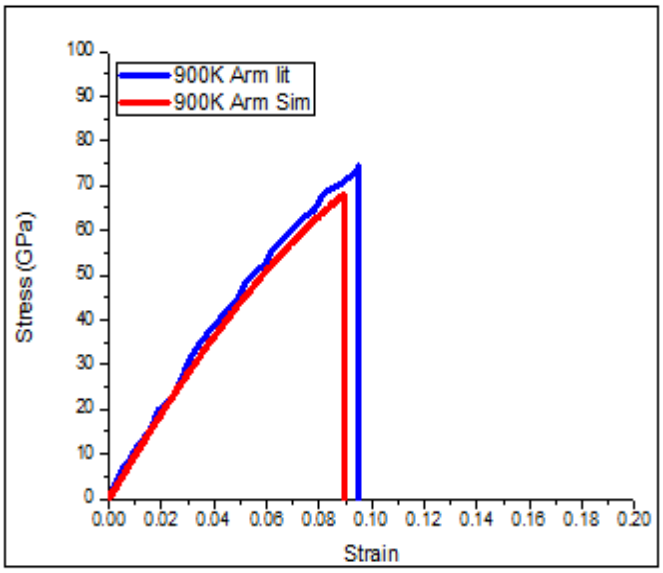

Figure 51: Graphene comparison of Stress-Strain curve at 900K for armchair simulation.(lit- Literature & Sim- Present study)

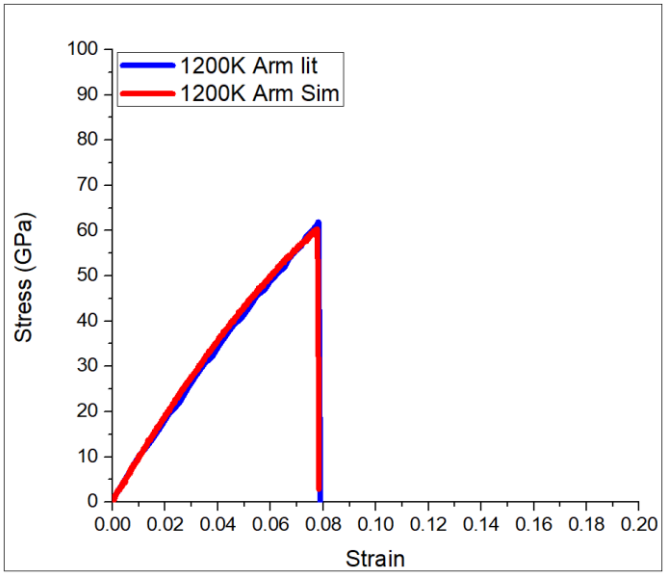

Figure 52: Graphene comparison of Stress-Strain curve at 1200K for armchair simulation. (lit- Literature & Sim- Present study.

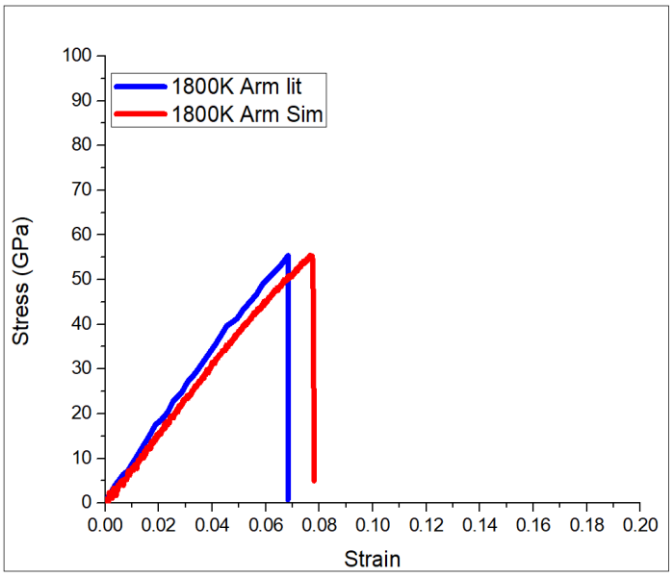

Figure 53: Graphene comparison of Stress-Strain curve at 1800K for armchair simulation. (lit- Literature & Sim- Present study).

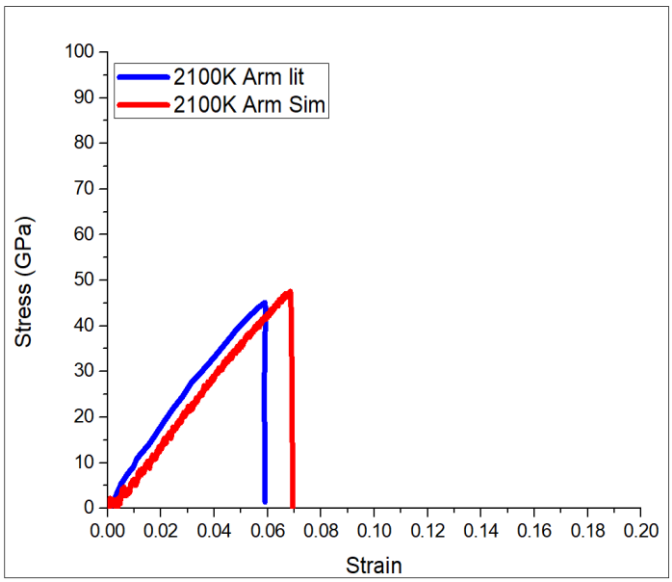

Figure 54: Graphene comparison of Stress-Strain curve at 2100K for armchair simulation.(lit- Literature & Sim- Present Study).

Fig.49-54 are of different temperatures express the good agreement between obtained fracture stress and literature with small insignificant deviation in some of them and all most exact result with others.

4.3.2. Validation of MoS_2.

As the confidence grew with the excellent result obtained with graphene, moving toward the TMDs materials after the structure was made for MoS_2, as discussed earlier in the upper section of this chapter.Validation of MoS_2 using Stillinger-Weber(SW) , it is a method was used in the present study as gate to TMDs materials . following Fig.55-57 are presenting some key results related to MoS_2 Validation.

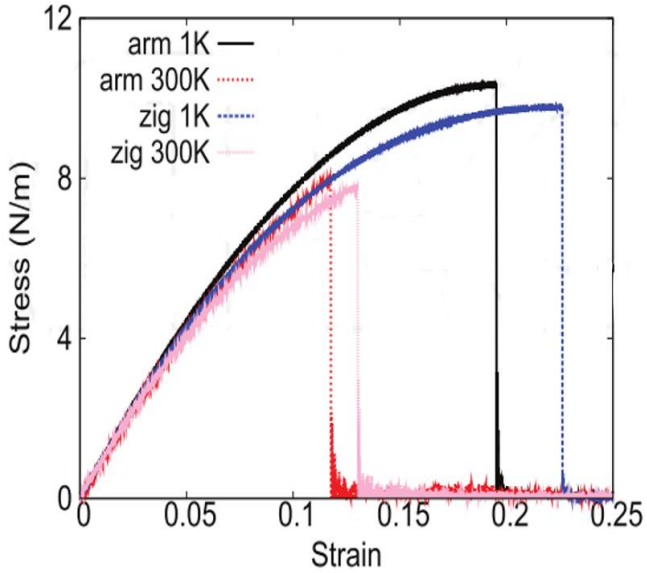

Figure 55: Stress-strain for single-layer 1H-MoS_2 of dimension 100 × 100 ˚A along the armchair and zigzag directions.[16].

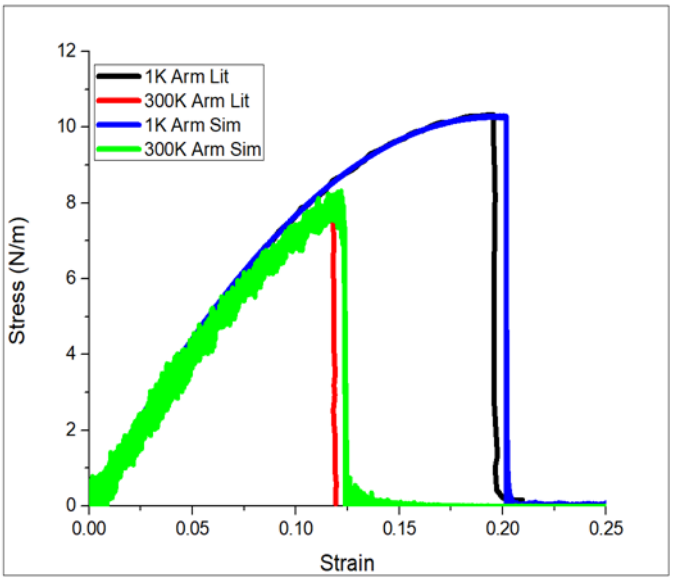

Figure 56: Stress-strain for single-layer 1K and 300K along the armchair.(lit- Literature & Sim- Present study).

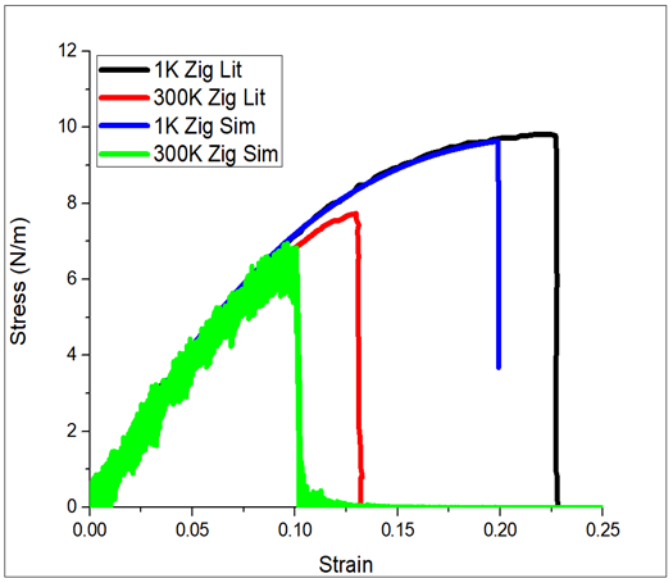

Figure 57: Stress-strain for single-layer comparison of 1K and 300K along the zigzag. (lit- Literature & Sim- Present study).

The validation result shown in the graphs in (Fig.56-57) are given for 1K and 300K in both directions, Armchair and Zigzag; the data show a perfect match with literature in the Armchair direction and with a slight deviation in a zigzag direction which is sufficient to initiate experiment with $MoTe_2$.

4.3.3. Validation of $MoTe_2$

The data from literature was taken for 1K and 300K for both direction as shown in the graph below. Following Fig.58-60 are presenting some key results related to $MoTe_2$ Validation.

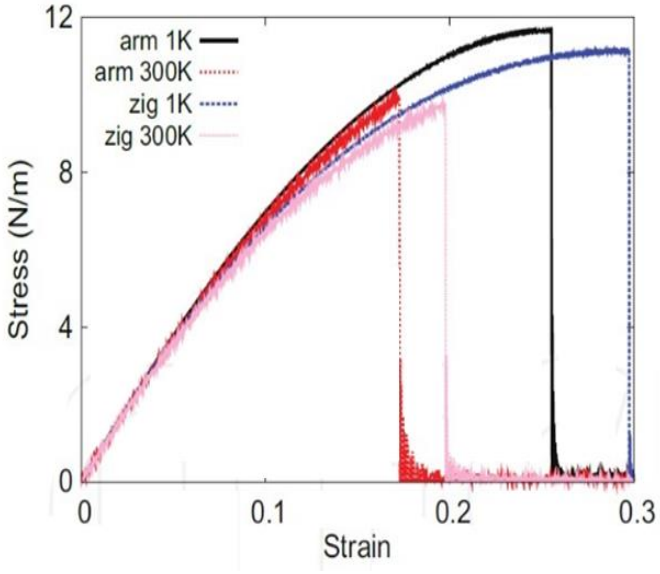

Figure 58: Stress-strain for single-layer 2H-$MoTe_2$ of dimension 100 × 100 ˚ along the armchair and zigzag directions[16].

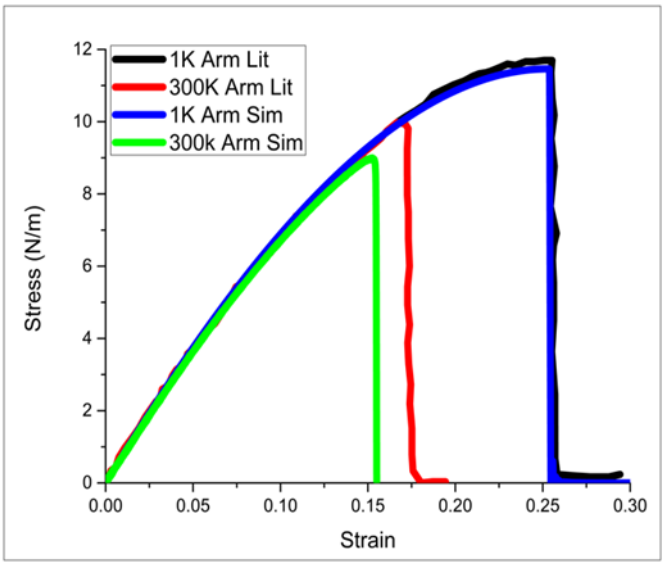

Figure 59: Stress-strain for single-layer 1K and 300K along the armchair.(lit- Literature & Sim- Present study).

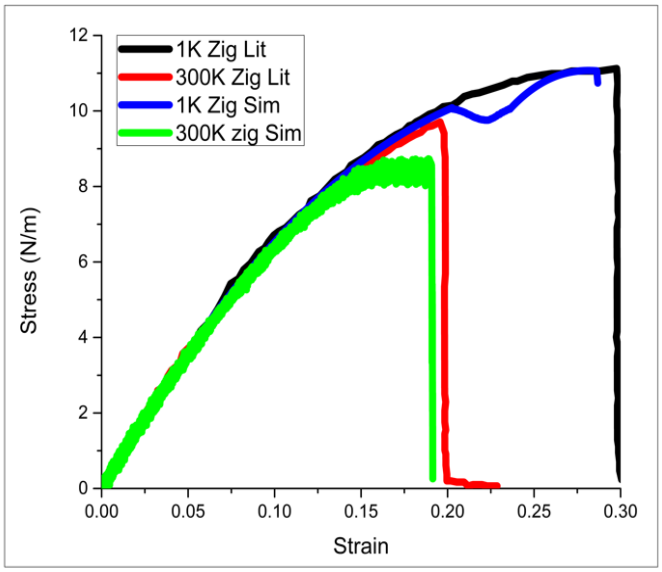

Figure 60: Stress-strain for single-layer comparison of 1K and 300K along the zigzag. (lit- Literature & Sim- Present study).

The graphs in Fig.57-60 showing the result of both directions for 1K and 300K and as it can be seen the obtained data is matching literature data with minor deviation. The amount of deviation for simulation is in the acceptable level.

4.4. THE SAMPLES OF FRACTURES OF 2D MATERIAL SIMULATION

The fracture behavior change is minor to none in the case of the same direction with different Temperatures; therefore, giving only one sample of each direction for every material used is enough to show the fracture behavior.

4.4.1. Fracture Sample of Graphene.

Following Fig. 61-65 are presenting some key results related to Fracture Sample of Graphene.

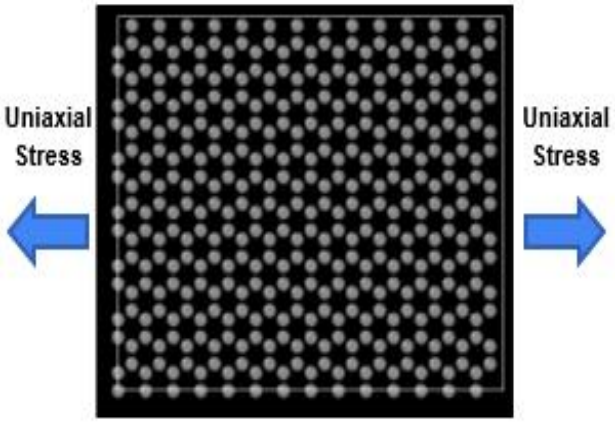

Figure 61:Single layer of graphene with stress direction applied on for visualization.

Fig.61 shows how the strain is applied to the graphene sheet; this figure only shows for Zigzag direction. This figure is an OVITO snapshot.

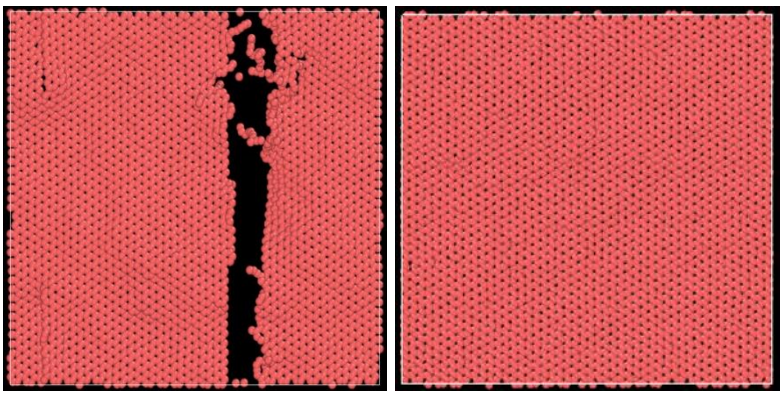

Strain: 0.13 0.14

Figure 62: The atomic configuration evolution during crack in Armchair direction at 300K.

Fig.62 shows snapshots, Which are taken from data output for visualization through OVITO, and they show the crack of graphene sheet of 5*5 nm in the armchair direction at 300K. The graph below Fig.63 is the graphical part of the data, which clearly shows the reflection of the fracture on the stress level.

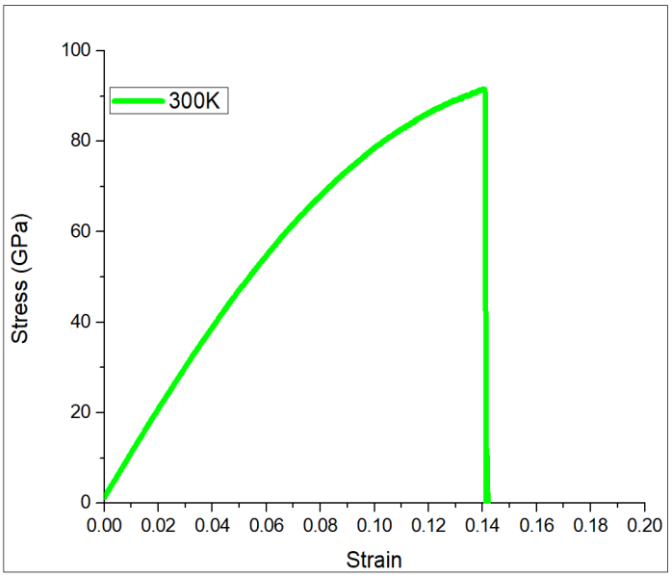

Figure 63: Plane Stress-strain for single-layer Graphene for Armchair at 300K.

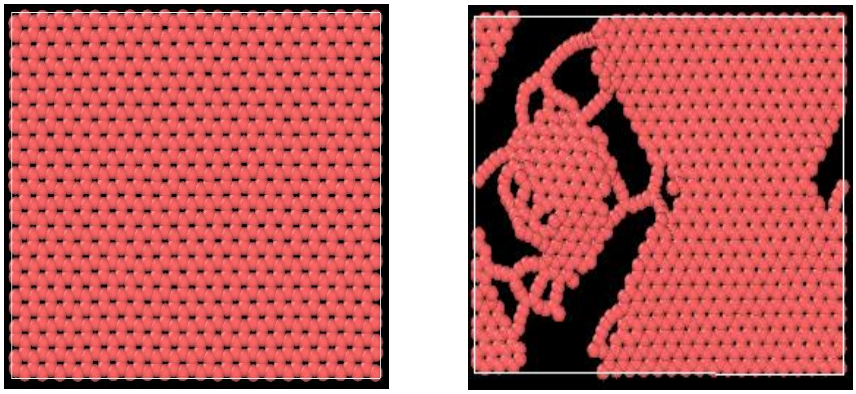

Strain: 0.17 0.19

Figure 64: The atomic configuration evolution during crack in Zigzag direction at 300K.

Fig.64 shows snapshots, Which are taken from data output for visualization through OVITO, and they show the crack of graphene sheet of 5*5 nm in the zigzag direction at 300K. The graph below Fig.65 is the graphical part of the data, which clearly shows the reflection of the fracture on the stress level.

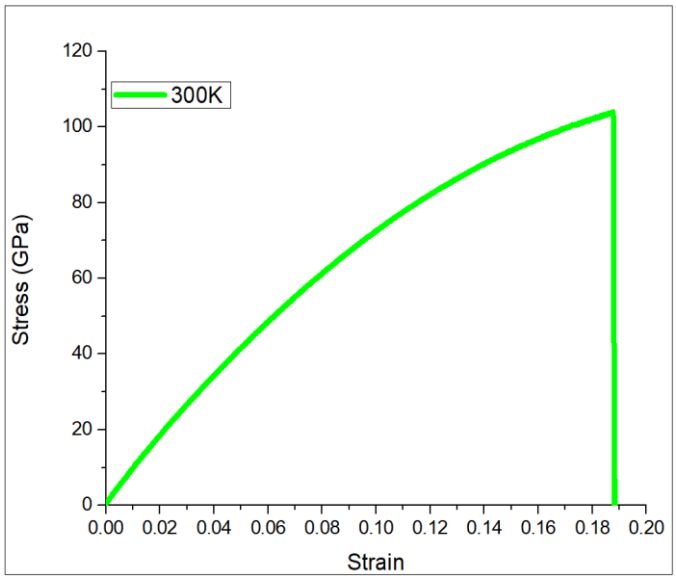

Figure 65: Plane Stress-strain for single-layer Graphene for Zigzag direction at 300K.

4.4.2. Fracture Sample of MoS2.

Following Fig.66-70 are presenting some key results related to Fracture Sample of MoS_2.

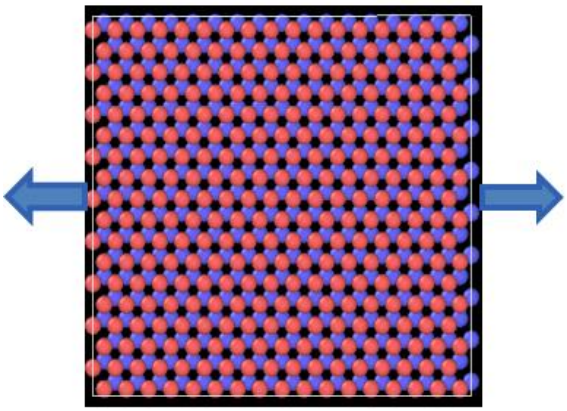

Figure 66: Single layer of MoS_2 with uniaxial stress.

Fig.66 show how the strain is applied on the MoS_2 sheet, this figure only shows for Zigzag direction. This figure is a OVITO snapshot.

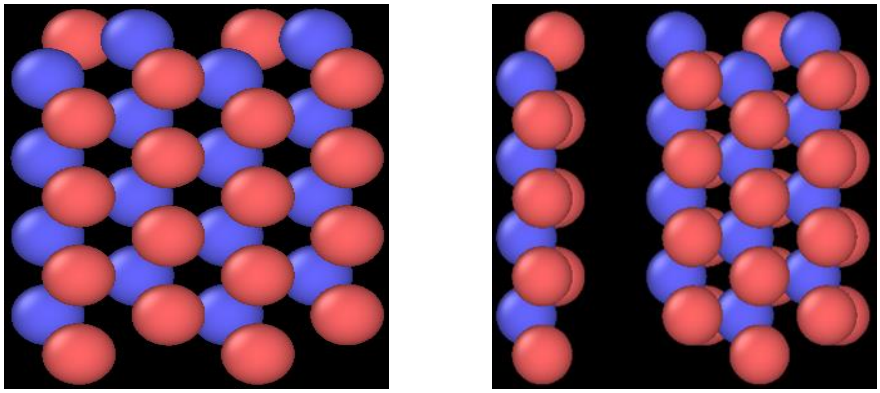

Strain: 0.19 0.20

Figure 67: The atomic configuration evolution during crack in Armchair direction at 1K.

Fig.67 shows snapshots, Which are taken from data output for visualization through OVITO, and they show the crack of the MoS_2 sheet of 1.2*1.1nm in the armchair direction at 1K. The graph below is the graphical part of the data, which clearly shows the reflection of the fracture on the stress level.

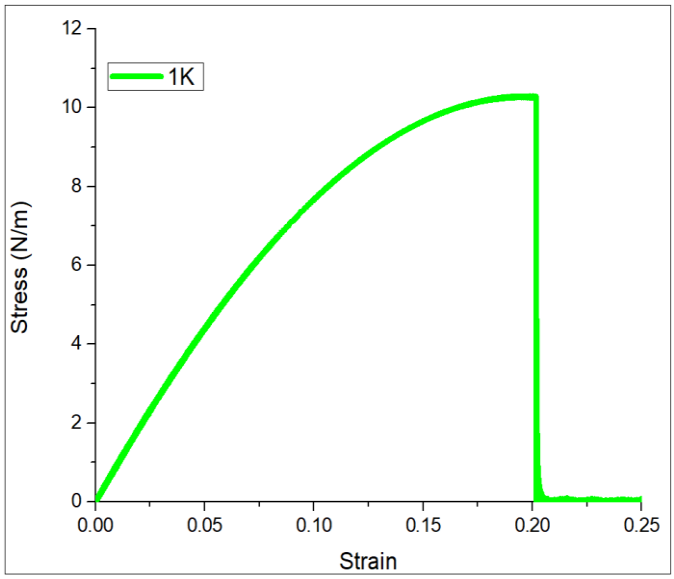

Figure 68: Plane Stress-strain for single-layer MoS_2 for Armchair at 1K.

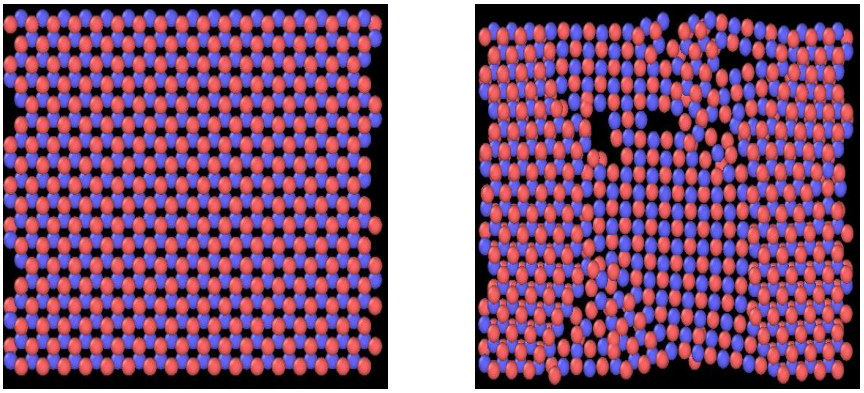

Strain: 0.19 0.20

Figure 69: The atomic configuration evolution during crack in Zigzag direction at 1K.

Fig.69 shows snapshots, Which are taken from data output for visualization through OVITO. They show the fracture of the MoS_2 sheet of 5.4*5 nm in the zigzag direction at 1K, which is of type of distortion and not similar behavior as Armchair direction. However, the graph below Fig.70 is the graphical part of the data, which clearly shows the reflection of the fracture on the stress level, it gives a similar trend to the Armchair graphical result.

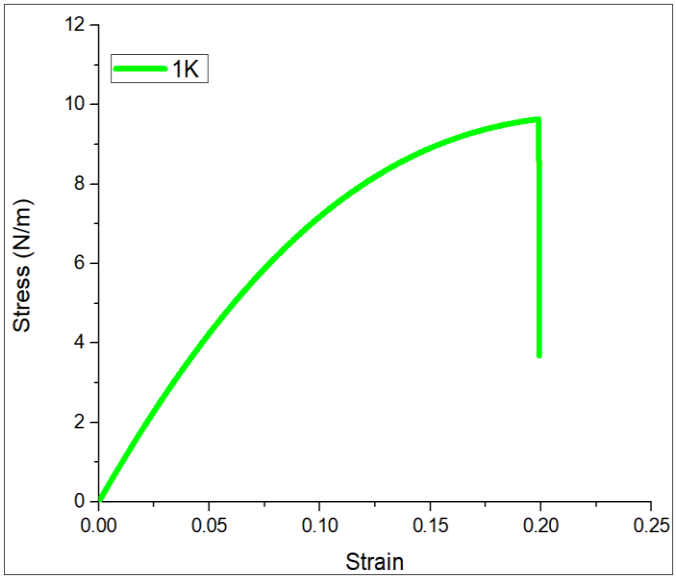

Figure 70: Plane Stress-strain for single-layer MoS_2 for Zigzag at 1K.

4.4.3. Fracture Sample of $MoTe_2$

As this material is the main focus, the sample present here is for two temperatures in each direction and with more detail on the propagation of the fracture snapshots. Following Fig. 71-77 are presenting some key results related to Fracture Sample of $MoTe_2$.

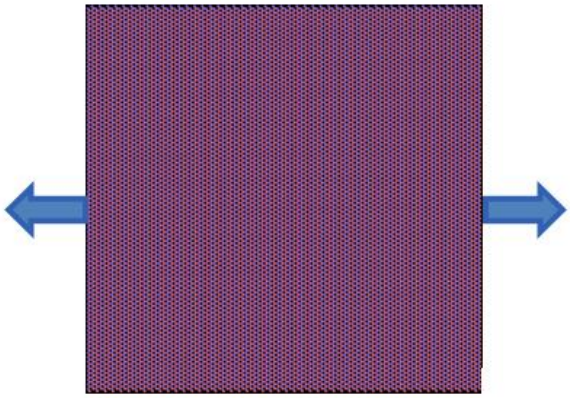

Figure 71:Single layer of $MoTe_2$ with uniaxial stress.

Fig.71 shows how the strain is applied on the $MoTe_2$ sheet; this figure only shows for Armchair direction. This figure is an OVITO snapshot.

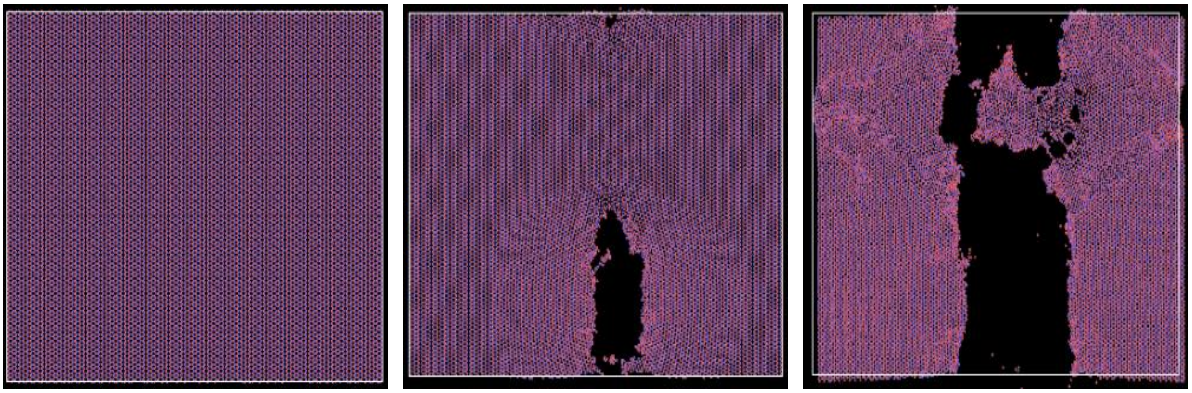

Strain: 24.56% *24.81%* *24.87%*

Figure 72: The atomic configuration evolution during crack in Armchair direction at 10K.

Fig.72 shows snapshots, Which are taken from data output for visualization through OVITO, and they show the crack propagation of $MoTe_2$ sheet of 30*30 nm in Armchair direction at 10K.

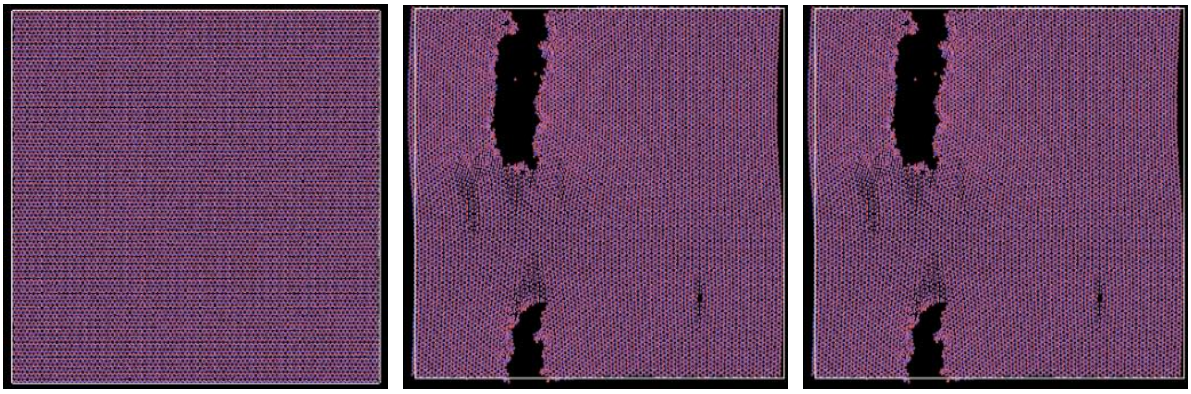

Strain: 15.00% *15.24%* *15.33%*

Figure 73 : The atomic configuration evolution during crack in Armchair direction at 300K.

Fig.73 shows snapshots, Which are taken from data output for visualization through OVITO, and they show the crack propagation of the $MoTe_2$ sheet of 30*30 nm in the armchair direction at 300K. The graph below Fig.74 is the graphical part of the data which clearly shows the reflection of the fracture on the stress level for both Temperatures at 10K and 300K.

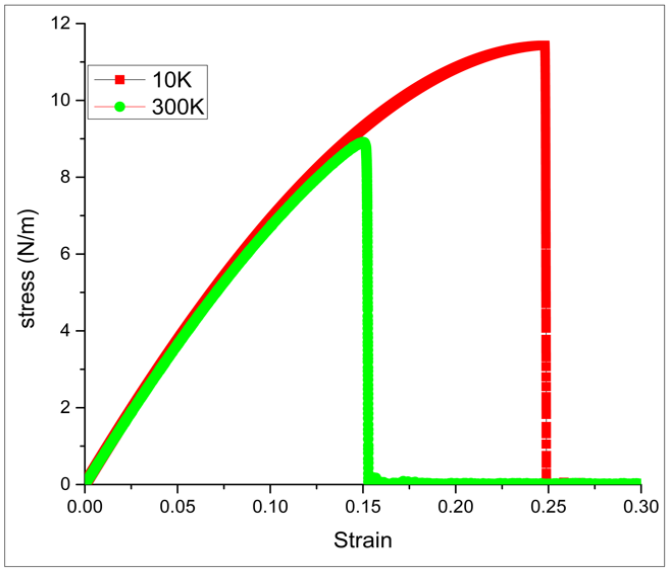

Figure 74: Plane Stress-strain for single-layer dimension 2H-$MoTe_2$ for Armchair at 10K and 300K.

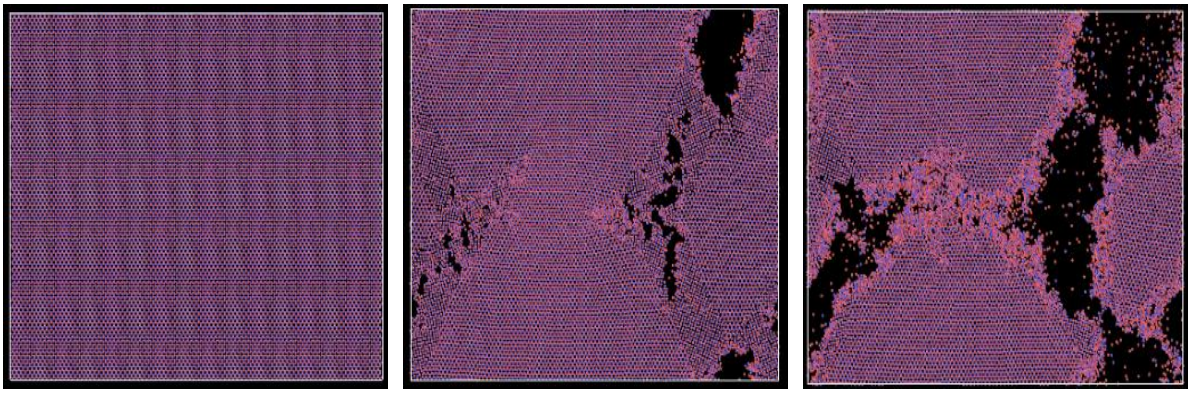

Strain: 18.17% *18.29%* *18.31%*

Figure 75: The atomic configuration evolution during crack in Zigzag direction at 10K.

Fig.75 shows snapshots, Which are taken from data output for visualization through OVITO, and they show the crack propagation of $MoTe_2$ sheet of 30*30 nm in Zigzag direction at 10K.

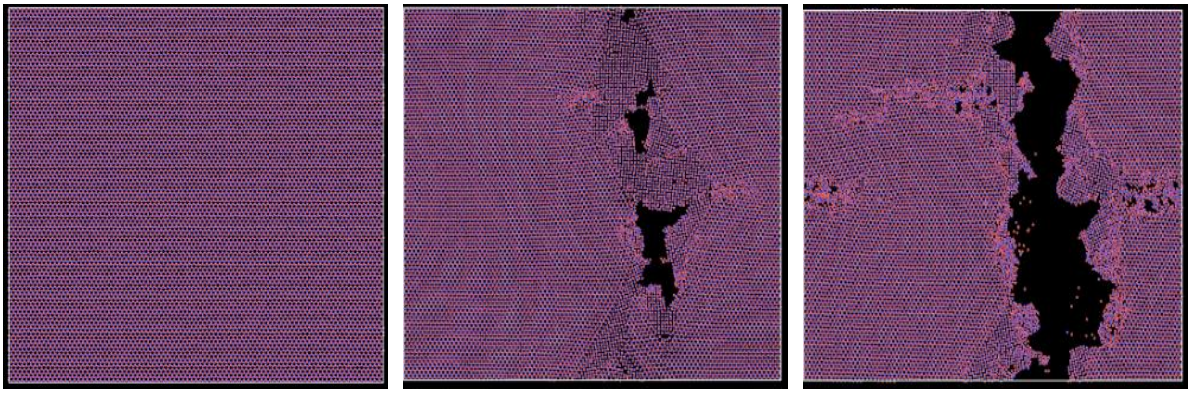

Strain: 13.74% *14.10%* *14.19%*

Figure 76: The atomic configuration evolution during crack in Zigzag direction at 300K.

Fig.76 shows snapshots, Which are taken from data output for visualization through OVITO, and they show the crack propagation of the $MoTe_2$ sheet of 30*30 nm in the zigzag direction at 300K. The graph below Fig.77 is the graphical part of the data which clearly shows the reflection of the fracture on the stress level for both Temperatures at 10K and 300K.

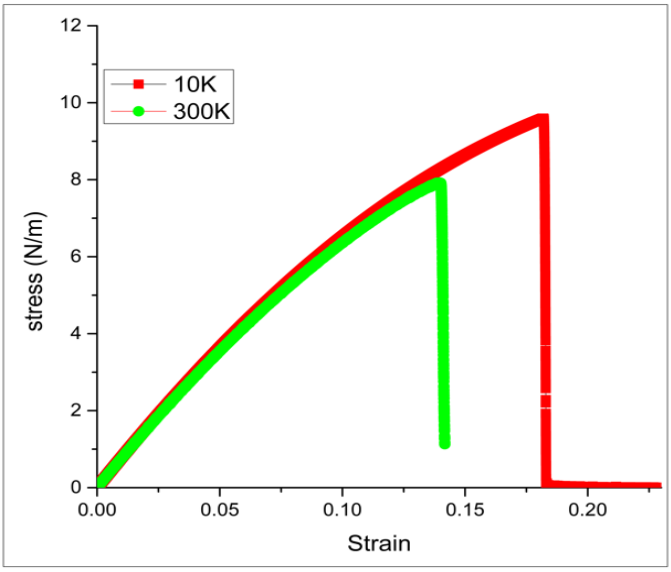

Figure 77: Plane Stress-strain for single-layer dimension 2H-$MoTe_2$ for zigzag at 10K and 300K.

4.5. RESULT OF $M_OT_{E_2}$ EXPLORATION

In the exploration of $MoTe_2$ following the latest trend and investigation of the $MoTe_2$, it is found that the gap is that the fracture stress and Young's Modulus of material have not been examined for a wide range of Temperatures. Therefore simulation experiments have been conducted on $MoTe_2$ to find out the fracture stress and Young's Modulus for an interval of 100K starting from 100K to 600K. The result is presented below. Following Fig. 78-81 are presenting the results.

4.5.1. Armchair Direction.

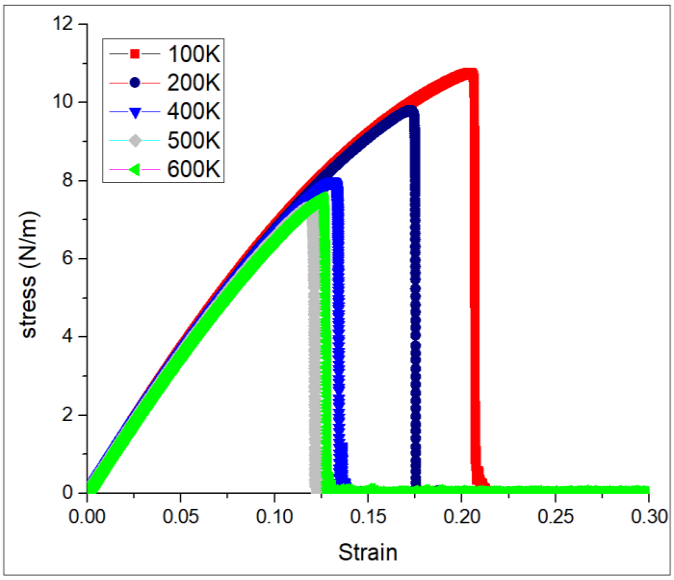

Figure 78: Plane Stress-strain for single-layer dimension 2H-$MoTe_2$ for Armchair from 100K to 600K.

Fig.78 of different Temperature stress-strain shows the trend of decreasing Fracture stress in the Armchair direction with Temperatures increasing except for 600K. Fracture stress increases from 7.29N/m to 7.564 N/m as it goes from 500K to 600K. The below Table.7 shows the exact values of each Temperature for Young's Modulus, Fracture Stress, and Fracture Strain.

Table 7 : Mechanical properties of Armchair simulation at different temperature.

Properties	10K	100K	200K	300K	400K	500K	600K
Young's Modulus	72.267	71.72673	70.99966	70.56126	69.88554	69.27886	68.75177
Fracture Stress	11.430	10.774	9.805	8.902	7.988	7.290	7.564
Fracture Strain	0.2480	0.2038	0.1725	0.1508	0.1309	0.1187	0.12524

4.5.2. Zigzag Direction.

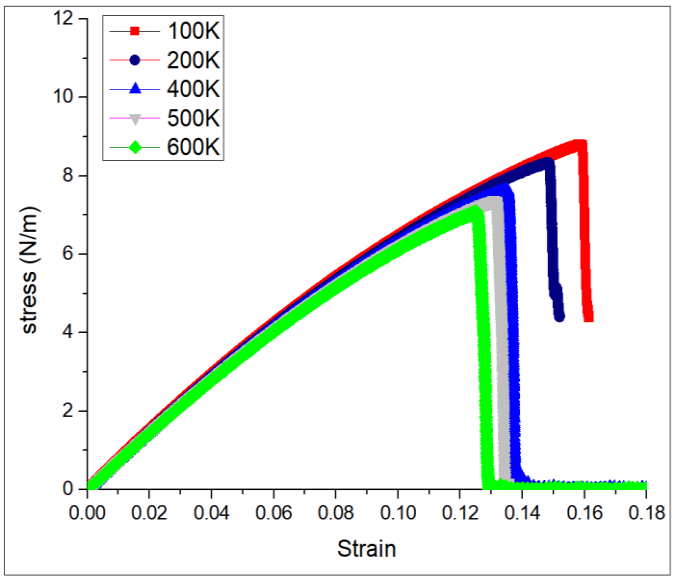

Figure 79: Plane Stress-strain for single-layer dimension 2H-$MoTe_2$ for Zigzag from 100K to 600K.

Fig.8 shows the different Temperatures stress-strain of the trend of decreasing Fracture stress in the zigzag direction with Temperature increase. The below Table.8 shows the exact values of each Temperature for Young's Modulus, Fracture Stress, and Fracture Strain.

Table 8: Mechanical properties of Zigzag simulation at different temperatures.

Properties	10K	100K	200K	300K	400K	500K	600K
Young's Modulus	69.17	68.63155	68.03227	67.40723	66.85901	66.25541	65.56633
Fracture Stress	9.600	8.816	8.333	7.914	7.626	7.373	7.091
Fracture Strain	0.1817	0.1583	0.1482	0.1390	0.1353	0.1314	0.1247

4.5.3. Findings and Discussion

Elastic Modulus for both direction exhibits a very excellent stability with very small insignificant change in wide range of Temperatures from 100K to 600K as shown in the graph below Fig.80.

The Fig.81 shows the comparison of Armchair and Zigzag direction of $MoTe_2$ at 300K. This is a sample to show the difference in strength between both directions, which is being evident through the wide range of the Temperatures. The data is given in the tables of $MoTe_2$ 2D sheet for both configrations . The Armchair direction is more potent than in Zigzag direction.

In this chapter, the results have been demonstrated in graphs and tables and the finding has been discussed in a detailed manner where all the qualitative and quantitative results are compared.

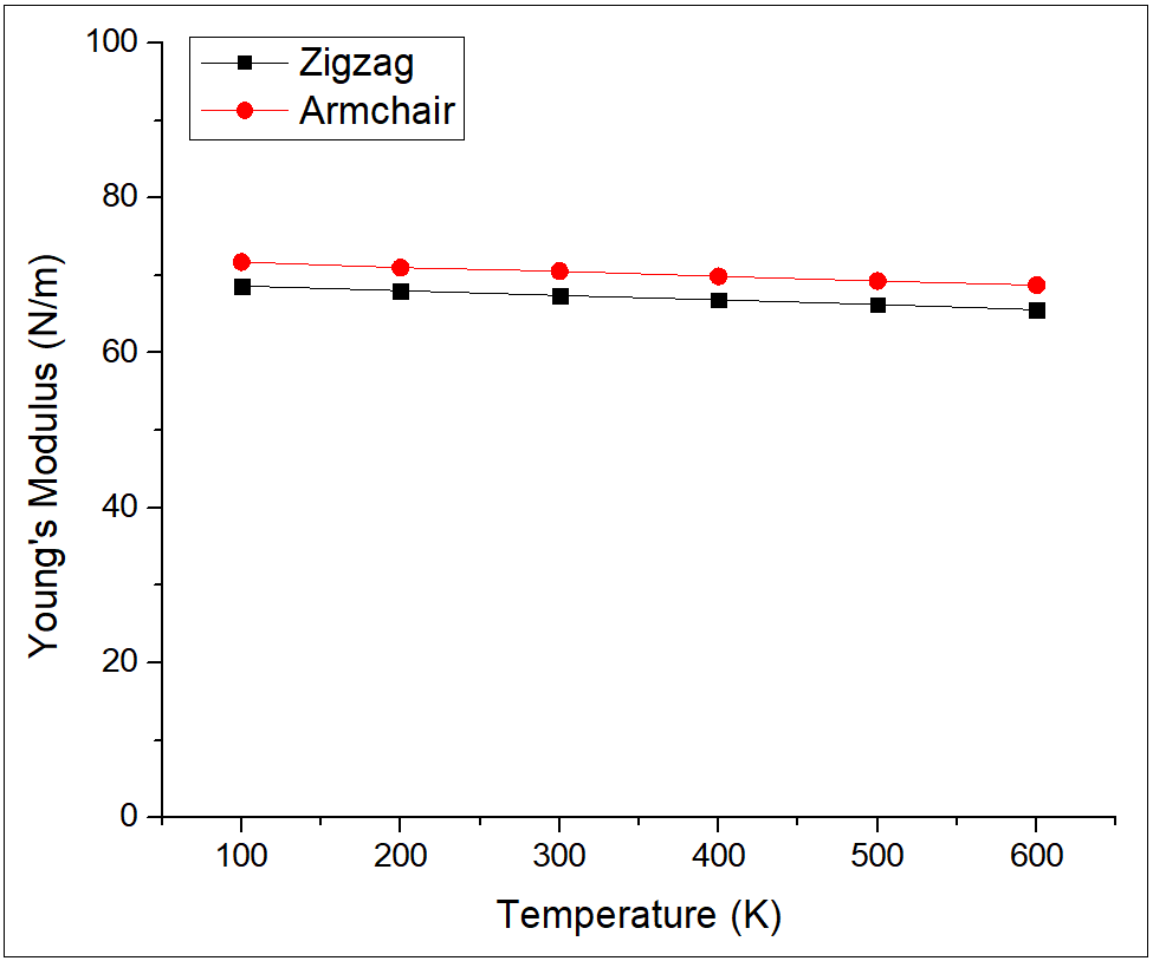

Figure 80: Elastic modulus at different temperatures for armchair and zigzag.

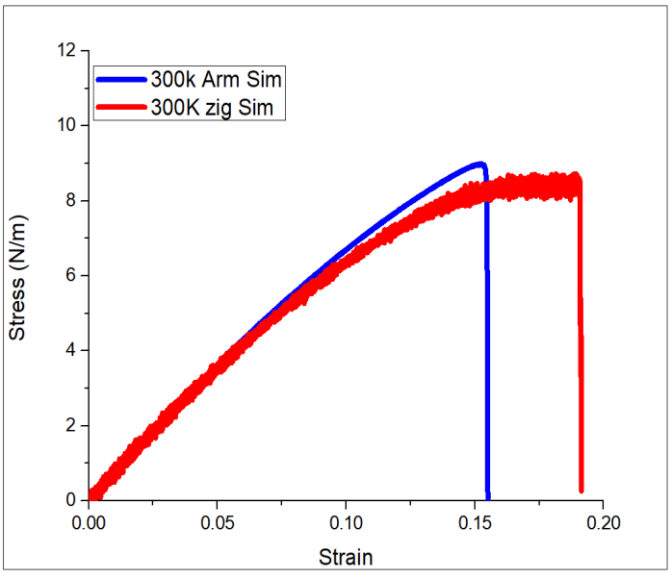

Figure 81: Plane stress-strain for single-layer dimension 2H-$MoTe_2$ armchair and zigzag at 300K.

Chapter 5
CONCULSION

5.1. SUMMARY OF THE WORK

In hand of this work , the Validation of published computational stress and strain result of Graphene, MoS_2 and, $MoTe_2$. Further in investigation of $MoTe_2$ found Ultimate tensile stress of $MoTe_2$ Reduces with the increase of the temperature , the elastic modulus stable with wide range of temperature and Armchair configuration is stronger than Zigzag configuration of $MoTe_2$.

5.2. KEY RESEARCH OUTCOME

- The skill of modifying Creating different materials lattice structures amd varying 2D material sheets size was learned and mastered to some extend.
- Molecules dynamic simulation experiments art was explored and apllied on 2D materials succesfuly.
- Difference between Classical and Quantum mechanics has been explored and some material and introductory course has been taken.
- Through the research phase the Fundamentals of computational and material science been scaned and generally understood.
- Ther interatomic intraction and interatomic forces influnceing the mechanical properties of the 2D materials partially Understood through the usage of different interatomic potentials.
- The application of 2D material in electronics industry with the design requirements was explored and we have enlightened with.
- Different softwares and developer packged have been deelt with which gave first hand experience of intgral usage of different supplementary tools. I.e. (OVITO, ATOMSK, VESTA AND ORGIN) and programing tools. I.e.(CodeBlock, Command Prompt),and some programing languages such Python and Matlab.

5.3. LIMITATIONS AND FUTURE WORK

- Computational Power for Processing large number of atoms.
- Experimental step for 2D materials.
- Assumptions of Standard conditions.

- Inherited Computational error.
- Approximation in governing equations.
- Random initial condition. I.e: Initial Velocity, Relaxation, Minimization Energy.
- In future could work with doping and vacancy effect in fracture and electrical properties of TMDs (around **40** compounds) .
- Composite 2D heterostructure fracture points could be investigated in farthure study.

5.4. RECOMMENDATION

- Modification of the SW potential for more realistic result for TMDs i.e. incorporating specific bonding angles.
- Machine Learning Algorithm to characterized mechanical properties of TMDs.

REFERENCES

[1] A. Gupta, T. Sakthivel, and S. Seal, "Recent development in 2D materials beyond graphene," *Prog. Mater. Sci.*, vol. 73, no. February, pp. 44–126, Aug. 2015, doi: 10.1016/j.pmatsci.2015.02.002.

[2] M. H. Kang, D. Lee, J. Sung, J. Kim, B. H. Kim, and J. Park, "Structure and chemistry of 2D materials," in *Comprehensive Nanoscience and Nanotechnology*, vol. 1–5, 2019.

[3] M. Yi and Z. Shen, "A review on mechanical exfoliation for the scalable production of graphene," *Journal of Materials Chemistry A*, vol. 3, no. 22. 2015, doi: 10.1039/c5ta00252d.

[4] J. Guo and K. Liu, "Recent Progress in Two-Dimensional MoTe2 Hetero-Phase Homojunctions," *Nanomaterials*, vol. 12, no. 1, Jan. 2022, doi: 10.3390/NANO12010110.

[5] X. Song, F. Yuan, and L. M. Schoop, "The properties and prospects of chemically exfoliated nanosheets for quantum materials in two dimensions," *Applied Physics Reviews*, vol. 8, no. 1. 2021, doi: 10.1063/5.0038644.

[6] A. P. Thompson *et al.*, "LAMMPS - a flexible simulation tool for particle-based materials modeling at the atomic, meso, and continuum scales," *Comput. Phys. Commun.*, vol. 271, 2022, doi: 10.1016/j.cpc.2021.108171.

[7] *Numerical Simulation in Molecular Dynamics*. 2007.

[8] P. Hirel, "Atomsk: A tool for manipulating and converting atomic data files," *Comput. Phys. Commun.*, vol. 197, 2015, doi: 10.1016/j.cpc.2015.07.012.

[9] K. Momma and F. Izumi, "VESTA: A three-dimensional visualization system for electronic and structural analysis," *J. Appl. Crystallogr.*, vol. 41, no. 3, 2008, doi: 10.1107/S0021889808012016.

[10] A. Stukowski, "Visualization and analysis of atomistic simulation data with OVITO–the Open Visualization Tool," *Model. Simul. Mater. Sci. Eng.*, vol. 18, no. 1, p. 015012, Dec. 2009, doi: 10.1088/0965-0393/18/1/015012.

[11] K. Vollmayr-Lee, "Introduction to molecular dynamics simulations," *Am. J. Phys.*, vol. 88, no. 5, pp. 401–422, 2020, doi: 10.1119/10.0000654.

[12] S. Deng and V. Berry, "Wrinkled, rippled and crumpled graphene: An overview of formation mechanism, electronic properties, and applications," *Materials Today*, vol. 19, no. 4. 2016, doi: 10.1016/j.mattod.2015.10.002.

[13] A. Castellanos-Gomez *et al.*, "Local strain engineering in atomically thin MoS2," *Nano*

Lett., vol. 13, no. 11, 2013, doi: 10.1021/nl402875m.

[14] T. Cui *et al.*, "Graphene fatigue through van der Waals interactions," *Sci. Adv.*, vol. 6, no. 42, Oct. 2020, doi: 10.1126/SCIADV.ABB1335.

[15] X. Wang, A. Tabarraei, and D. E. Spearot, "Fracture mechanics of monolayer molybdenum disulfide," *Nanotechnology*, vol. 26, no. 17, p. 175703, May 2015, doi: 10.1088/0957-4484/26/17/175703.

[16] J.-W. Jiang and Y.-P. Zhou, "Parameterization of Stillinger-Weber Potential for Two-Dimensional Atomic Crystals," *Handb. Stillinger-Weber Potential Parameters Two-Dimensional At. Cryst.*, Dec. 2017, doi: 10.5772/INTECHOPEN.71929.

[17] R. Mas-Ballesté, C. Gómez-Navarro, J. Gómez-Herrero, and F. Zamora, "2D materials: To graphene and beyond," *Nanoscale*, vol. 3, no. 1. 2011, doi: 10.1039/c0nr00323a.

[18] K. S. Novoselov *et al.*, "Two-dimensional gas of massless Dirac fermions in graphene," *Nature*, vol. 438, no. 7065, pp. 197–200, Nov. 2005, doi: 10.1038/nature04233.

[19] P. R. Wallace, "The band theory of graphite," *Phys. Rev.*, vol. 71, no. 9, pp. 622–634, 1947, doi: 10.1103/PhysRev.71.622.

[20] Q. H. Wang, K. Kalantar-Zadeh, A. Kis, J. N. Coleman, and M. S. Strano, "Electronics and optoelectronics of two-dimensional transition metal dichalcogenides," *Nature Nanotechnology*, vol. 7, no. 11. 2012, doi: 10.1038/nnano.2012.193.

[21] K. S. Novoselov, V. I. Fal'Ko, L. Colombo, P. R. Gellert, M. G. Schwab, and K. Kim, "A roadmap for graphene," *Nature*, vol. 490, no. 7419. 2012, doi: 10.1038/nature11458.

[22] R. Zhang and R. Cheung, "Mechanical Properties and Applications of Two-Dimensional Materials," in *Two-dimensional Materials - Synthesis, Characterization and Potential Applications*, 2016.

[23] D. Er and K. Ghatak, "Atomistic modeling by density functional theory of two-dimensional materials," in *Synthesis, Modelling and Characterization of 2D Materials and their Heterostructures*, 2020.

[24] A. K. Geim and I. V. Grigorieva, "Van der Waals heterostructures," *Nat. 2013 4997459*, vol. 499, no. 7459, pp. 419–425, Jul. 2013, doi: 10.1038/nature12385.

[25] M. Huang, H. Yan, C. Chen, D. Song, T. F. Heinz, and J. Hone, "Phonon softening and crystallographic orientation of strained graphene studied by Raman spectroscopy," *Proc. Natl. Acad. Sci. U. S. A.*, vol. 106, no. 18, pp. 7304–7308, May 2009, doi: 10.1073/PNAS.0811754106.

[26] A. K. Geim and K. S. Novoselov, "The rise of graphene," *Nat. Mater.*, vol. 6, no. 3, 2007,

doi: 10.1038/nmat1849.

[27] A. D. Zdetsis and E. N. Economou, "A Pedestrian Approach to the Aromaticity of Graphene and Nanographene: Significance of Huckel's (4n+2)π Electron Rule," *J. Phys. Chem. C*, vol. 119, no. 29, 2015, doi: 10.1021/acs.jpcc.5b04311.

[28] P. Harris, "Transmission Electron Microscopy of Carbon: A Brief History," *C*, vol. 4, no. 1, 2018, doi: 10.3390/c4010004.

[29] M. A. Poothanari, Y. B. Pottathara, and S. Thomas, "Carbon nanostructures for electromagnetic shielding applications," in *Industrial Applications of Nanomaterials*, 2019.

[30] N. Mounet *et al.*, "Two-dimensional materials from high-throughput computational exfoliation of experimentally known compounds," *Nat. Nanotechnol.*, vol. 13, no. 3, 2018, doi: 10.1038/s41565-017-0035-5.

[31] P. Joensen, R. F. Frindt, and S. R. Morrison, "Single-layer MoS2," *Mater. Res. Bull.*, vol. 21, no. 4, 1986, doi: 10.1016/0025-5408(86)90011-5.

[32] S. Beniwal *et al.*, "Graphene-like Boron-Carbon-Nitrogen Monolayers," *ACS Nano*, vol. 11, no. 3, 2017, doi: 10.1021/acsnano.6b08136.

[33] Z. Shi, Z. Zhang, A. Kutana, and B. I. Yakobson, "Predicting Two-Dimensional Silicon Carbide Monolayers," *ACS Nano*, vol. 9, no. 10, 2015, doi: 10.1021/acsnano.5b02753.

[34] Z. Zhang, X. Liu, B. I. Yakobson, and W. Guo, "Two-dimensional tetragonal tic monolayer sheet and nanoribbons," *J. Am. Chem. Soc.*, vol. 134, no. 47, 2012, doi: 10.1021/ja308576g.

[35] Z. Xiong, L. Zhong, H. Wang, and X. Li, "Structural defects, mechanical behaviors and properties of two-dimensional materials," *Materials*, vol. 14, no. 5. 2021, doi: 10.3390/ma14051192.

[36] K. V. Emtsev *et al.*, "Towards wafer-size graphene layers by atmospheric pressure graphitization of silicon carbide," *Nat. Mater. 2009 83*, vol. 8, no. 3, pp. 203–207, Feb. 2009, doi: 10.1038/nmat2382.

[37] Y. Y. Zhang, Q. X. Pei, and C. M. Wang, "Mechanical properties of graphynes under tension: A molecular dynamics study," *Appl. Phys. Lett.*, vol. 101, no. 8, 2012, doi: 10.1063/1.4747719.

[38] D. Malko, C. Neiss, F. Viñes, and A. Görling, "Competition for graphene: Graphynes with direction-dependent dirac cones," *Phys. Rev. Lett.*, vol. 108, no. 8, 2012, doi: 10.1103/PhysRevLett.108.086804.

[39] G. Li, Y. Li, H. Liu, Y. Guo, Y. Li, and D. Zhu, "Architecture of graphdiyne nanoscale films," *Chem. Commun.*, vol. 46, no. 19, 2010, doi: 10.1039/b922733d.

References

[40] Y. Li, L. Xu, H. Liu, and Y. Li, "Graphdiyne and graphyne: From theoretical predictions to practical construction," *Chemical Society Reviews*, vol. 43, no. 8. 2014, doi: 10.1039/c3cs60388a.

[41] X. Wu *et al.*, "Epitaxial Growth and Air-Stability of Monolayer Antimonene on PdTe2," *Adv. Mater.*, vol. 29, no. 11, Mar. 2017, doi: 10.1002/ADMA.201605407.

[42] C. Lee, X. Wei, J. W. Kysar, and J. Hone, "Measurement of the elastic properties and intrinsic strength of monolayer graphene," *Science (80-.).*, vol. 321, no. 5887, pp. 385–388, Jul. 2008, doi: 10.1126/SCIENCE.1157996/SUPPL_FILE/LEE-SOM.PDF.

[43] J. Wang, F. Ma, W. Liang, and M. Sun, "Electrical properties and applications of graphene, hexagonal boron nitride (h-BN), and graphene/h-BN heterostructures," *Materials Today Physics*, vol. 2. 2017, doi: 10.1016/j.mtphys.2017.07.001.

[44] A. K. Geim, "Graphene: Status and Prospects," *Science (80-.).*, vol. 324, no. 5934, pp. 1530–1534, Jun. 2009, doi: 10.1126/SCIENCE.1158877.

[45] N. D. Mueller, J. S. Gerber, M. Johnston, D. K. Ray, N. Ramankutty, and J. A. Foley, "Closing yield gaps through nutrient and water management," *Nat. 2012 4907419*, vol. 490, no. 7419, pp. 254–257, Aug. 2012, doi: 10.1038/nature11420.

[46] M. Chhowalla, H. S. Shin, G. Eda, L. J. Li, K. P. Loh, and H. Zhang, "The chemistry of two-dimensional layered transition metal dichalcogenide nanosheets," *Nat. Chem. 2013 54*, vol. 5, no. 4, pp. 263–275, Mar. 2013, doi: 10.1038/nchem.1589.

[47] R. Kappera *et al.*, "Phase-engineered low-resistance contacts for ultrathin MoS2 transistors," *Nat. Mater.*, vol. 13, no. 12, 2014, doi: 10.1038/nmat4080.

[48] Y.-C. Lin, D. O. Dumcenco, Y.-S. Huang, and K. Suenaga, "Atomic mechanism of phase transition between metallic and semiconducting MoS2 single-layers," 2013.

[49] K. A. N. Duerloo, Y. Li, and E. J. Reed, "Structural phase transitions in two-dimensional Mo-and W-dichalcogenide monolayers," *Nat. Commun.*, vol. 5, 2014, doi: 10.1038/ncomms5214.

[50] X. Chen, C. Liu, and S. Mao, "Environmental Analysis with 2D Transition-Metal Dichalcogenide-Based Field-Effect Transistors," *Nano-Micro Lett. 2020 121*, vol. 12, no. 1, pp. 1–24, Apr. 2020, doi: 10.1007/S40820-020-00438-W.

[51] "On the theory of superconductivity: the one-dimensional case," *Proc. R. Soc. London. Ser. A. Math. Phys. Sci.*, vol. 223, no. 1154, 1954, doi: 10.1098/rspa.1954.0116.

[52] K. Kang, S. Chen, and E. H. Yang, "Synthesis of transition metal dichalcogenides," in *Synthesis, Modelling and Characterization of 2D Materials and their Heterostructures,*

2020.

[53] S. Manzeli, D. Ovchinnikov, D. Pasquier, O. V. Yazyev, and A. Kis, "2D transition metal dichalcogenides," *Nat. Rev. Mater. 2017 28*, vol. 2, no. 8, pp. 1–15, Jun. 2017, doi: 10.1038/natrevmats.2017.33.

[54] "2D Materials: An Introduction to Two-Dimensional Materials | Ossila." [Online]. Available: https://www.ossila.com/pages/introduction-2d-materials. [Accessed: 31-May-2022].

[55] E. Yang, H. Ji, and Y. Jung, "Two-Dimensional Transition Metal Dichalcogenide Monolayers as Promising Sodium Ion Battery Anodes," *J. Phys. Chem. C*, vol. 119, no. 47, 2015, doi: 10.1021/acs.jpcc.5b09935.

[56] P. Gao, L. Wang, Y. Zhang, Y. Huang, and K. Liu, "Atomic-Scale Probing of the Dynamics of Sodium Transport and Intercalation-Induced Phase Transformations in MoS2," *ACS Nano*, vol. 9, no. 11, 2015, doi: 10.1021/acsnano.5b04950.

[57] D. Su, S. Dou, and G. Wang, "Ultrathin MoS2 nanosheets as anode materials for sodium-ion batteries with superior performance," *Adv. Energy Mater.*, vol. 5, no. 6, 2015, doi: 10.1002/aenm.201401205.

[58] X. Sun, Z. Wang, and Y. Q. Fu, "Defect-Mediated Lithium Adsorption and Diffusion on Monolayer Molybdenum Disulfide," *Sci. Rep.*, vol. 5, 2015, doi: 10.1038/srep18712.

[59] Y. M. Chen, X. Y. Yu, Z. Li, U. Paik, and X. W. Lou, "Hierarchical MoS2 tubular structures internally wired by carbon nanotubes as a highly stable anode material for lithium-ion batteries," *Sci. Adv.*, vol. 2, no. 7, 2016, doi: 10.1126/sciadv.1600021.

[60] V. Sharma, K. Ghatak, and D. Datta, "Two-dimensional materials and its heterostructures for energy storage," in *Synthesis, Modelling and Characterization of 2D Materials and their Heterostructures*, 2020.

[61] B. Radisavljevic, A. Radenovic, J. Brivio, V. Giacometti, and A. Kis, "Single-layer MoS2 transistors," *Nat. Nanotechnol.*, 2011, doi: 10.1038/nnano.2010.279.

[62] A. A. Soluyanov *et al.*, "Type-II Weyl semimetals," *Nat. 2015 5277579*, vol. 527, no. 7579, pp. 495–498, Nov. 2015, doi: 10.1038/nature15768.

[63] B. A. Joyce, "Molecular beam epitaxy," *Reports Prog. Phys.*, vol. 48, no. 12, p. 1637, Dec. 1985, doi: 10.1088/0034-4885/48/12/002.

[64] J. W. Chung, Z. R. Dai, and F. S. Ohuchi, "WS2 thin films by metal organic chemical vapor deposition," *J. Cryst. Growth*, vol. 186, no. 1–2, pp. 137–150, Mar. 1998, doi: 10.1016/S0022-0248(97)00479-X.

References

[65] "Epitaxial growth of a 2D transition metal dichalcogenide lateral heterojunction." [Online]. Available: https://spie.org/news/6470-epitaxial-growth-of-a-2d-transition-metal-dichalcogenide-lateral-heterojunction?SSO=1. [Accessed: 31-May-2022].

[66] A. Kuc, N. Zibouche, and T. Heine, "Influence of quantum confinement on the electronic structure of the transition metal sulfide TS2," *Phys. Rev. B - Condens. Matter Mater. Phys.*, vol. 83, no. 24, pp. 1–4, 2011, doi: 10.1103/PhysRevB.83.245213.

[67] P. Geerlings, F. De Proft, and W. Langenaeker, "Conceptual density functional theory," *Chem. Rev.*, vol. 103, no. 5, pp. 1793–1873, 2003, doi: 10.1021/cr990029p.

[68] W. Kohn, "Nobel lecture: Electronic structure of matter - Wave functions and density functional," *Rev. Mod. Phys.*, vol. 71, no. 5, pp. 1253–1266, 1999, doi: 10.1103/revmodphys.71.1253.

[69] P. Johari and V. B. Shenoy, "Tuning the Electronic Properties of Semiconducting Transition Metal Dichalcogenides by Applying Mechanical Strains," *ACS Nano*, vol. 6, no. 6, pp. 5449–5456, Jun. 2012, doi: 10.1021/nn301320r.

[70] I. S. I. Web, S. This, H. Press, M. Science, N. York, and A. Nw, "Graphene : Status and Prospects," vol. 1530, no. 2009, 2012, doi: 10.1126/science.1158877.

[71] X. Xu, W. Yao, D. Xiao, and T. F. Heinz, "Spin and pseudospins in layered transition metal dichalcogenides," *Nature Physics*, vol. 10, no. 5. 2014, doi: 10.1038/nphys2942.

[72] A. Splendiani *et al.*, "Emerging photoluminescence in monolayer MoS2," *Nano Lett.*, vol. 10, no. 4, pp. 1271–1275, 2010, doi: 10.1021/nl903868w.

[73] K. F. Mak, C. Lee, J. Hone, J. Shan, and T. F. Heinz, "Atomically thin MoS2: A new direct-gap semiconductor," *Phys. Rev. Lett.*, 2010, doi: 10.1103/PhysRevLett.105.136805.

[74] P. Cudazzo, I. V. Tokatly, and A. Rubio, "Dielectric screening in two-dimensional insulators: Implications for excitonic and impurity states in graphane," *Phys. Rev. B - Condens. Matter Mater. Phys.*, vol. 84, no. 8, pp. 1–7, 2011, doi: 10.1103/PhysRevB.84.085406.

[75] A. Ramasubramaniam, "Large excitonic effects in monolayers of molybdenum and tungsten dichalcogenides," *Phys. Rev. B - Condens. Matter Mater. Phys.*, vol. 86, no. 11, p. 115409, Sep. 2012, doi: 10.1103/PhysRevB.86.115409.

[76] H. P. Komsa and A. V. Krasheninnikov, "Effects of confinement and environment on the electronic structure and exciton binding energy of MoS2 from first principles," *Phys. Rev. B - Condens. Matter Mater. Phys.*, vol. 86, no. 24, 2012, doi: 10.1103/PhysRevB.86.241201.

References

[77] T. C. Berkelbach, M. S. Hybertsen, and D. R. Reichman, "Theory of neutral and charged excitons in monolayer transition metal dichalcogenides," *Phys. Rev. B - Condens. Matter Mater. Phys.*, vol. 88, no. 4, 2013, doi: 10.1103/PhysRevB.88.045318.

[78] D. Y. Qiu, F. H. Da Jornada, and S. G. Louie, "Optical spectrum of MoS2: Many-body effects and diversity of exciton states," *Phys. Rev. Lett.*, vol. 111, no. 21, 2013, doi: 10.1103/PhysRevLett.111.216805.

[79] A. Chernikov *et al.*, "Exciton binding energy and nonhydrogenic Rydberg series in monolayer WS2," *Phys. Rev. Lett.*, vol. 113, no. 7, 2014, doi: 10.1103/PhysRevLett.113.076802.

[80] K. He *et al.*, "Tightly bound excitons in monolayer WSe2," *Phys. Rev. Lett.*, vol. 113, no. 2, 2014, doi: 10.1103/PhysRevLett.113.026803.

[81] Z. Ye *et al.*, "Probing excitonic dark states in single-layer tungsten disulphide," *Nature*, vol. 513, no. 7517, pp. 214–218, 2014, doi: 10.1038/nature13734.

[82] G. Wang *et al.*, "Giant Enhancement of the Optical Second-Harmonic Emission of WSe2 Monolayers by Laser Excitation at Exciton Resonances," *Phys. Rev. Lett.*, vol. 114, no. 9, 2015, doi: 10.1103/PhysRevLett.114.097403.

[83] C. Zhang, A. Johnson, C. L. Hsu, L. J. Li, and C. K. Shih, "Direct imaging of band profile in single layer MoS2 on graphite: Quasiparticle energy gap, metallic edge states, and edge band bending," *Nano Lett.*, vol. 14, no. 5, 2014, doi: 10.1021/nl501133c.

[84] J. S. Ross *et al.*, "Electrical control of neutral and charged excitons in a monolayer semiconductor," *Nat. Commun.*, vol. 4, 2013, doi: 10.1038/ncomms2498.

[85] D. Sanvitto *et al.*, "Observation of charge transport by negatively charged excitons," *Science (80-.).*, vol. 294, no. 5543, 2001, doi: 10.1126/science.1064847.

[86] M. M. Fogler, L. V. Butov, and K. S. Novoselov, "High-temperature superfluidity with indirect excitons in van der Waals heterostructures," *Nat. Commun.*, vol. 5, 2014, doi: 10.1038/ncomms5555.

[87] H. Zeng, J. Dai, W. Yao, D. Xiao, and X. Cui, "Valley polarization in MoS 2 monolayers by optical pumping," *Nat. Nanotechnol.*, vol. 7, no. 8, 2012, doi: 10.1038/nnano.2012.95.

[88] S. Yang *et al.*, "The piezotronic effect of zinc oxide nanowires studied by in situ TEM," *Adv. Mater.*, vol. 24, no. 34, 2012, doi: 10.1002/adma.201104420.

[89] K. F. Mak, K. He, J. Shan, and T. F. Heinz, "Control of valley polarization in monolayer MoS2 by optical helicity," *Nat. Nanotechnol.*, vol. 7, no. 8, 2012, doi: 10.1038/nnano.2012.96.

References

[90] J. A. Reyes-Retana, G. G. Naumis, and F. Cervantes-Sodi, "Centered honeycomb NiSe2 nanoribbons: Structure and electronic properties," *J. Phys. Chem. C*, vol. 118, no. 6, 2014, doi: 10.1021/jp409504f.

[91] X. Zhang, M. Zhen, J. Bai, S. Jin, and L. Liu, "Efficient NiSe-Ni3Se2/Graphene Electrocatalyst in Dye-Sensitized Solar Cells: The Role of Hollow Hybrid Nanostructure," *ACS Appl. Mater. Interfaces*, vol. 8, no. 27, 2016, doi: 10.1021/acsami.6b02350.

[92] F. Wang *et al.*, "Selenium-Enriched Nickel Selenide Nanosheets as a Robust Electrocatalyst for Hydrogen Generation," *Angew. Chemie - Int. Ed.*, vol. 55, no. 24, 2016, doi: 10.1002/anie.201602802.

[93] K. F. Mak and J. Shan, "Photonics and optoelectronics of 2D semiconductor transition metal dichalcogenides," *Nature Photonics*, vol. 10, no. 4. Nature Publishing Group, pp. 216–226, Apr-2016, doi: 10.1038/nphoton.2015.282.

[94] W. L. McMillan, "Theory of discommensurations and the commensurate-incommensurate charge-density-wave phase transition," *Phys. Rev. B*, vol. 14, no. 4, 1976, doi: 10.1103/PhysRevB.14.1496.

[95] S. Manzeli, D. Ovchinnikov, D. Pasquier, O. V. Yazyev, and A. Kis, "2D transition metal dichalcogenides," *Nat. Rev. Mater.*, vol. 2, no. 8, p. 17033, Aug. 2017, doi: 10.1038/natrevmats.2017.33.

[96] K. Kaasbjerg, K. S. Thygesen, and K. W. Jacobsen, "Phonon-limited mobility in n-type single-layer MoS 2 from first principles," *Phys. Rev. B - Condens. Matter Mater. Phys.*, vol. 85, no. 11, 2012, doi: 10.1103/PhysRevB.85.115317.

[97] K. Kaasbjerg, K. S. Thygesen, and A. P. Jauho, "Acoustic phonon limited mobility in two-dimensional semiconductors: Deformation potential and piezoelectric scattering in monolayer MoS2 from first principles," *Phys. Rev. B - Condens. Matter Mater. Phys.*, vol. 87, no. 23, 2013, doi: 10.1103/PhysRevB.87.235312.

[98] W. Zhang, Z. Huang, W. Zhang, and Y. Li, "Two-dimensional semiconductors with possible high room temperature mobility," *Nano Res.*, vol. 7, no. 12, 2014, doi: 10.1007/s12274-014-0532-x.

[99] R. Ganatra and Q. Zhang, "Few-layer MoS2: A promising layered semiconductor," *ACS Nano*. 2014, doi: 10.1021/nn405938z.

[100] J. W. Jiang, Z. Qi, H. S. Park, and T. Rabczuk, "Elastic bending modulus of single-layer molybdenum disulfide (MoS 2): Finite thickness effect," *Nanotechnology*, vol. 24, no. 43, 2013, doi: 10.1088/0957-4484/24/43/435705.

References

[101] X. Fan, W. T. Zheng, J. L. Kuo, and D. J. Singh, "Structural stability of single-layer MoS2 under large strain," *J. Phys. Condens. Matter*, vol. 27, no. 10, 2015, doi: 10.1088/0953-8984/27/10/105401.

[102] S. Bertolazzi, J. Brivio, and A. Kis, "Stretching and breaking of ultrathin MoS 2," *ACS Nano*, vol. 5, no. 12, 2011, doi: 10.1021/nn203879f.

[103] J. Wu *et al.*, "Grain-Size-Controlled Mechanical Properties of Polycrystalline Monolayer MoS2," *Nano Lett.*, vol. 18, no. 2, 2018, doi: 10.1021/acs.nanolett.7b05433.

[104] S. Xiong and G. Cao, "Molecular dynamics simulations of mechanical properties of monolayer MoS2," *Nanotechnology*, vol. 26, no. 18, 2015, doi: 10.1088/0957-4484/26/18/185705.

[105] M. Hasanian, B. Mortazavi, A. Ostadhossein, T. Rabczuk, and A. C. T. van Duin, "Hydrogenation and defect formation control the strength and ductility of MoS2 nanosheets: Reactive molecular dynamics simulation," *Extrem. Mech. Lett.*, vol. 22, pp. 157–164, Jul. 2018, doi: 10.1016/j.eml.2018.05.008.

[106] B. Mortazavi, A. Ostadhossein, T. Rabczuk, and A. C. T. Van Duin, "Mechanical response of all-MoS2 single-layer heterostructures: A ReaxFF investigation," *Phys. Chem. Chem. Phys.*, vol. 18, no. 34, 2016, doi: 10.1039/c6cp03612k.

[107] N. Ghobadi, "A comparative study of the mechanical properties of multilayer MoS2 and graphene/MoS2 heterostructure: effects of temperature, number of layers and stacking order," *Curr. Appl. Phys.*, vol. 17, no. 11, pp. 1483–1493, 2017, doi: 10.1016/j.cap.2017.08.018.

[108] Q. Qin, T. Heil, M. Antonietti, and M. Oschatz, "Single-Site Gold Catalysts on Hierarchical N-Doped Porous Noble Carbon for Enhanced Electrochemical Reduction of Nitrogen," *Small Methods*, vol. 2, no. 12, p. 1800202, Dec. 2018, doi: 10.1002/SMTD.201800202.

[109] R. A. S. I. Subad, T. S. Akash, P. Bose, and M. M. Islam, "Engineered defects to modulate fracture strength of single layer MoS2: An atomistic study," *Phys. B Condens. Matter*, vol. 592, no. October 2019, p. 412219, Sep. 2020, doi: 10.1016/j.physb.2020.412219.

[110] J.-W. Jiang, H. S. Park, and T. Rabczuk, "Molecular dynamics simulations of single-layer molybdenum disulphide (MoS 2): Stillinger-Weber parametrization, mechanical properties, and thermal conductivity," *J. Appl. Phys.*, vol. 114, no. 6, p. 064307, Aug. 2013, doi: 10.1063/1.4818414.

[111] H. Zhao, K. Min, and N. R. Aluru, "Size and chirality dependent elastic properties of graphene nanoribbons under uniaxial tension," *Nano Lett.*, vol. 9, no. 8, 2009, doi:

10.1021/nl901448z.

[112] C. D. Reddy, A. Ramasubramaniam, V. B. Shenoy, and Y. W. Zhang, "Edge elastic properties of defect-free single-layer graphene sheets," *Appl. Phys. Lett.*, vol. 94, no. 10, 2009, doi: 10.1063/1.3094878.

[113] Z. Islam and A. Haque, "Defects and grain boundary effects in MoS2: A molecular dynamics study," *J. Phys. Chem. Solids*, vol. 148, p. 109669, Jan. 2021, doi: 10.1016/j.jpcs.2020.109669.

[114] M. Dey, M. Dey, M. A. Matin, and N. Amin, "Design of highly stable and efficient molybdenum telluride PV cells with arsenic telluride BSF," in *2016 3rd International Conference on Electrical Engineering and Information and Communication Technology, iCEEiCT 2016*, 2017, doi: 10.1109/CEEICT.2016.7873153.

[115] K. Balakrishnan and P. Ramasamy, "Study of anomalous electrical behaviour of molybdenum ditelluride single crystals," *J. Cryst. Growth*, vol. 137, no. 1–2, 1994, doi: 10.1016/0022-0248(94)91291-2.

[116] R. F. Frindt, "The optical properties of single crystals of WSe2 and MoTe2," *J. Phys. Chem. Solids*, vol. 24, no. 9, 1963, doi: 10.1016/0022-3697(63)90024-6.

[117] D. Puotinen and R. E. Newnham, " The crystal structure of MoTe 2 ," *Acta Crystallogr.*, vol. 14, no. 6, 1961, doi: 10.1107/s0365110x61002084.

[118] B. E. Brown, " The crystal structures of WTe 2 and high-temperature MoTe 2 ," *Acta Crystallogr.*, vol. 20, no. 2, 1966, doi: 10.1107/s0365110x66000513.

[119] M. K. Agarwal and M. J. Capers, "The measurement of the lattice parameters of molybdenum ditelluride," *J. Appl. Crystallogr.*, vol. 5, no. 2, 1972, doi: 10.1107/s0021889872008787.

[120] O. Knop and R. D. MacDonald, "CHALKOGENIDES OF THE TRANSITION ELEMENTS: III. MOLYBDENUM DITELLURIDE," *Can. J. Chem.*, vol. 39, no. 4, 1961, doi: 10.1139/v61-110.

[121] M. K. Agarwal and M. J. Capers, "Dislocations in molybdenum ditelluride," *J. Appl. Crystallogr.*, vol. 9, no. 5, 1976, doi: 10.1107/s0021889876011710.

[122] E. Revolinsky and D. J. Beerntsen, "Electrical properties of α- and β-MoTe2 as affected by stoichiometry and preparation temperature," *J. Phys. Chem. Solids*, vol. 27, no. 3, 1966, doi: 10.1016/0022-3697(66)90195-8.

[123] M. B. Vellinga, R. de Jonge, and C. Haas, "Semiconductor to metal transition in MoTe2," *J. Solid State Chem.*, vol. 2, no. 2, 1970, doi: 10.1016/0022-4596(70)90085-X.

References

[124] C. Manolikas, J. van Landuyt, and S. Amelinckx, "Electron microscopy and electron diffraction study of the domain structures, the dislocation fine structure, and the phase transformations in β-MoTe2," *Phys. status solidi*, vol. 53, no. 1, 1979, doi: 10.1002/pssa.2210530138.

[125] K. Ueno and K. Fukushima, "Changes in structure and chemical composition of α-MoTe2 and β-MoTe2 during heating in vacuum conditions," *Appl. Phys. Express*, vol. 8, no. 9, 2015, doi: 10.7567/APEX.8.095201.

[126] G. Qiu, Z. Gai, Y. Tao, J. Schmitt, G. A. Kullak-Ublick, and J. Wang, "Dual-Functional Plasmonic Photothermal Biosensors for Highly Accurate Severe Acute Respiratory Syndrome Coronavirus 2 Detection," *ACS Nano*, vol. 14, no. 5, pp. 5268–5277, May 2020, doi: 10.1021/ACSNANO.0C02439/ASSET/IMAGES/LARGE/NN0C02439_0005.JPEG.

[127] Y. Sun *et al.*, "Elastic Properties and Fracture Behaviors of Biaxially Deformed, Polymorphic MoTe2," *Nano Lett.*, vol. 19, no. 2, pp. 761–769, 2019, doi: 10.1021/acs.nanolett.8b03833.

[128] S. Song, D. H. Keum, S. Cho, D. Perello, Y. Kim, and Y. H. Lee, "Room Temperature Semiconductor-Metal Transition of MoTe2 Thin Films Engineered by Strain," *Nano Lett.*, vol. 16, no. 1, 2016, doi: 10.1021/acs.nanolett.5b03481.

[129] Q. Zhang *et al.*, "Simultaneous synthesis and integration of two-dimensional electronic components," *Nat. Electron.*, vol. 2, no. 4, 2019, doi: 10.1038/s41928-019-0233-2.

[130] R. Ma *et al.*, "MoTe2 Lateral Homojunction Field-Effect Transistors Fabricated using Flux-Controlled Phase Engineering," *ACS Nano*, vol. 13, no. 7, 2019, doi: 10.1021/acsnano.9b02785.

[131] F. Ercolessi, "A molecular dynamics primer," *J. Chem. Inf. Model.*, vol. 53, no. 9, 2013.

[132] "Sandia National Laboratories: News Releases : LAMMPS supercomputer code developer earns special recognition." [Online]. Available: https://newsreleases.sandia.gov/lammps/. [Accessed: 31-May-2022].

[133] S. Plimpton, "LAMMPS documentation," *... . cs. sandia. gov/~ sjplimp/lammps/doc/Manual. html*, 2007.

[134] "Typical time and length scales of different computer simulation... | Download Scientific Diagram." [Online]. Available: https://www.researchgate.net/figure/Typical-time-and-length-scales-of-different-computer-simulation-techniques-Figure-is_fig1_346392670. [Accessed: 31-May-2022].

[135] B. Fiedler, M. Hojo, S. Ochiai, K. Schulte, and M. Ando, "Failure behavior of an epoxy

matrix under different kinds of static loading," *Compos. Sci. Technol.*, vol. 61, no. 11, pp. 1615–1624, Aug. 2001, doi: 10.1016/S0266-3538(01)00057-4.

[136] A. G. Evans, "Slow crack growth in brittle materials under dynamic loading conditions," *Int. J. Fract. 1974 102*, vol. 10, no. 2, pp. 251–259, Jun. 1974, doi: 10.1007/BF00113930.

[137] L. Yi and T. Chang, "Loading direction dependent mechanical behavior of graphene under shear strain," *Sci. China Physics, Mech. Astron.*, vol. 55, no. 6, pp. 1083–1087, Jun. 2012, doi: 10.1007/s11433-012-4721-x.

[138] S. Q. Yang, W. L. Tian, Y. H. Huang, P. G. Ranjith, and Y. Ju, "An experimental and numerical study on cracking behavior of brittle sandstone containing two non-coplanar fissures under uniaxial compression," *Rock Mech. Rock Eng.*, vol. 49, no. 4, pp. 1497–1515, Apr. 2016, doi: 10.1007/S00603-015-0838-3/FIGURES/19.

[139] G. M. Pharr and W. C. Oliver, "Measurement of Thin Film Mechanical Properties Using Nanoindentation," *MRS Bull.*, vol. 17, no. 7, pp. 28–33, 1992, doi: 10.1557/S0883769400041634.

[140] C. Wei, K. Cho, and D. Srivastava, "Tensile strength of carbon nanotubes under realistic temperature and strain rate," *Phys. Rev. B*, vol. 67, no. 11, p. 115407, Mar. 2003, doi: 10.1103/PhysRevB.67.115407.

[141] R. Ansari, B. Motevalli, A. Montazeri, and S. Ajori, "Fracture analysis of monolayer graphene sheets with double vacancy defects via MD simulation," *Solid State Commun.*, vol. 151, no. 17, pp. 1141–1146, Sep. 2011, doi: 10.1016/J.SSC.2011.05.021.

[142] T. Ohtsuki, K. Ohno, K. Shiga, Y. Kawazoe, Y. Maruyama, and K. Masumoto, "Systematic study of foreign-atom-doped fullerenes by using a nuclear recoil method and their MD simulation," *J. Chem. Phys.*, vol. 112, no. 6, p. 2834, Jan. 2000, doi: 10.1063/1.480858.

[143] E. H. Chowdhury, M. H. Rahman, S. Fatema, and M. M. Islam, "Investigation of the mechanical properties and fracture mechanisms of graphene/WSe2 vertical heterostructure: A molecular dynamics study," *Comput. Mater. Sci.*, vol. 188, p. 110231, Feb. 2021, doi: 10.1016/J.COMMATSCI.2020.110231.

[144] M. A. N. Dewapriya, R. K. N. D. Rajapakse, and A. S. Phani, "Atomistic and continuum modelling of temperature-dependent fracture of graphene," *Int. J. Fract.*, vol. 187, no. 2, pp. 199–212, Jun. 2014, doi: 10.1007/S10704-014-9931-Y/FIGURES/11.

[145] M. C. Wang, C. Yan, L. Ma, N. Hu, and M. W. Chen, "Effect of defects on fracture strength of graphene sheets," *Comput. Mater. Sci.*, vol. 54, no. 1, pp. 236–239, Mar. 2012, doi: 10.1016/J.COMMATSCI.2011.10.032.

References

[146] M. S. R. Elapolu, A. Tabarraei, X. Wang, and D. E. Spearot, "Fracture mechanics of multi-layer molybdenum disulfide," *Eng. Fract. Mech.*, vol. 212, no. September 2018, pp. 1–12, 2019, doi: 10.1016/j.engfracmech.2019.02.027.

[147] M. L. Pereira Júnior *et al.*, "On the Elastic Properties and Fracture Patterns of MoX2 (X = S, Se, Te) Membranes: A Reactive Molecular Dynamics Study," *Condens. Matter*, vol. 5, no. 4, p. 73, Nov. 2020, doi: 10.3390/condmat5040073.

[148] S. A. Chowdhury *et al.*, "Mechanical Properties and Strain Transfer Behavior of Molybdenum Ditelluride (MoTe2) Thin Films," *J. Eng. Mater. Technol.*, vol. 144, no. 1, Jan. 2022, doi: 10.1115/1.4051306.

[149] M. L. Pereira Júnior *et al.*, "On the Elastic Properties and Fracture Patterns of MoX2 (X = S, Se, Te) Membranes: A Reactive Molecular Dynamics Study," *Condens. Matter 2020, Vol. 5, Page 73*, vol. 5, no. 4, p. 73, Nov. 2020, doi: 10.3390/CONDMAT5040073.

[150] S. J. Stuart, A. B. Tutein, and J. A. Harrison, "A reactive potential for hydrocarbons with intermolecular interactions," *J. Chem. Phys.*, vol. 112, no. 14, p. 6472, Mar. 2000, doi: 10.1063/1.481208.

[151] D. W. Brenner, O. A. Shenderova, J. A. Harrison, S. J. Stuart, B. Ni, and S. B. Sinnott, "A second-generation reactive empirical bondorder (REBO) potential energy expression for hydrocarbons," *J. Phys. Condens. Matter*, vol. 14, no. 4, p. 783, Jan. 2002, doi: 10.1088/0953-8984/14/4/312.

[152] K. Chenoweth, A. C. T. Van Duin, and W. A. Goddard, "ReaxFF reactive force field for molecular dynamics simulations of hydrocarbon oxidation," *J. Phys. Chem. A*, vol. 112, no. 5, pp. 1040–1053, Feb. 2008, doi: 10.1021/JP709896W/SUPPL_FILE/JP709896W-FILE005.PDF.

[153] T. R. Shan, B. D. Devine, T. W. Kemper, S. B. Sinnott, and S. R. Phillpot, "Charge-optimized many-body potential for the hafnium/hafnium oxide system," *Phys. Rev. B - Condens. Matter Mater. Phys.*, vol. 81, no. 12, p. 125328, Mar. 2010, doi: 10.1103/PHYSREVB.81.125328/FIGURES/4/MEDIUM.

[154] A. P. Thompson *et al.*, "LAMMPS - a flexible simulation tool for particle-based materials modeling at the atomic, meso, and continuum scales," *Comput. Phys. Commun.*, vol. 271, p. 108171, Feb. 2022, doi: 10.1016/J.CPC.2021.108171.

[155] S. J. Plimpton and C. Knight, "Rendezvous algorithms for large-scale modeling and simulation," *J. Parallel Distrib. Comput.*, vol. 147, pp. 184–195, Jan. 2021, doi: 10.1016/J.JPDC.2020.09.001.

References

[156] J.-W. Jiang and Y.-P. Zhou, "Parameterization of Stillinger-Weber Potential for Two-Dimensional Atomic Crystals," in *Handbook of Stillinger-Weber Potential Parameters for Two-Dimensional Atomic Crystals*, vol. i, no. tourism, InTech, 2017, p. 13.

[157] J.-W. Jiang, "Misfit Strain-Induced Buckling for Transition-Metal Dichalcogenide Lateral Heterostructures: A Molecular Dynamics Study," *Acta Mech. Solida Sin.*, vol. 32, no. 1, pp. 17–28, Feb. 2019, doi: 10.1007/s10338-018-0049-z.

[158] J. W. Jiang, "Misfit Strain-Induced Buckling for Transition-Metal Dichalcogenide Lateral Heterostructures: A Molecular Dynamics Study," *Acta Mech. Solida Sin.*, vol. 32, no. 1, pp. 17–28, Feb. 2019, doi: 10.1007/S10338-018-0049-Z.

[159] A. H. Castro Neto, F. Guinea, N. M. R. Peres, K. S. Novoselov, and A. K. Geim, "The electronic properties of graphene," *Rev. Mod. Phys.*, vol. 81, no. 1, pp. 109–162, Jan. 2009, doi: 10.1103/REVMODPHYS.81.109.

[160] M. Z. S. Flores, P. A. S. Autreto, S. B. Legoas, and D. S. Galvao, "Graphene to graphane: A theoretical study," *Nanotechnology*, vol. 20, no. 46, 2009, doi: 10.1088/0957-4484/20/46/465704.

[161] "Molecular Dynamics Simulation of the Uniaxial Tensile Test of a Graphene Sample." [Online]. Available: https://www.linkedin.com/pulse/how-perform-uniaxial-tensile-tests-graphene-sample-lammps-dewapriya/. [Accessed: 08-May-2022].

[162] "Crystallography Open Database." [Online]. Available: http://www.crystallography.net/cod/. [Accessed: 08-May-2022].

[163] A. Molina-Sánchez and L. Wirtz, "Phonons in single and few-layer MoS 2 and WS 2."

[164] "Molybdenum Disulfide, MoS2: Theory, Structure & Applications | Ossila." [Online]. Available: https://www.ossila.com/pages/molybdenum-disulfide-mos2. [Accessed: 08-May-2022].

[165] B. Mortazavi, G. R. Berdiyorov, M. Makaremi, and T. Rabczuk, "Mechanical responses of two-dimensional MoTe 2 ; pristine 2H, 1T and 1T' and 1T'/2H heterostructure."

[166] "Molybdenum Ditelluride, MoTe2 | CAS 12058-20-7 | Ossila." [Online]. Available: https://www.ossila.com/products/molybdenum-ditelluride. [Accessed: 08-May-2022].

[167] H. Zhao and N. R. Aluru, "Temperature and strain-rate dependent fracture strength of graphene," *J. Appl. Phys.*, vol. 108, no. 6, p. 064321, Sep. 2010, doi: 10.1063/1.3488620.